ASSESSING CLIMATE CHANGE IMPACT ACROSS KBK (KALAHANDI-BOLANGIR-KORAPUT) REGION OF ODISHA

KALAHANDI-BOLANGIR-KORAPUT (KBK)

WATER RESOURCES SYSTEMS DIVISION
NATIONAL INSTITUTE OF HYDROLOGY
ROORKEE- 247 667, UTTARAKHAND, INDIA
June, 2016

DIRECTOR

Er. R. D. Singh

HEAD

Dr. Sharad Kumar Jain

INVESTIGATING TEAM

Shri Prabhash Kumar Mishra	:	Scientist 'B'
Dr. Sharad Kumar Jain	:	Scientist 'G' & Head
Dr. Sanjay Kumar Jain	:	Scientist 'G'

TABLE OF CONTENTS

LIST OF FIGURES

LIST OF TABLES

1

INTRODUCTION

1.1 GENERAL

In the recent few decades, importance of climate change has immensely increased due to global warming and its projected effects on hydrologic cycle. Rainfall pattern is extremely varied both spatially and temporally. Temperature is also changing fast. Any change in the rainfall magnitude and pattern will have considerable impact on the water resources. According to IPCC's Fifth Assessment Report (AR5), precipitation trends, including extremes, are characterized by strong variability, with both increasing and decreasing trends observed in different parts and seasons of Asia. Over India, the increase in the number of monsoon break days and the decline in the number of monsoon depressions are consistent with the overall decrease in seasonal mean rainfall. But an increase in extreme rainfall events occurred at the expense of weaker rainfall events over the central Indian region and in many other areas. Almost all models and all scenarios project an increase in both the mean and extreme precipitation in the Indian summer monsoon. In a study of the Mahanadi River Basin in India, a water availability projection (A2, CGCM2) indicated increasing possibility of floods in September but increasing water scarcity in April (Asokan and Dutta, 2008). Constant occurrences of events like flood, drought, high intensity rainfall, hailstorm etc. are being reported throughout the world (Mirza, 2003; Kundzewicz et. al, 2005; Kyselý, 2008). These increasing extreme incidents have led to the rising concern of climate change. Changes in the spatial and temporal distribution of precipitation and temperature are a major component in many studies.

Climate change is a reality. The impact of climate change is multipronged and affects water resources and many other sectors including agriculture, forestry, health, fresh and marine aquaculture, etc. (IPCC, 2007; IPCC, 2013). Climate change is a global phenomenon. Any change in the climate globally, affects India taking into account its vast and varied geographical area. Sea level rise becoming a threat to the people living along the coastal stretch. Temperature

rise affects Himalaya glacier, which is abode to rivers such as the Ganga, the Brahmaputra, and many more.

In India, many studies have been undertaken to understand climate change. A number of researches have been conducted on the precipitation pattern of India. Pal and Al-Tabbaa (2010) indicated variability in seasonal rainfall among different geographical regions of India and no significance was noticed in seasonal and annual rainfall from 1871 to 2005. Basistha et al., 2009 reported 1964 as the most probable year when a shift is detected in the annual and monsoon rainfall over Himalaya. Ghosh et al., 2009 analyzed the Indian summer monsoon rainfall at different scales. Kumar and Jain (2010) analyzed rainfall trend in Kashmir valley. The study indicated decreasing trend in monsoon rainfall, while increasing trend is found in annual, pre-monsoon, post-monsoon and winter rainfall. Kumar et al., 2010 carried out the regional trend analysis of long-term rainfall. The study showed no significant trend in the annual, seasonal and monthly rainfall in most of the months. For the whole of India no significant trend was detected for annual, seasonal, or monthly rainfall. Work on Indian Summer Monsoon (ISM) has been done with Mann-Kendall Test by Duncan et al., 2012 who found that major parts of the country experienced significant rising trend in inter-annual rainfall variation. Patra et al., 2012 analyzed rainfall trend over Orissa state for the period 1871-2006. The analysis revealed non-significant decreasing trend of annual and monsoon rainfall, whereas increasing trend in post-monsoon season over the state. However, rainfall during winter and summer seasons showed an increasing trend. Jain and Kumar (2012) reviewed trends of rainfall, rainy days, and temperature at basin level for India. The study indicated decreasing annual rainfall trends in sixteen basins, one basin with significant decreasing trend with 95% confidence level. The study also showed a rising trend in the mean maximum temperature series at most of the stations. The mean minimum temperature showed a rising as well as a falling trend. At most of the stations in the south, central and western parts of India a rising trend was found. Some stations located in the north and northeastern India showed a falling trend in annual mean temperature. Similarly, temperature trend analysis has been done across India and other countries by different researchers to detect the temperature effects (De and Rao, 2004; Arora et al., 2005; Kothawale and Kumar, 2005; Hundecha and Bardossy, 2005; Jhajharia and Singh, 2011). Thus, wide variability in the precipitation and temperature trend has triggered the growing concern of climate change and its future impact on the environment.

The research work involves finding monotonic trend of rainfall, temperature (minimum, maximum, mean) and potential evapotranspiration across the KBK (Kalahandi-Bolangir-Koraput) region. The research work also includes downscaling the future climate of the region using Global Circulation Models (GCMs), here HadCM3 A2 and B2 scenarios. Finally, the water availability and utilization has been assessed for a representative basin, here Tel basin of the KBK region. This study will help the agricultural planners and managers dealing with the water resources of the area.

1.2 BASIS OF THE STUDY

A study on drought was carried out for Kalahandi district in Orissa (presently, Odisha) by National Institute of Hydrology (NIH) Roorkee a few years back. This particular district along with two nearby districts i.e. Bolangir & Koraput are very much drought prone and have more or less similar climatic conditions. A lot of changes have taken place in the region in the last few decades. Large-scale watershed management activities are also going on funded by NABARD and other Commercial Banks. Development of KBK region is one of the most priority areas for State government also. Thereby, if a holistic study is taken for this region dominated by tribal population with traditional rich culture covering the three KBK districts will be more justified. Keeping in view these facts, the present study has been envisaged to study the water resources problem considering climate change and land use change occurring in the study region.

1.3 STUDY OBJECTIVES

The research work envisages assessing the climate change effects in KBK region, Odisha which is regularly facing drought, water scarcity, and flood as well. The study focuses on the following major three objectives:

- ➢ To analyze long-term historical climatic data to determine trend in rainfall, temperature, PET, etc.
- ➢ To analyze the future climate in the region based on downscaled GCM data.
- ➢ To assess the current potential and gap in utilization of water resources in the region to develop management plan.

The study was undertaken during April 2013, and was completed during June 2016.

1.4 CHAPTERIZATION

The report is organized as follows:

Chapter one describes the background and the importance of the topic, particularly in the context of KBK region. The chapter also specifies the major objectives. It also summaries the organization of the report.

Chapter two describes the study area, here KBK region. Eight administrative districts falling in the KBK region are discussed separately in this chapter.

Chapter three discusses the historical trend for rainfall, temperature, and potential evapotranspiration for the KBK region, Odisha. The chapter also discusses the database preparation, and methodology adopted in the study for finding trends of different variables.

Chapter four describes the expected future rainfall and temperature in the region utilizing Multiple Linear Regression (MLR) based statistical downscaling technique. The proposed technique uses the National Centre for Environmental Prediction (NCEP reanalysis 1961-2001) and Hadley Centre Coupled Model (HadCM3) climatic model for the A2 and B2 emission scenarios (relevant to India) for the period of 1961-2099. Thus, the impact of climate change on expected rainfall and temperature is studied by way of estimating the future rainfall and temperature for different time steps, i.e., past (1961-2010), 2020s, 2050s and 2080s under the suggested scenarios HadCM3-A2 and B2.

Chapter five discusses the water resources availability in the Tel basin. The chapter also discusses the water utilization in the basin. The water resources availability has been done using Soil and Water Assessment Tool (SWAT) model.

Chapter six discusses the summary, important conclusions drawn from the study. It also discusses the scope of future work.

STUDY AREA

2.1 KBK (KALAHANDI-BOLANGIR-KORAPUT) REGION

The Kalahandi-Koraput-Bolangir (KBK) is three individual district administrations in the state of Odisha. During 1992-93, the three districts were reorganized into eight districts viz. Malkangiri, Nabarangpur, Rayagada, Nuapada, Sonepur, Kalahandi, Koraput and Bolangir. It may be noted that after the re-organization of the old districts, the KBK region now consists of eight districts namely, Kalahandi and Nuapada forming part of undivided Kalahandi; Bolangir and Sonepur forming part of undivided Bolangir; and Koraput, Malkangiri, Nabarangpur and Rayagada forming part of undivided Koraput. These eight districts comprise of 14 Subdivisions, 37 Tehsils, 80 Community Development (CD) Blocks, 1,437 Gram Panchayats and 12,293 villages. The geographical and administrative divisions of these districts are summarized in Table 2.1.

Geographically, the KBK region is not homogeneous, and the districts are all highland districts. The eight districts which form the KBK region account for 19.72% population and occupy over 30.59% of the geographical area of the State (1,55,820 km^2). The population details as per the Census 2011 is presented in Table 2.2. The KBK region is unfortunately famous for all possible poverty indices set forth by different study groups. The region, though witnesses an annual rainfall of 956-1375 mm spread over four monsoon months viz. June, July, August and September, has historically faced drought in every 3-4 years. The climate in the area is sub-humid, dry with extreme summer and winter. The population in the region is a mixed group dominated by tribals, like Khonds, Bondas, Koyas, etc.

The area is endowed with mineral dominated natural resources and Non-Timber Forest Produce (NTFP) in the large encompasses of forest. Rain-fed agriculture is the principal occupation of the inhabitants. The location of the study area has been shown in Figure 2.1.

Table 2.1: Geographical and administrative divisions of KBK districts (source: www.kbk.nic.in)

Sl. No.	District	Area (Sq.km)	Number of					
			Blocks	TSP	Sub-div.	Tahsils	GP	Villages
1	Kalahandi	7920	13	2	2	7	273	2236
2	Bolangir	6575	14	-	3	6	285	1794
3	Koraput	8807	14	14	2	7	226	2028
4	Nuapada	3852	5	-	1	2	109	663
5	Sonepur	2337	6	-	2	4	96	959
6	Rayagada	7073	11	11	2	4	171	2667
7	Malkangiri	5791	7	7	1	3	108	1045
8	Nabarangpur	5291	10	10	1	4	169	901
Total		**47646**	**80**	**44**	**14**	**37**	**1437**	**12293**

Table 2.2: Demography in the KBK region (Source: Census of India, 2011)

Sl. No.	District	Area (km²)	Population					
			Total	Male	Female	% decadal growth since 2001	Sex ratio	Density (Persons / km²)
1	Kalahandi	7920	15,73,054	7,85,179	7,87,875	17.79	1003	199
2	Bolangir	6575	16,48,574	8,31,349	8,17,225	23.29	983	251
3	Koraput	8807	13,76,934	6,77,864	6,99,070	16.63	1031	156
4	Nuapada	3852	6,06,490	3,00,307	3,06,183	14.28	1020	157
5	Subarnapur	2337	6,52,107	3,32,897	3,19,210	20.35	959	279
6	Rayagada	7073	9,61,959	4,69,672	4,92,287	15.74	1048	136
7	Malkangiri	5791	6,12,727	3,03,913	3,08,814	21.53	1016	106
8	Nabarangpur	5291	12,18,762	6,04,046	6,14,716	18.81	1018	230
KBK		**47646**	**86,50,607**	**43,05,227**	**43,45,380**	**18.55**	**1009**	**182**
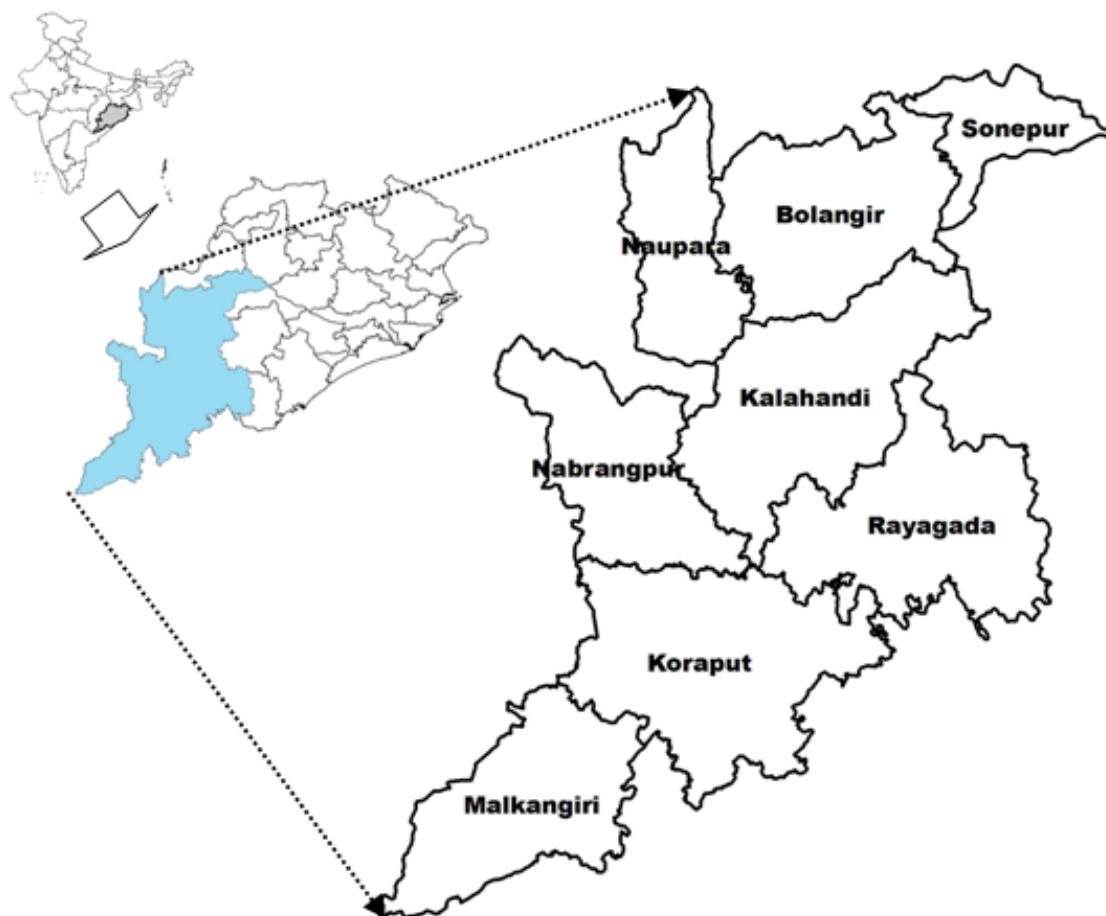
Fig. 2.1 KBK districts in the state of Odisha

A brief description of each district follows.

2.2   KALAHANDI DISTRICT

Kalahandi district covers a geographical area of 7920 km^2. It lies between 19°18'00" to 21°30'00" North Latitude and 82°12'00" to 83°28'12" East Longitude. The district is situated in the South Western part of Odisha, bordered to the North by the Bolangir district and Nuapada district, to the South by the Nabarangpur district, Koraput district and Rayagada district, and to the East by the Rayagada, Kandhamal and Boudh district. The district has two distinct physiographic regions, the hilly-tracts and the plain lands. It has many magnificent scenic spots with towering hills and deep valleys. The plain forms around 50 percent of the total land area and covers the entire Nuapada subdivision (the present Nuapada district) and then runs southward up to Bhawanipatna and westward up to Junagarh and Dharamgarh. The hilly tracts are mostly

located in the western part of Nuapada subdivision and southwestern part of Bhawanipatna subdivision. The climate of the Kalahandi district is of extreme type. It is dry except during monsoon. The maximum temperature of the district reaches up to 45°C, whereas the minimum temperature recorded is 11°C. The district experiences an average annual rainfall of 1378.20 mm. The monsoon starts late in June and generally lasts up to September. The principal rivers flowing in Kalahandi district are Tel, Indravati and Jonk. They are tributaries of major rivers like Mahanadi and Godavari. Besides, there are many perennial streams originating from the hills of the district. However, the rivers and streams in the open country seldom carry a large flow of water during winter and summer seasons and those are scarcely subjected to high floods. Kalahandi district is largely an agriculture based economy. It is rich with agriculture. Forest based products like Mahua, Kendu leaf, Wood, Timber and Bamboos also contribute to local economy largely. The district is a rich land in terms of art and crafts. The location map of the Kalahandi district has been shown in Figure 2.2.
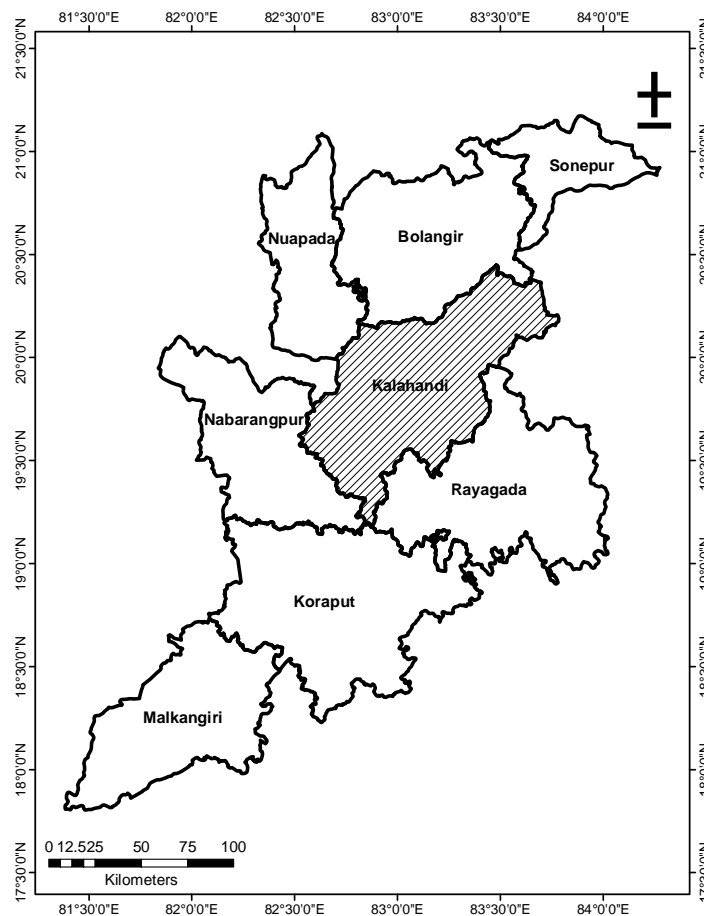
Fig. 2.2 Kalahandi district in the KBK region

2.3 BOLANGIR DISTRICT

The Bolangir district also a part of the KBK region is surrounded by Subarnapur district in the east, Nuapada district in the west, Kalahandi district in the south and Bargarh district in the north. The district lies between 20°11'40" to 21°05'08" North latitude and 82°41'15" to 83°40'22" East longitude. It covers an area of 6575 km^2. Bolangir district has 3 subdivisions, 14 Tahasils, 14 Blocks, 1 Municipality, 3 NACs, and 285 gram panchayats, and 1794 villages. The district witnesses a dry climate with minimum temperature stands at 16.6°C and maximum temperature about 48.7°C. The average annual rainfall in the district stands at 1215.6 mm. The economy of the Bolangir district is basically agrarian with 70 percent of the population depends on agriculture. The tourism industry of Bolangir district also contributes to its economy. The predominant soil groups found in the Bolangir district are red, mixed red, black and alluvial soils. In the district paddy is the principal crop, which accounts for 61 percent of gross cropped area. The other important crops grown in the district are pulses grown in 14 percent of the cropped area followed by oil seeds, which is grown in 3 percent, fibre in 4 percent, vegetable in 2 percent and other food crops like spices and condiments etc. The location map of the Bolangir district has been shown in Figure 2.3.
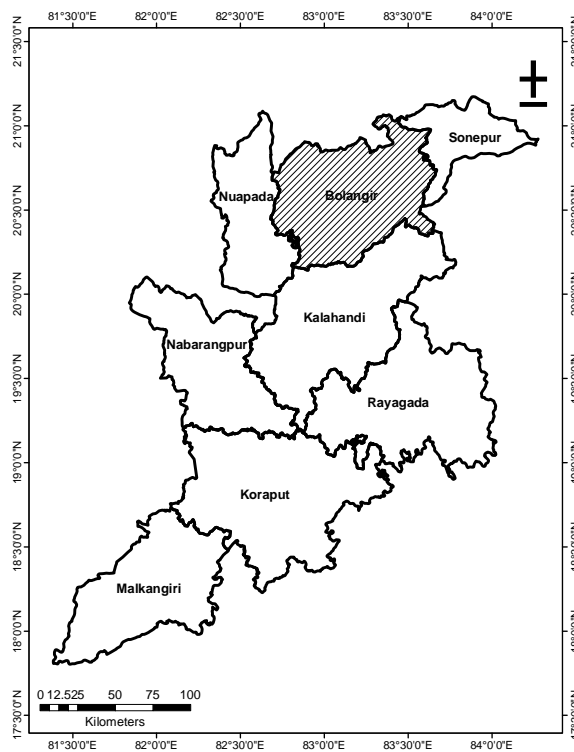
Fig 2.3 Bolangir district in the KBK region

2.4   KORAPUT DISTRICT

The Koraput district is the third administrative district of the undivided KBK region extent from 17°23'60" to 20°41'60" North latitude and 81°14'24" to 84°12'00" East longitude. The Koraput district covers a total geographical area of 8379 km^2. It is bounded by Rayagada district in the east, Bastar district of Chhatisgarh in the west and Nabarangpur district in the south. The district has got 2 sub divisions namely Koraput and Jeypore. The administrative set-up in the district is 14 Tahsils, 14 Blocks, 1 Municipality, 3 NACs, 226 Gram Panchayats, and 2028 Villages The district experiences three seasons i.e. summer, winter and rainy with summer occurring from April to June, Rainy season is from June to October and Winter is from November to March. Koraput district experiences a minimum of 12°C and maximum of 38°C temperature. The annual average rainfall in the district is 1522 mm. The Economy of Koraput district is primarily based upon forestry and agriculture (including shifting cultivation). Agriculture is the mainstay of the economy of the Koraput district with 83% of the population depends on it. The soil and climate in the district are favorable for taking up of agro-horticultural crops like coffee, cashew, cotton, tobacco, vegetables, fruits, etc. The major food crops grown in the district are paddy, millet, maize and pulses. The location map of the Koraput district has been shown in Figure 2.4.
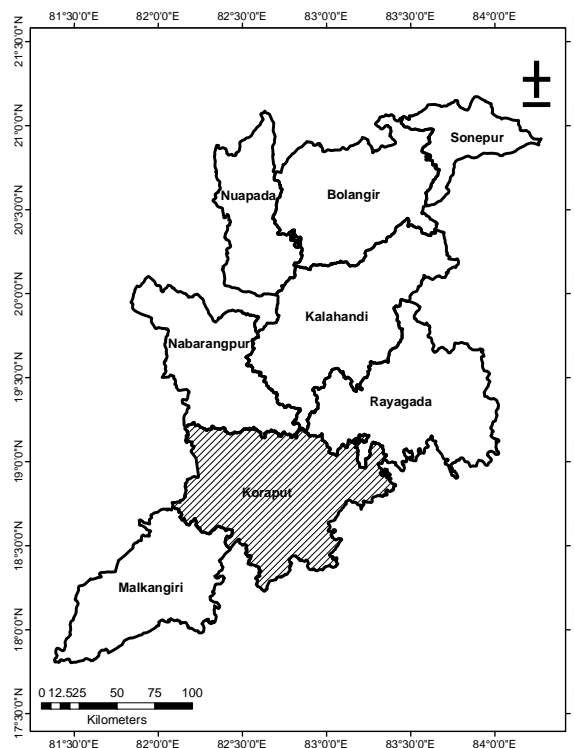
Fig. 2.4 Koraput district in the KBK region

2.5   NUAPADA DISTRICT

The district of Nuapada, a part of undivided Kalahandi district, was divided into two parts i.e. Kalahandi and Nuapada for administrative convenience in 1993. The present Nuapada district comprises of one sub-division (Nuapada), five Tahsils (Nuapada, Khariar, Komna, Boden and Sinapali) and five Blocks (Khariar, Sinapalli, Boden, Nuapada and Komna). The district is located in the western part of Odisha. It extends between 20°00'00" to 21°05'00" North latitude and 82°40'00" to 82°60'00" East longitude. The Nuapada district is surrounded in the north, west and south by Raipur district of Chattishgarh and in the east to Bargarh, Bolangir and Kalahandi districts of Odisha. This district is spread over in an area of 3407.5 km^2. River Jonk flowing in the district seprates it from the state of Chhatisgarh. Patora Dam (Upper Jonk Irrigation Project) is built on Jonk river, in the Nuapada district which is one of the major sources of irrigation. Timber is by far the major forest products and Sal is a major constituent of these products. Other important species of Nuapada forests, are Bija, Asan, Bandhan. There are some other minor forest produces of this region which include Kendu leaf, Broom-grass, Mohua flower. The location map of the Nuapada district has been shown in Figure 2.5.
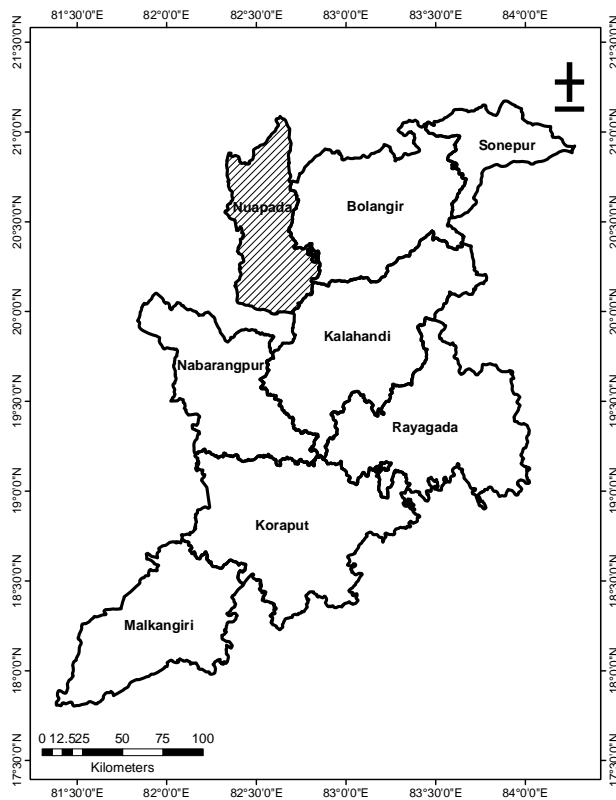
Fig. 2.5 Nuapada district in the KBK region

2.6   SONEPUR DISTRICT

Sonepur (also known as Subarnapur) district is a newly created district which also known as second Varanasi of India. It is bounded on the north by Sambalpur district, on the south and the South–East by Boudh district, on the East by Rairakhol sub–division of Sambalpur district and on the West by Bolangir district. Majaraja Sudhansu Sekher Singh Deo in 1937, who happens to be the last chouhan ruler of Sonepur undertaken number of progressive reforms in the state established a council of Ministers headed by a Chief Minister in March 1943. During his rule, Sonepurr kingdom was merged with the Odisha province on 1st January 1948 and became a Sub–Division under Bolangir district. However from 1st April 1993 Sonepur was given the status of a district Headquarter. The total geographical area of the district is 2285 km^2. As per the administrative is concerned there are 2 sub-divisions, 6 tehsils, 1 municipality, 2 NACs, and 829 inhabited villages. The climate in the region is dry. The general physiography is undulating with river Mahanadi draining through the district. The district receives an average annual rainfall of 1443 mm. The annual average temperature is about 30°C with summer temperature reaching about 45°C and winter temperature about 24°C. The economy in the region is mainly driven by agriculture. Important rivers flowing through the district are Mahanadi, Jeera, Aun, Tel, Suktel, etc. The location map of the Sonepur district has been shown in Figure 2.6.
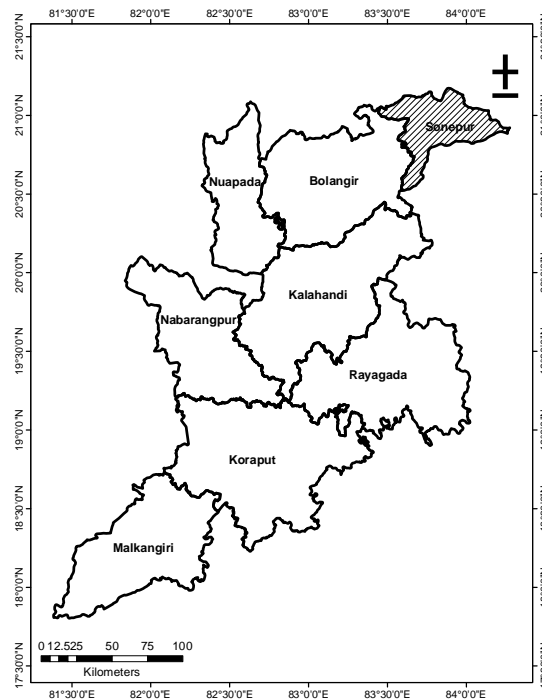
Fig. 2.6 Sonepur district in the KBK region

2.7   MALKANGIRI DISTRICT

Malkangiri district is named after its headquarters town, Malkangiri. The present Malkangiri got its identity as an independent district due to reorganization of districts of Odisha as per a notification on 1st October, 1992 and with effect from 2nd October 1992. The total geographical area of the district stands at 5,791 km^2. It extends between 17°45'00" to 18°40'00" North latitude and 81°10'00" to 82°00'00" East longitude. The district is divided into two distinct physical divisions. The eastern part is covered with steep ghats, platues and valleys, sparsely inhabited by primitive tribes, notable among who are Bondas, Koyas, Porajas and Didayis. The district is moderately literate, with the number of literate males far out numbering the number of literate females. The climate in the district is generally cold during winter and hot in summer with temperature ranging from 13°C to 47°C. The average annual rainfall is about 1700 mm. Relative humidity is generally high, especially in the monsoon and post–monsoon months. River Saberi is flowing in the district. Important water resources project in the district are Balimela Dam, Satiguda Dam, etc. The location map of the Malkangiri district has been shown in Figure 2.7.
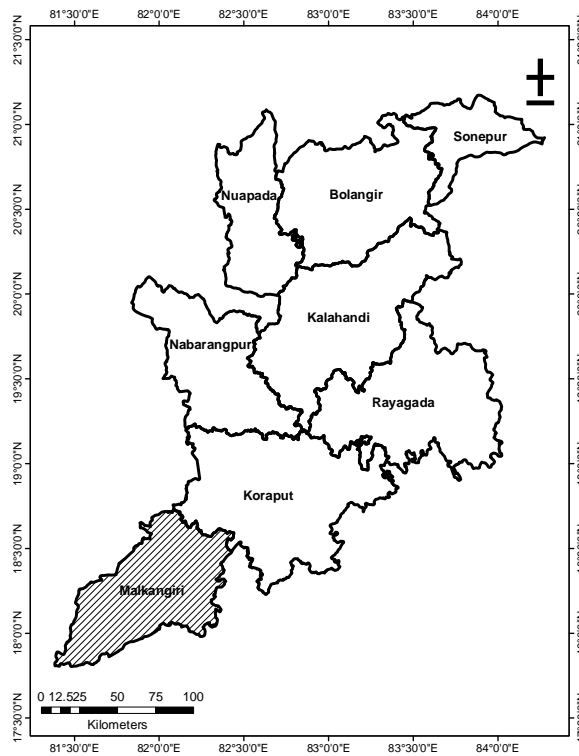
Fig. 2.7 Malkangiri district in the KBK region

2.8   NABARANGPUR DISTRICT

Prior to the creation of Nabarangpur district in the year 1993, it was a sub-division of the erstwhile Koraput district. It is situated at 20°18'00" to 17°30'00" North latitude and 81°16'12" to 84°6'00" East longitude. Its boundary stretches in the north to Raipur and west to Bastar districts of Chhatisgarh. The east side of Nabarangpur touches Kalahandi and Rayagada districts and south to the Koraput districts of Odisha. The river Indravati forms the border between Nabarangpur and Koraput districts. Nabarangpur district covers an area of 5294 km^2 of which 1583.4 km^2 covered by forests. The administrative headquarters of the district is located at Nabarangpur city. At present Nabarangpur district comprises of 1 sub division (Nabarangpur), 10 tehsils and 10 blocks, 169 GPs, 1 NAC and 10 Police Stations. As per 2011 census, the district has 12.19 lakhs population. More than ten types of tribes are living in the district covering half of the population. The district enjoys 1691.57 mm total rainfall annually. More than 90 per cent of its inhabitants depend on farming for their livelihood. Special crops like paddy, maize, sugarcane, groundnut, biri, mung, arhar, ragi, and seasamum are grown in the district. The location map of the Nabarangpur district has been shown in Figure 2.8.
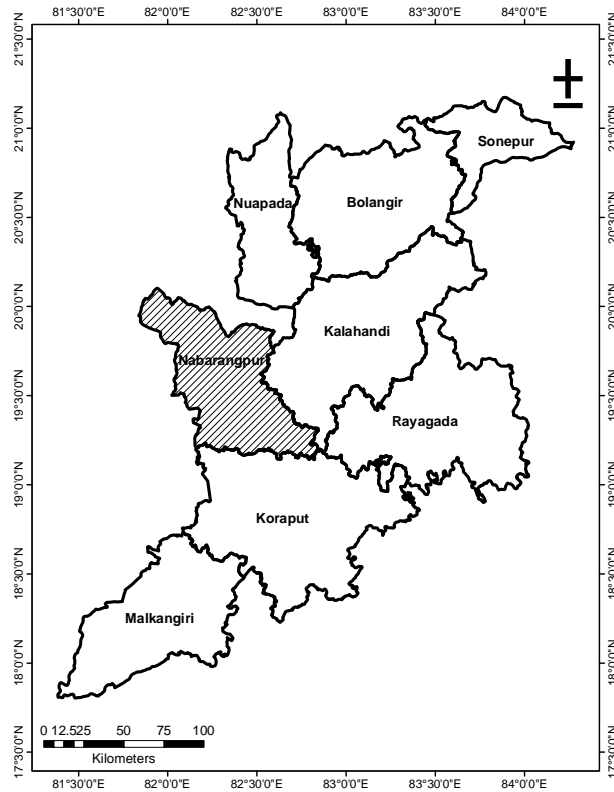
Fig. 2.8 Nabarangpur district in the KBK region

2.9   RAYAGADA DISTRICT

Rayagada is a district of meadows, forests, waterfalls and terraced valleys surrounded by Koraput district in the South-West, Kalahandi district in North-West, Kandhamal in the North-East and Ganjam district in the East. The total geographical area of the district is 7073 km^2 of which 40% of the total area is under forest. The climate in the region is hot and humid. The annual average rainfall is 1455 mm. As per Census 2001, the total population stands at 8.31 lakhs with more than 80% living in the villages. The population of this district consists mainly of tribals. The Kondhas or Kondhs form the majority of population followed by Souras. The district has 2 sub-divisions, 11 tehsils, 1 municipality, 2 NACs, 171 GPs, 15 police stations and 2467 inhabited villages. It is a mineral (viz. bauxite, silicon) rich district. The district generates income mainly through agriculture based activities. Paddy, wheat, ragi, mung, biri, ground nut, potato and maize are the major crops grown in the area. Nagavali and Vamsadhara are the two important rivers flowing in the district. The location map of the Rayagada district has been shown in Figure 2.9.
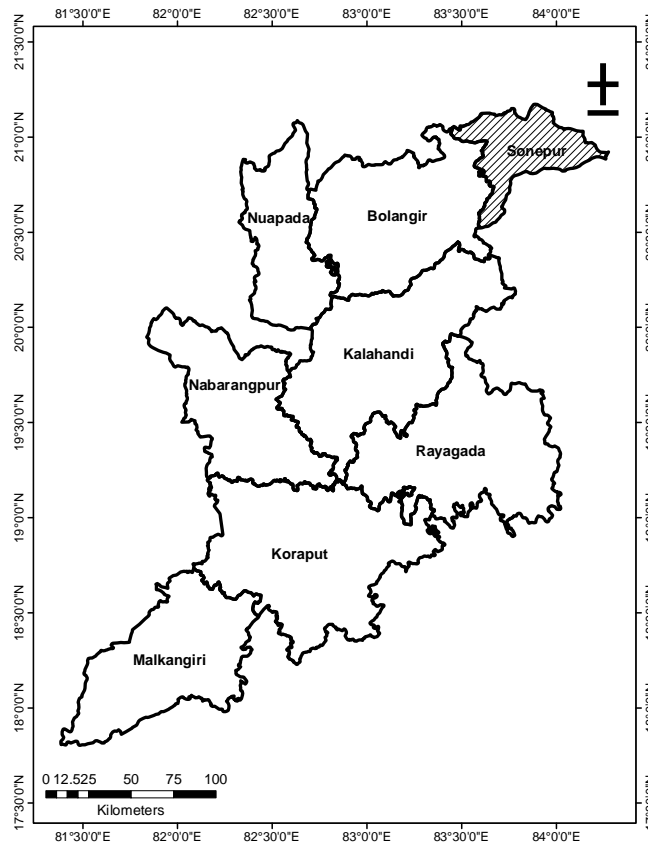
Fig. 2.9 Rayagada district in the KBK region

3

HISTORICAL TREND ANALYSIS

3.1 GENERAL

Over recent decades the scientific community has amassed a wealth of observational data. The last one hundred years have been a period of rapid climate change, partly in response to human influences. Social, economic, industrial, and land use developments all contribute to human impact on our climate, locally, nationally and globally. The changes already observed have had, and continue to have, impacts on many aspects of society, including health, agriculture, water resources and energy demand. In order to make appropriate plans for the future it is vital to investigate observed changes in climate. In doing so, models of past and present climate can be validated and scenarios of future climate put into the context of any change already recorded. In order to plan for adaptation to climate change there is a need to know the degree of change already experienced in specific locations throughout the seasons. Having sufficient information about climatic change in the recent past is necessary to improve the certainty and accuracy of estimates about the future, and the role of this information is particularly important in assessments of regional climate change. Identification of long-term trends in climate change is providing information for decision makers and resource managers that allow them to better anticipate and plan for the potential impacts of climate variability and change.

A temporal trend is the general increase or decrease in observed values over time. The trend describes the long smooth movement of the variable lasting over the span of observations, ignoring the short term fluctuations. The purpose of a trend test is to determine whether the values of a series generally increase or decrease. Trend analysis is used to determine the significance of a trend and to estimate the magnitude of that trend. Trend analysis determines whether the measured values of a variable increase or decrease during a time period.

Detection of trends in long time series of hydrological data is of paramount scientific and practical significance. Water resources systems have been designed and operated based on the assumption of stationary hydrology. If this assumption is incorrect then existing procedures for designing levees, dams, reservoirs, etc. will have to be revised. Without revision there is a danger

that systems are over or under designed and either do not serve their purpose adequately or are overly costly. Studies of change are also of importance because of our need to understand the impact that man is having on the "natural" world.

There are many parametric and non-parametric methods that have been applied for detection of trends. Parametric testing procedures are widely used in classical statistics. In parametric testing, it is necessary to assume an underlying distribution for the data (often the normal distribution), and to make assumptions that data observations are independent of one another. For many hydrological series, these assumptions are not appropriate. Firstly hydrological series rarely have a normal distribution. Secondly, there is often temporal dependence in hydrological series, particularly if the time series interval is short (e.g. today's flow tells us quite a bit about what tomorrow's flow is likely to be). If parametric techniques are to be used, it may be necessary to (a) transform data so that its distribution is nearly normal and (b) restrict analyses to annual series, for which independence assumptions are acceptable, rather than using the more detailed monthly, daily or hourly flow series. In non-parametric and distribution-free methods, fewer assumptions about the data need to be made. With such methods it is not necessary to assume a distribution. However, many of these methods still rely on assumptions of independence.

In the recent research, while finding the trends of different climatic variables, administrative units i.e. districts rather than the common basin approach has been adopted. This is done due to three major reasons. First, the entire KBK region falls within Mahanadi basin in two prominent sub-basins viz. Tel basin draining into the river Mahanadi and Saberi basin draining into the river Godavari (Fig. 3.1). Apart from this, several basins exist mainly in the district of Rayagada which drains into the Bay of Bengal. Secondly, KBK region is an administrative unit recognized by the Govt. of Odisha where KBK specific funding is received from Central as well as State Govt. Third, data pertaining to climatic variables is available district-wise.
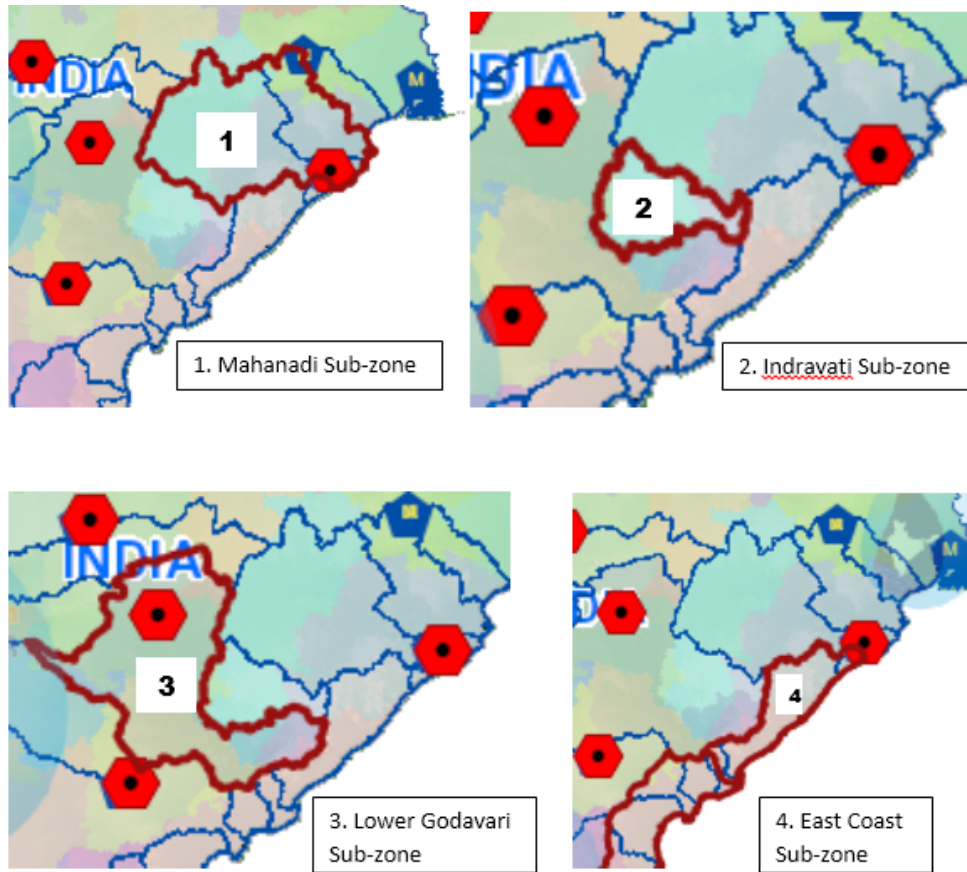
Fig. 3.1 Sub-basins within the Mahanadi basin

The trend analysis has been done with parametric (regression line) and non-parametric viz. Mann-Kendall (MK) test in 8 different districts *viz. Bolangir, Kalahandi, Koraput, Malkangiri, Nabarangpur, Nuapada, Rayagada and Sonepur*. Seasonal trend analysis for all the three factors has also been carried out for the period 1901 to 2010 (110 years).

3.2 DATA USED

In the present study, monthly rainfall data of 110 years (1901-2010), temperature (minimum, maximum, and mean) data of 102 years (1901-2002), and potential evapotranspiration data of 102 years (1901-2002) has been considered for trend analysis in the study across eight KBK districts (source: www.indiawaterportal.org). Data was analysed on monthly (Jan-Dec), seasonal (pre-monsoon, monsoon, post-monsoon, winter) and annual basis.

3.3 APPROACH AND METHODOLOGY OF FINDING TRENDS

3.3.1 Trend analysis using parametric method

3.3.1.1 Outlier test

Outliers are data points that depart significantly from the trend of the training data. These data when used during analysis can considerably affect the magnitude of statistical parameters computed from the data, especially for small sample. As per U.S. Water Resources Council, 1981, when the skewness of a series lie between ±0.4, test for both high and low outliers should be performed using the following frequency equation before eliminating the outliers:

$$Y_H = \bar{y} + K_n S_y \quad \text{(High outliers)} \tag{3.1}$$

$$Y_L = \bar{y} - K_n S_y \quad \text{(Low outliers)} \tag{3.2}$$

Where Y_H is the high outlier threshold in log unit, $\bar{y}$ is the mean of the sample data in log unit, K_n is the constant that is determined from the sample size n, S_y is the standard deviation of the sample size in log unit and Y_L is the low outlier threshold in log unit. For a sample size of 40 and 32, K_n value is taken as 2.682 and 2.591 respectively (Chow et al., 1988).

3.3.1.2 Linear Regression Method

Trends in time-series data were analyzed using simple linear regression. Hydrologic data were reduced to a single value for each year of the selected time period. The annual series of values then was related to time by an equation of the form:

$$Y = mX + C \tag{3.3}$$

Where,

Y = a hydrologic variable, such as rainfall; X = time in years; and
C = intercept.

The slope, m, indicates the average rate of change in the hydrologic characteristic during each year of the time period. If the slope is significantly different from zero, the trend in the hydrologic variable is equal to the magnitude of the slope and the direction of the trend is defined by the sign of the slope: increasing if the sign is positive and decreasing if the sign is

negative. If the slope is not significantly different from zero, there is no trend in the hydrologic variable. One advantage of this method of trend analysis is that it is easy to apply to a large number of sites. A disadvantage is that it can fail to detect trends that are nonlinear but still monotonic (generally in one direction).

3.3.1.3 AR/ MA/ ARMA Method

Three basic models exist, AR (autoregressive), MA (moving average) and a combined ARMA. When regular differencing is applied together with AR and MA, they are referred to as ARIMA, with the I indicating "integrated" and referencing the differencing procedure. AutoRegressive (AR) models were first introduced by Yule in 1926. They were consequently supplemented by Slutsky who in 1937 presented Moving Average (MA) schemes. It was Wold (1938), however, who combined both AR and MA schemes and showed that ARMA processes can be used to model all stationary time.

Box-Jenkins Forecasting Method is also utilized for forecasting based on statistical concepts and principles and are able to model a wide spectrum of time series behavior. In statistics, a moving average, also called running average, is used to analyze a set of data by creating a series of averages of different subsets of the full data set. Given a series of numbers and a fixed subset size, the moving average can be obtained by first taking the average of the first subset. The fixed subset size is then shifted forward, creating a new subset of numbers, which is averaged. This process is repeated over the entire data series. The plot line connecting all the (fixed) averages is the moving average. Thus, a moving average is not a single number, but it is a set of numbers, each of which is the average of the corresponding subset of a larger set of data points (Wikipedia, 2013).

3.3.2 Trend analysis using non-parametric method

3.3.2.1 Autocorrelation test

Presence of positive or negative autocorrelation affects the trend in a series (Yue et al., 2002; Yue et al., 2003). The autocorrelation (also known as serial correlation coefficients) test was performed to check the randomness and periodicity, if any, in the time series of all data (Madarres and Silva, 2007). If randomness is found, pre-whitening method was applied for

removing the effect of correlation on MK Test (Storch, 1993; Cunderlik and Burn, 2002; Cunderlik and Burn, 2004). MK test was then applied on the pre-whitened series (Mann, 1945; Kendall, 1975; Xu et al., 2003; Bayazit and Onoz, 2007) together with the Theil-Sen's estimator (Theil, 1950; Sen, 1968) for obtaining the monotonic trend and magnitude of the three climatic variables viz. rainfall, temperature, and potential evapotranspiration.

The autocorrelation coefficient r_k of a discrete time series for lag-k is estimated as follows:

$$r_k = \frac{\sum_{k=1}^{n-k}(X_t - \overline{X_t})\,(X_{t+k} - \overline{X_{t+k}})}{\left[\sum_{k=1}^{n-k}(X_t - \overline{X_t})^2\,(X_{t+k} - \overline{X_{t+k}})^2\right]^{0.5}} \tag{3.4}$$

Where, r_k is the lag-k serial correlation coefficient of the series. The hypothesis of serial independence is then tested by the lag-1 autocorrelation coefficient as $H_0 : r_1 = 0$ against $H_1 : |r_1| > 0$ using the test of significance of serial correlation (Yevjevich, 1971) following Rai et al., 2010).

$$(r_k)_{t_g} = \frac{-1 \pm t_g(n - k - 1)^{1/2}}{n - k} \tag{3.5}$$

Where, $(r_k)_{t_g}$ is the normally distributed value of r_k, t_g is the normally distributed statistic at g level of significance. The value of t_g are 1.645, 1.965 and 2.326 at significance level of 0.10, 0.05 and 0.01 respectively. If $|r_k| \geq (r_k)_{t_g}$, the null hypothesis about serial independence is rejected at the significance level α (here 0.05). For the non-normal series, MK test is appropriate choice for the trend analysis (Yue and Pilon, 2004; Basistha et al., 2008). Therefore, the MK test has been used wherever the autocorrelation is not significant at 5% significance level.

3.3.2.2 Mann-Kendall Test

One of the widely used non-parametric tests for detecting a trend in hydro-climatic time series is the Mann Kendall (MK) test. A statistical method, Mann Kendall Test is used in this study to analyze the spatial variation and temporal trends of the hydro-climatic series. Mann Kendall test which was originally devised by Mann (1945) as a non-parametric test for detecting trends and the distribution of the test statistic derived by Kendall (1975) is used to test the non-linear trend as well as turning point. This Mann Kendall test searches for a trend in a time series without specifying whether the trend is linear or nonlinear. The trend test is applied to a time series x_i

ranked from i = 1,2……….n-1, and x_j ranked from j = i+1,2,……….n. Each data point x_i is used as a reference point and is compared with all other data points x_j such that, the MK statistic is

$$Z_c = \begin{cases} \dfrac{S-1}{\sqrt{Var(S)}} & if, S > 0 \\ 0 & if, S = 0 \\ \dfrac{S+1}{\sqrt{Var(S)}} & if, S < 0 \end{cases}$$

(3.6)

Where,

$$S = \sum_{i=1}^{n-1} \sum_{j=i+1}^{n} sgn(x_j - x_i)$$

(3.7)

Where,

$$sgn(x_j - x_i) = \begin{cases} 1.......if (x_j - x_i) > 0 \\ 0.......if (x_j - x_i) = 0 \\ -1.......if (x_j - x_i) < 0 \end{cases}$$

(3.8)

Here x_j and x_i show the data values which are in sequence with n data, sgn (θ) is equivalent to 1, 0 and -1 in case θ is more than, equal to or less than 0 respectively. If Z_c found to be more than $Z_{\alpha/2}$ then the trend is believed to be significant where α is the level of significance (Yue and Hashino, 2003). While trend magnitude can be determined with little ambiguity, the corresponding statistical significance, sometimes cited to bolster scitific argument, is less certain (Cohn and Lins, 2005).

The trend magnitude was calculated by Theil-Sen's estimator (Theil, 1950; Sen, 1968).

$$\beta = median\left(X_i - X_j / i - j\right), \qquad \forall j < i$$

(3.9)

Where $1<j<i<n$ and β estimator give the median of the entire data set of all combination of pairs and gives resistance to the effect of extreme values.

3.3.2.3 Sen's Slope Estimator Test

In cases where a linear trend is present in a time series, then the true slope can be estimated by using a simple non-parametric procedure developed by Sen (1968). The slope estimate of N pairs of data are first computed by

$$Q_i = \frac{xj - xk}{j - k} \quad \text{for i=1,…………N} \tag{3.10}$$

Where x_j and x_k are data values at times j and k (j>k) respectively. The meridian of these N values of Q_i is Sen's estimator of slope. If N is odd, then Sen's estimator is computed by $Q_{med} = Q_{(N+1)/2}$ and if N is even, then Sen's estimator is computed by $Q_{med}=[Q_{N/2}+Q_{(N+2)/2}]/2$. Finally Q_{med} is tested by a two sided test at 100 (1-α)% confidence interval and true slope may be obtained by the non-parametric test.

3.3.2.4 Mann-Whitney-Pettitt method (MWP)

The time series {X1, X2…, Xn} with length *n* is taken. *t* was taken as the time of the most expected change point. Two samples {X1, X2, …, Xt} and {Xt+1, Xt+2, …, Xn} then can be obtained by dividing the time series at *t* time. The *Ut* index was obtained in the following way:

$$U_t = \sum_{i=1}^{t} \sum_{j=t+1}^{n} \mathrm{sgn}(X_i - X_j) \tag{3.11}$$

Where,

$$\mathrm{sgn}(x_j - x_i) = \begin{cases} 1.......if(x_j - x_i) > 0 \\ 0.......if(x_j - x_i) = 0 \\ -1.......if(x_j - x_i) < 0 \end{cases} \tag{3.12}$$

Plotting of *Ut* value against *t* in a time series will results in a continuously increasing value of |Ut| with no change point. Yet, if there is a change point (even a local change point), then |Ut| will increase up to the change point level and then will begin to decrease. The major significant change point *t* gives the point where value of |Ut | remains highest:

$$K_T = \max_{1 \leq t \leq T} |U_\tau| \tag{3.13}$$

The approximated significant probability *p(t)* for a change point is represented as:

$$p = 1 - \exp\left[\frac{-6K_T^2}{n^3 + n^2}\right] \tag{3.14}$$

When probability $p(t)$ surpasses $(1 - \alpha)$, then the change point becomes significant statistically at time t with the significance level of α (Pettitt, 1979).

3.3.2.5 Homogeneity test

Homogeneity test was done on the series with Pettitt's test and Standard Normal Homogeneity Test (SNHT) at 5% significance level (Alexandersson, 1986; Alexandersson and Moberg, 1997). The critical value of T_0 of SNHT for 110 samples of rainfall is 9.255 at 95% significant level (Khaliq and Ouarda, 2007). The series is homogeneous if T_0 is less than critical values. Other tests to detect change in a time series are Median change point, Rank-sum test, CUSUM test, the Kruskal-Wallis test, Students' t test, Wilcoxon-Mann-Whitney test, etc. (Kundzewicz and Robson, 2004).

3.4 RESULTS AND DISCUSSION

3.4.1 Rainfall trend

The study investigates monthly, annual and seasonal trend of mean rainfall of KBK region for the period 1901 to 2010 (110 years). Seasonal analysis has been carried out for Pre-monsoon (Mar-May), Monsoon (Jun-Sept), Post-monsoon (Oct-Nov), Winter (Dec-Feb). The basic statistics of the annual series of rainfall is presented in Table 3.1. Annual average rainfall in the region varies from 1139.26 mm (Malkangiri) to 1429.31 mm (Nabarangpur) for the period 1901 to 2010. The standard deviation during the same period varies from 199.52 mm to 295.61 mm. The skewness in the annual average rainfall varied from 0.51 to 2.40, with an average positive skewness of 1.07 indicating a skewed asymmetric curve. The dispersion in the annual rainfall series is expressed through coefficient of variation varying between 15% (Bolangir) to 23% (Koraput). The average variation is 18% in the entire region. Figure 3.2 shows the temporal variation of annual rainfall with linear trend line for the eight KBK districts during the period 1901 to 2010 without considering the outliers. As seen from Figure 3.2, rainfall in the districts of Bolangir and Nuapada show a decreasing trend, Koraput and Malkangiri districts an increasing trend and others as no clear trend.

The rainfall series for all the eight districts are tested for presence of outliers. The details of the existence of outliers in the rainfall series for the district are presented in Table 3.2. After removing the outliers existing in the districts of Koraput, Malkangiri, Sonepur, and whole KBK region, the linear regression was once again fitted. The linear trends before/ after removal of the outliers are presented in Figures 3.3 to 3.10 for the districts where outliers exist (Table 3.2). The slope of the linear regression trend line before/ after removal of the outliers is presented in Table 3.3.

Before applying MK test and Sen's Slope Estimate, all the series are tested for serial correlation using Lag-1 auto-correlation at 5% significance level (Table 3.4). Serially correlated series are made independent by pre-whitening to remove effects due to serial correlation. The results of MK test (z-statistics) are presented in Table 3.5. The Sen's slope estimate is presented in Table 3.6. The test results indicate two districts with significant trend (Malkangiri with increasing and Nuapada with decreasing) in the annual rainfall (Fig.3.11). Fig.3.12 presents the interpolated Z value distributed across the KBK region by Kriging method.

The magnitude of the decreasing trends in the annual rainfall varies from 0.204 mm/ year (Kalahandi) to 1.419 mm/ year (Nuapada). The analysis also indicates a non-significant increasing trends in the annual rainfall in the districts of Koraput (+0.935 mm/ year) and Rayagada (+0.382 mm/ year). The annual rainfall series for the districts of Bolangir, Nabarangpur and Sonepur indicates non-significant decreasing trend. Seasonal analysis of trend showed non-significant increasing as well as decreasing trend in pre-monsoon, monsoon and post monsoon rainfall in the study area. Koraput, Nabarangpur and Rayagada districts showed non-significant increasing trends and Bolangir, Kalahandi, Malkangiri, Nuapada and Sonepur districts showed non-significant decreasing trends in the summer rainfall (pre-monsoon). However, in case of seasonal monsoon rainfall, five districts (Bolangir, Kalahandi, Nuapada, Rayagada and Sonepur) showed non-significant decreasing trend and the remaining (Koraput, Malkangiri and Nabarangpur) showed increasing trends. Winter rainfall in the entire region showed decreasing rainfall trend which will considerably affect the rabi crops grown. When closely investigated the rainfall trend with respect to different districts, it has been found that districts with significant forest coverage (Koraput, Malkangiri) are receiving more rainfall in comparison to other districts such as Kalahandi, Nuapada, Sonepur with less forest coverage.

Although several other factors govern the rainfall phenomenon in a region, this aspects requires further investigation.

Homogeneity test has been performed to find the shift year when a considerable change in the climate was witnessed in the region. Two widely used tests (Pettitt and SNHT) are employed to detect the change year for different series of rainfall and temperature. Table 3.7 presents change year for the annual series for different districts. Pettit test indicate shifting in annual rainfall mainly prior to 1961 and beyond, whereas SNHT test indicate to last decade (2005) as change year. Finally, the effect of outliers during finding trend of series using the parametric linear regression method is compared with and without outliers with respect to the trend detection using MK test is provided in Table 3.8. As expected, when the outliers are removed, trend for the rainfall series corresponding to the entire KBK region was reversed showing a decreasing trend unlike the increasing trend earlier shown without removal of outliers. When comparison is made on the trend analysis performed using parametric linear regression method and nonparametric MK test, it was revealed that except for the district of Nabarangpur, both methods indicate same trend (Table 3.8).

Table 3.1: Basic statistics of seasonal and annual mean rainfall series for KBK region

Rainfall series (mm)	Mean	Max	Min	Standard deviation	Coefficient of variation	Skewness	Kurtosis
Annual	1296.57	2123.48	928.28	205.49	0.16	0.88	1.80
Pre-monsoon	97.47	310.68	19.81	47.91	0.49	1.37	3.50
Monsoon	1063.36	1872.91	643.94	187.67	0.18	0.99	2.79
Post-monsoon	114.00	283.76	7.08	57.62	0.51	0.47	0.16
Winter	21.73	76.68	0.00	17.18	0.79	0.80	-0.04
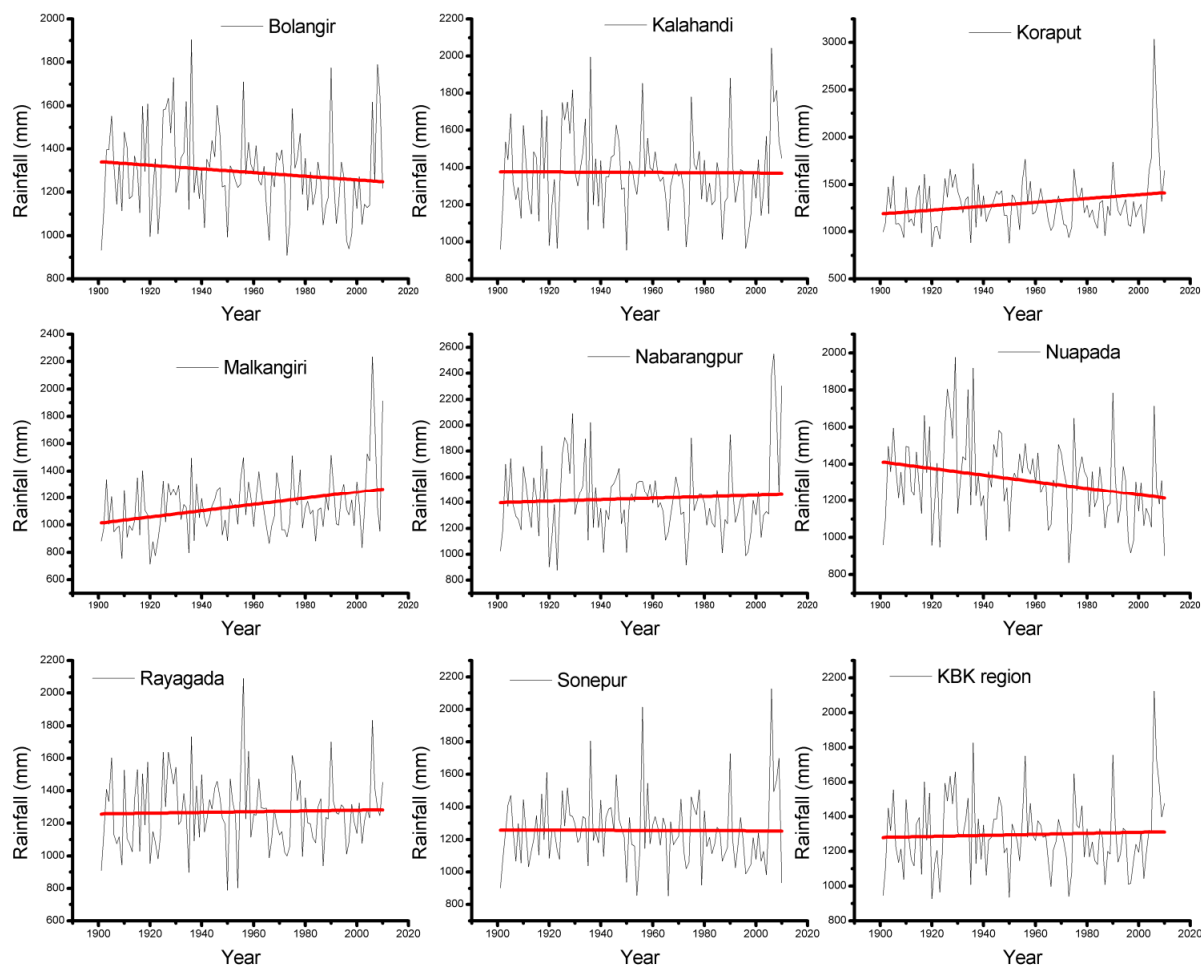
Fig. 3.2 Temporal variation of annual rainfall for the KBK region during 1901 to 2010

(Thick red lines represent linear trend lines)

Table 3.2: Presence of outliers in the rainfall series

Districts	Test of outliers				
	Max.	Min.	High	Low	Presence of outliers
Bolangir	1904.33	908.65	2030.81	806.24	No
Kalahandi	2042.60	953.57	2233.62	821.65	No
Koraput	**3035.60**	837.80	2331.59	694.61	Yes
Malkangiri	**2236.60**	713.46	1980.18	632.22	Yes
Nabarangpur	2546.90	875.42	2550.39	770.23	No
Nuapada	2142.45	782.55	1975.11	864.70	No
Rayagada	2110.83	741.45	2089.73	787.55	No
Sonepur	**2031.05**	755.48	2125.70	854.48	Yes
KBK region	**2047.42**	801.78	2123.48	928.28	Yes
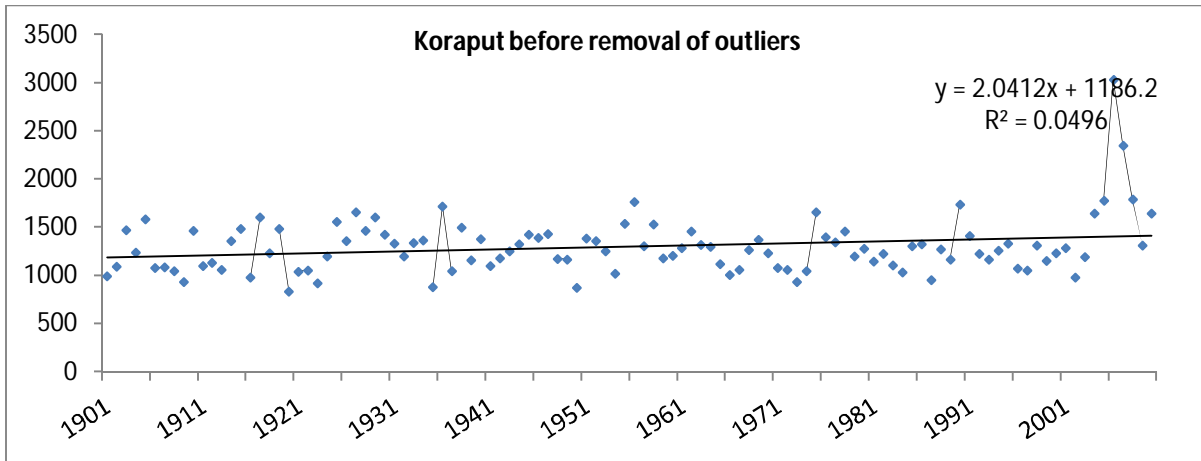
Fig. 3.3 Linear trend lines before removal of outliers in Koraput district
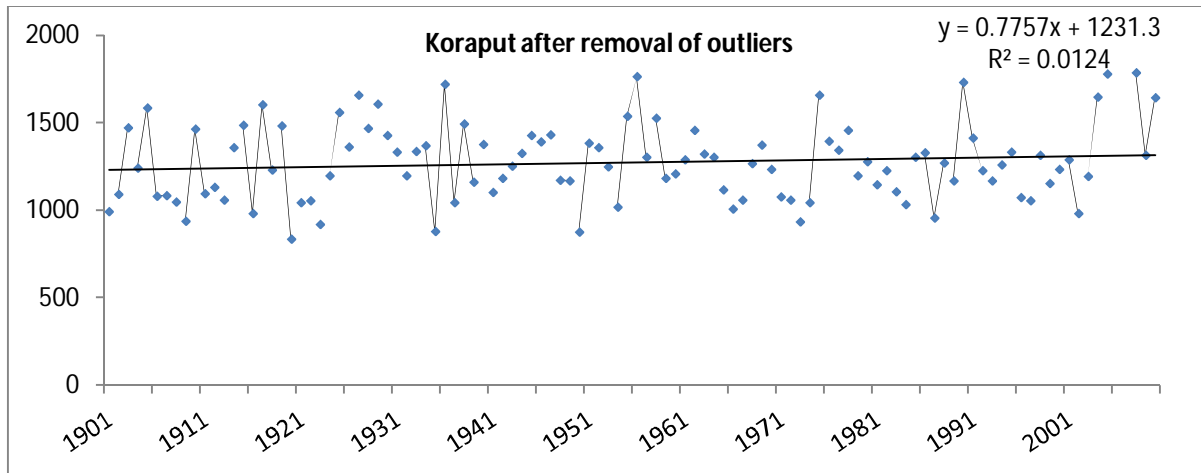
Fig. 3.4 Linear trend lines after removal of outliers in Koraput district
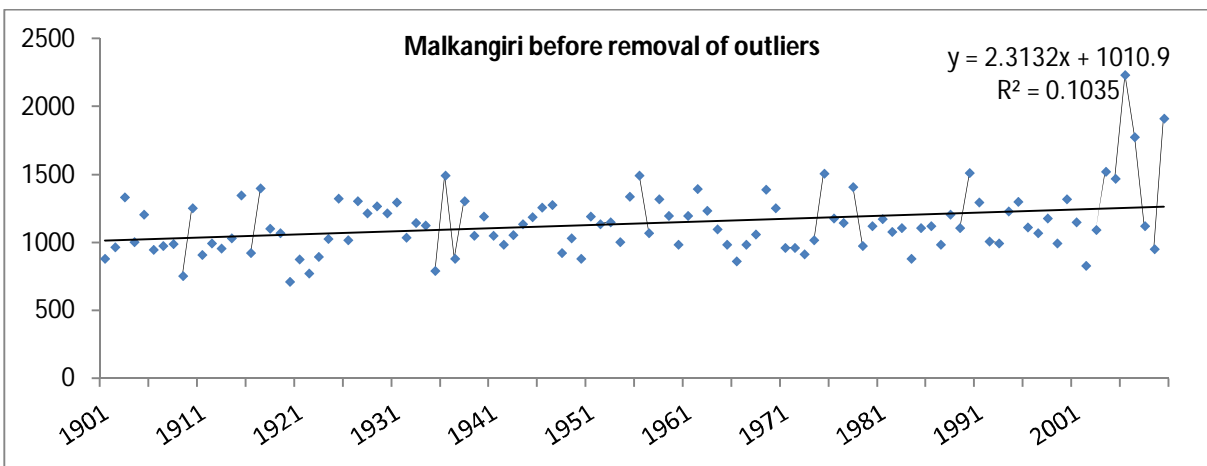
Fig. 3.5 Linear trend lines before removal of outliers in Malkangiri district
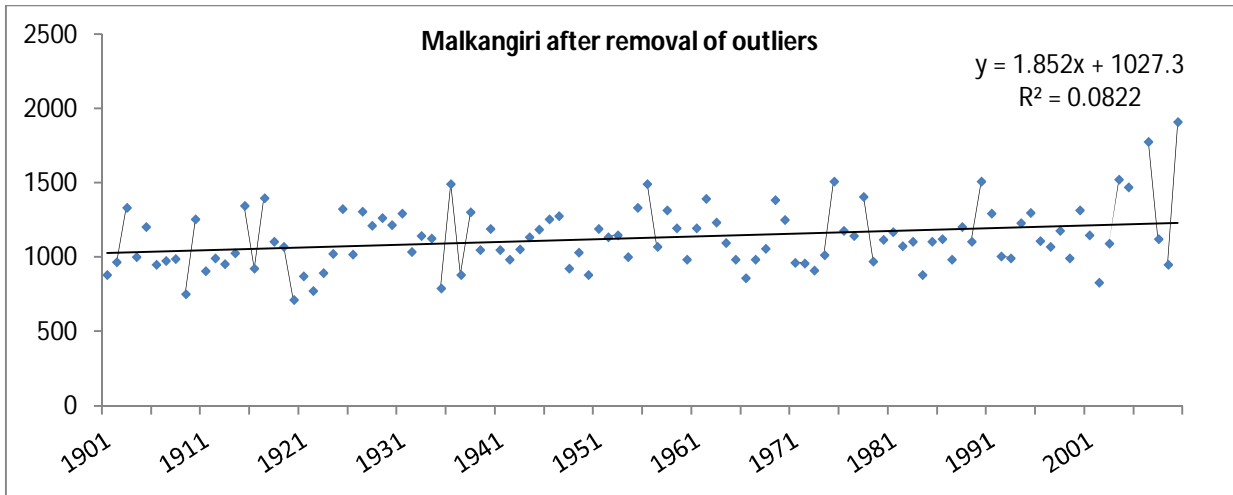
Fig. 3.6 Linear trend lines after removal of outliers in Malkangiri district
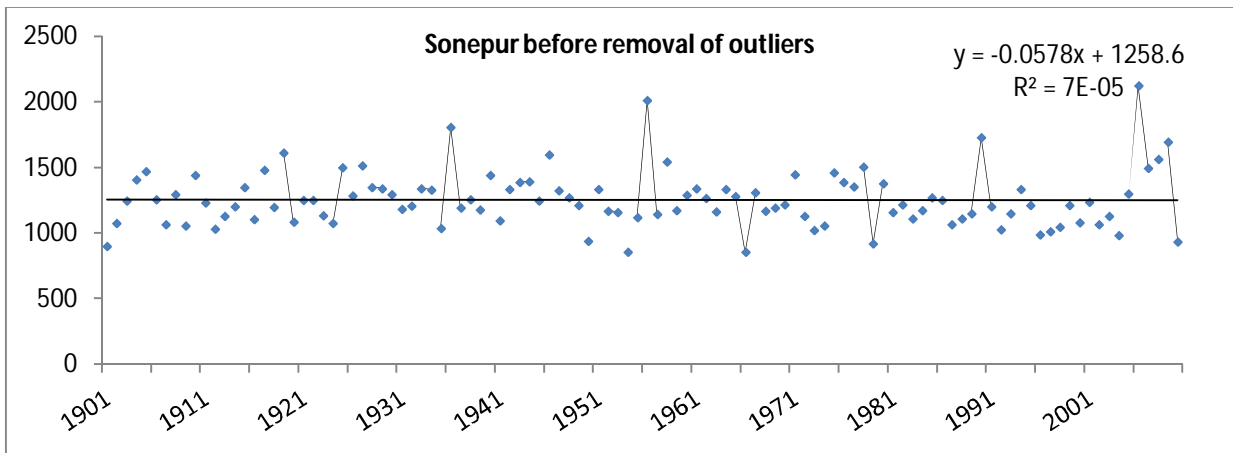
Fig. 3.7 Linear trend lines before removal of outliers in Sonepur district
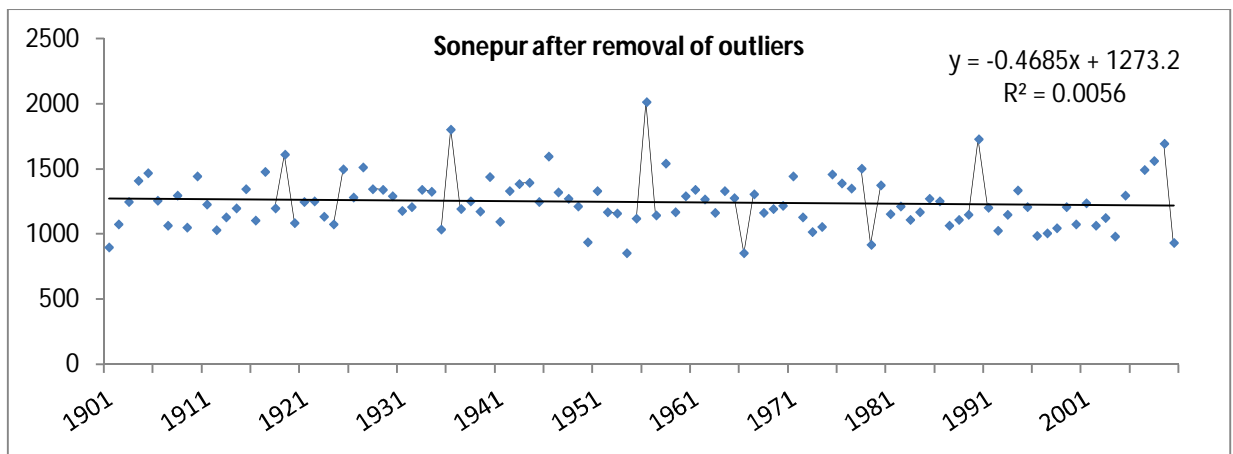
Fig. 3.8 Linear trend lines after removal of outliers in Sonepur district
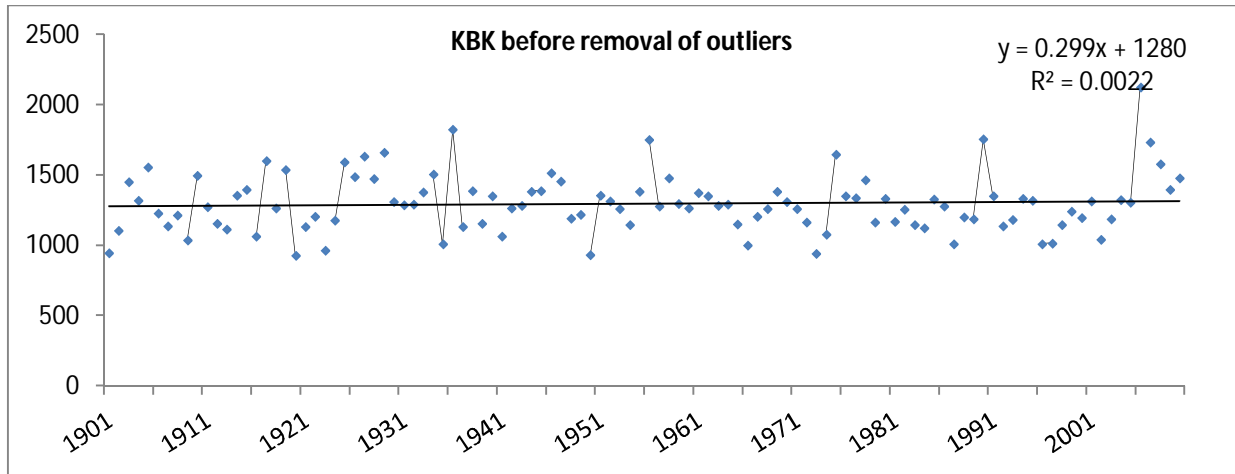
Fig. 3.9 Linear trend lines before removal of outliers in Whole KBK region
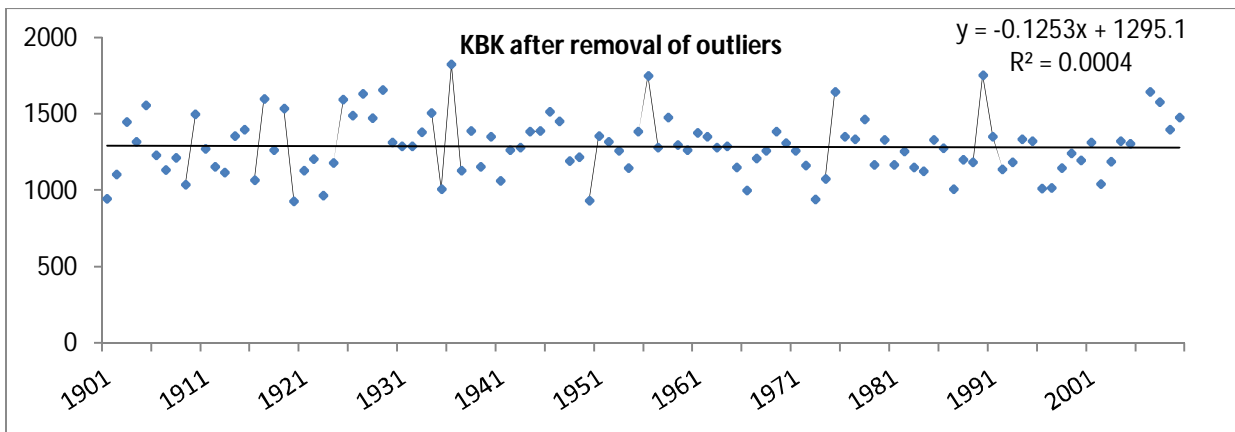
Fig. 3.10 Linear trend lines after removal of outliers in whole KBK region

Table 3.3: Slope of the linear regression trend line before/ after removal of the outliers

Districts	Slope of the linear regression trend line for the rainfall series		
	Outliers	Slope before removal of outliers	Slope after removal of outliers
Bolangir	No	-0.842	NA
Kalahandi	No	-0.066	NA
Koraput	Yes	2.041	0.775
Malkangiri	Yes	2.313	1.852
Nabarangpur	No	0.580	NA
Nuapada	No	-1.806	NA
Rayagada	No	0.229	NA
Sonepur	Yes	-0.057	-0.468
KBK region	Yes	0.055	-0.125

Table 3.4: Lag-1 serial autocorrelation

Districts	Rainfall				
	Annual	Pre-monsoon	Monsoon	Post-monsoon	Winter
Bolangir	0.129	-0.009	0.203	-0.038	-0.139
Kalahandi	0.118	0.004	0.231	-0.038	-0.060
Koraput	0.414	-0.115	0.486	0.020	0.030
Malkangiri	0.234	-0.061	0.226	0.117	-0.040
Nabarangpur	0.286	-0.061	0.401	-0.052	-0.006
Nuapada	0.161	-0.006	0.211	-0.041	-0.054
Rayagada	0.010	-0.014	-0.016	0.052	-0.042
Sonepur	0.010	0.062	0.071	0.027	-0.186
KBK region	0.183	-0.031	0.257	0.006	-0.069

Table 3.5: Mann-Kendall test statistics (Z value)

Districts	Rainfall				
	Annual	Pre-monsoon	Monsoon	Post-monsoon	Winter
Bolangir	-1.643	-0.305	-1.069	0.041	-0.625
Kalahandi	-0.279	-0.579	-0.015	-0.036	-1.348
Koraput	0.935	0.243	0.625	1.183	**-2.203**
Malkangiri	**2.041**	-0.641	1.715	1.860	-1.379
Nabarangpur	-0.398	0.858	0.031	0.439	-1.173
Nuapada	**-2.221**	-0.682	-1.555	-0.036	-0.863
Rayagada	0.382	1.137	-0.062	0.403	-1.193
Sonepur	-1.028	-0.517	-1.038	-0.212	-1.111
KBK region	0.062	-0.155	-0.098	0.465	-1.250

Table 3.6: Sen's slope (β-value)

Districts	Rainfall				
	Annual	Pre-monsoon	Monsoon	Post-monsoon	Winter
Bolangir	-0.852	-0.034	-0.661	0.003	-0.039
Kalahandi	-0.204	-0.099	-0.013	-0.007	-0.062
Koraput	0.673	0.038	0.428	0.278	-0.098
Malkangiri	1.312	-0.081	0.851	0.526	-0.046
Nabarangpur	-0.310	0.142	0.055	0.084	-0.048
Nuapada	-1.419	-0.077	-0.960	-0.006	-0.034
Rayagada	0.259	0.225	-0.027	0.098	-0.051
Sonepur	-0.599	-0.080	-0.538	-0.020	-0.069
KBK region	0.055	-0.026	-0.053	0.098	-0.057

Table 3.7: Homogeneity test

Districts	Pettitt's test				SNHT test			
	K	t	P value	Homogeneity	$T_0^{\#}$	t	P value	Homogeneity
Bolangir	815.0	1961	0.080	H_0 cannot be rejected.	5.744	2005	0.287	H_0 cannot be rejected.
Kalahandi	472.0	1962	0.610	H_0 cannot be rejected.	12.204	2005	0.014	H_a is true.
Koraput	642.0	1924	0.247	H_0 cannot be rejected.	35.723	2003	0.0002	H_a is true.
Malkangiri	920.0	1924	0.032	H_a is true.	26.635	2003	0.0003	H_a is true.
Nabarangpur	539.0	1961	0.449	H_0 cannot be rejected.	31.575	2005	0.0001	H_a is true.
Nuapada	1061.0	1961	0.008	H_a is true.	9.512	1961	0.047	H_a is true.
Rayagada	540.0	1924	0.450	H_0 cannot be rejected.	3.464	2005	0.642	H_0 cannot be rejected.
Sonepur	556.0	1978	0.417	H_0 cannot be rejected.	10.837	2005	0.066	H_0 cannot be rejected.
KBK region	471.0	2003	0.624	H_0 cannot be rejected.	16.553	2005	0.004	H_a is true.

H_0=null hypothesis i.e. series showing homogeneity; H_a=alternate hypothesis

Fig. 3.11 Map showing increasing or decreasing trend for the KBK districts
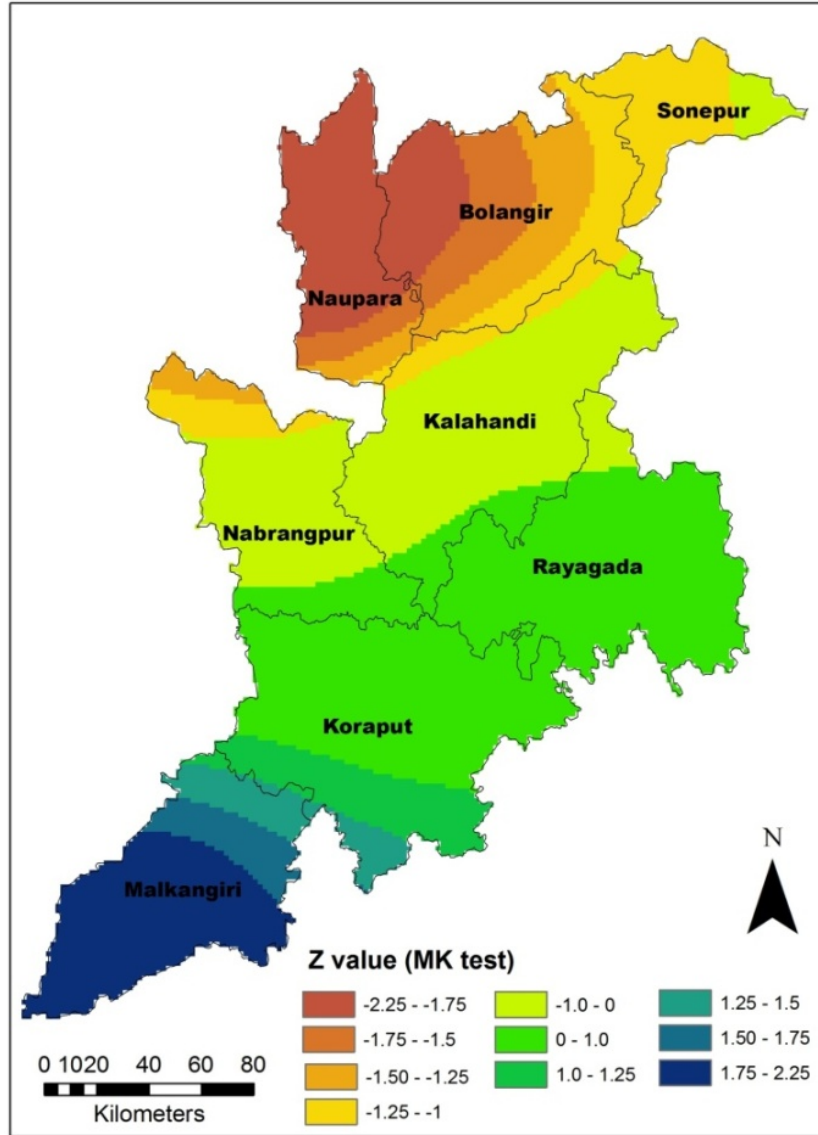
Fig. 3.12 Z value (MK test) for the annual rainfall (110 years) of the KBK districts

Table 3.8: Effect of outliers in the rainfall trend

District	With outliers	Presence of outliers	Without outliers	MK test
Bolangir	-	x	-	-
Kalahandi	+/-	x	+/-	-
Koraput	+	√	+	+
Malkangiri	+	√	+	+
Nabarangpur	+	x	+	-
Nuapada	-	x	-	-
Rayagada	+	x	+	+
Sonepur	+/-	√	+/-	-
KBK	+	√	-	+

3.4.2 Temperature trend

3.4.2.1 Mean temperature

Temperature is one of the important variables affecting the climate in a region. Therefore, in the study monthly, annual and seasonal trend of mean temperature of KBK region for the period 1901 to 2002 (102 years) have been investigated. Seasonal analysis has also been carried out for the annual mean temperature. The basic statistics of the annual mean temperature series for the KBK region is presented in Table 3.9. Further, trend lines using simple linear regression method have been detected for the entire KBK region as well as individual districts as shown in Figures 3.13 to 3.21. The monthly, seasonal and annual series are tested for existence of any outliers. The outlier test indicates absence of outliers as presented in Table 3.10. Z statistics (MK test) and Sen's slope is presented in Table 3.11 and Table 3.12 respectively. Both regression method and MK test indicate a significant increasing temperature trend in the mean annual series. The districts like Kalahandi, Koraput, Malkangiri, Nabarangpur, and Nuapada, the increasing temperature trend is significant at alpha = 0.001 level of significance. The seasonal mean temperature is also showing an increasing trend in the region. The northern part of the KBK region covering districts of Sonepur and Bolangir, showing increasing trend at alpha = 0.01 level of significance. The spatial distribution of the Z value (Kriging interpolation) is shown in Fig. 3.22.

Table 3.9: Basic statistics of annual mean temperature series for KBK region

Annual mean temperature series (^{o}C)	Mean	Max	Min	Standard deviation	Coefficient of variation	Skewness	Kurtosis
Jan-Dec	25.43	26.25	24.41	0.37	0.01	-0.12	-0.31
Mar-May	29.13	30.65	27.48	0.65	0.02	-0.20	-0.10
Jun-Sep	26.93	27.96	26.05	0.43	0.02	0.19	-0.66
Oct-Nov	23.67	25.25	22.13	0.70	0.03	0.19	-0.44
Dec-Feb	20.92	22.27	19.66	0.57	0.03	0.09	-0.58
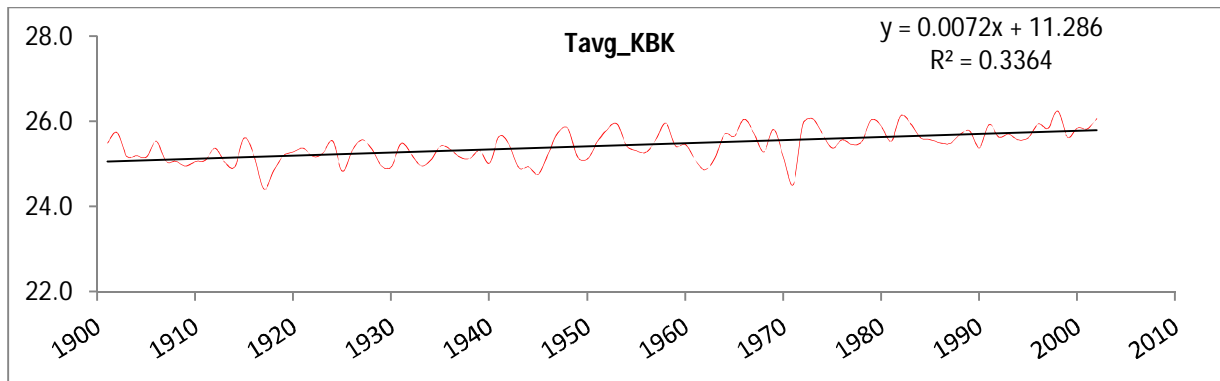
Fig. 3.13 Linear trend lines for the annual mean temperature (102 years) in whole KBK region
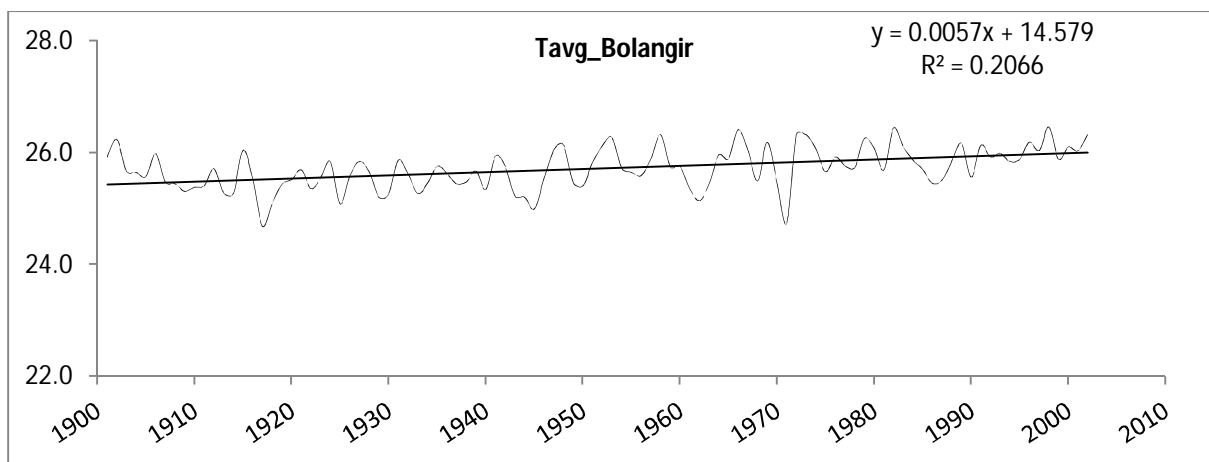
Fig. 3.14 Linear trend lines for the annual mean temperature (102 years) in Bolangir district
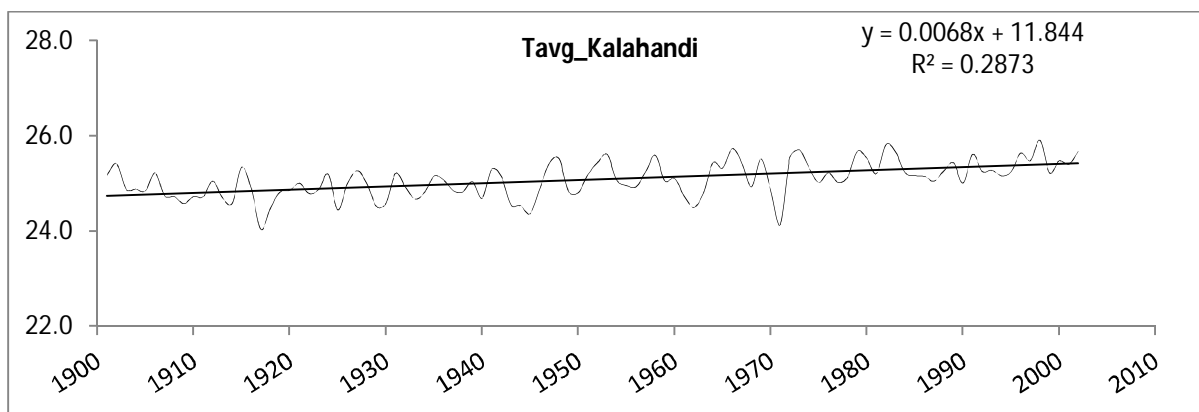
Fig. 3.15 Linear trend lines for the annual mean temperature (102 years) in Kalahandi district
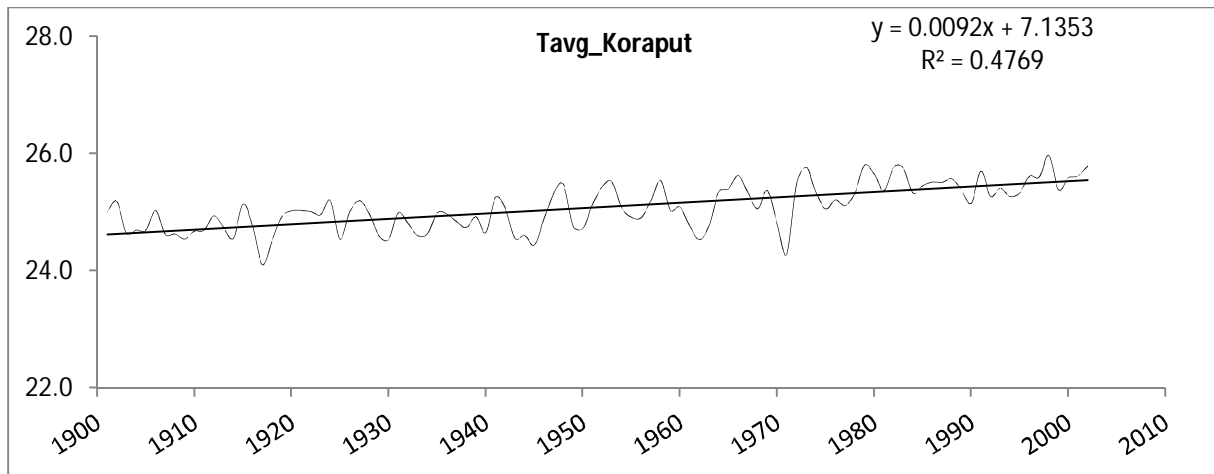
Fig. 3.16 Linear trend lines for the annual mean temperature (102 years) in Koraput district
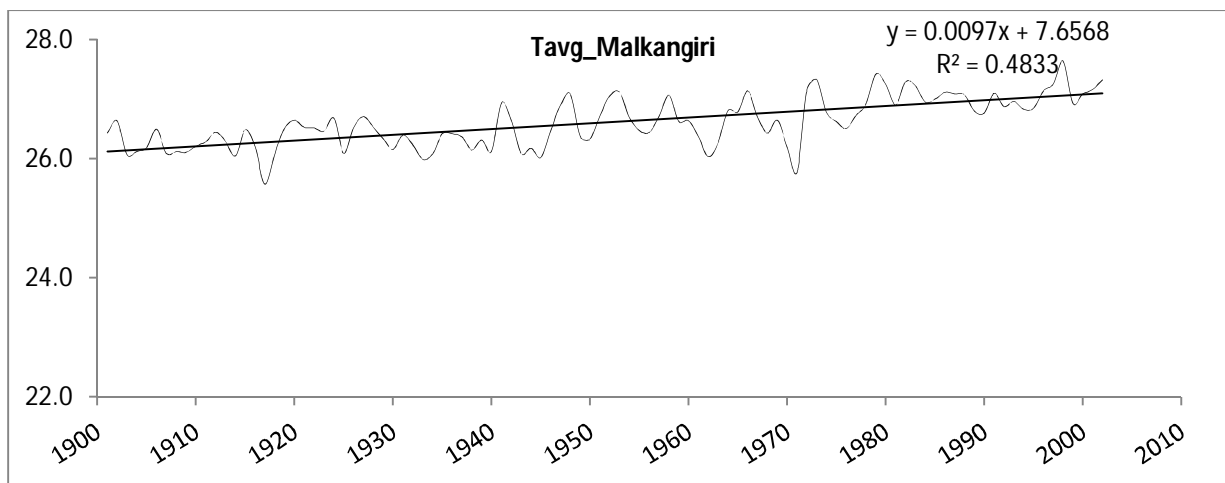
Fig. 3.17 Linear trend lines for the annual mean temperature (102 years) in Malkangiri district
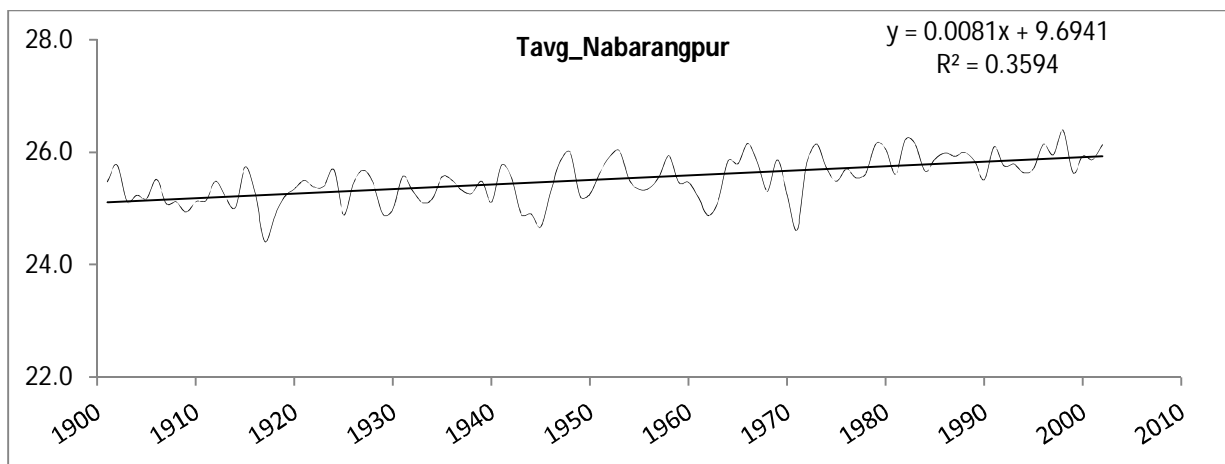
Fig. 3.18 Linear trend lines after removal of outliers in Nabarangpur district
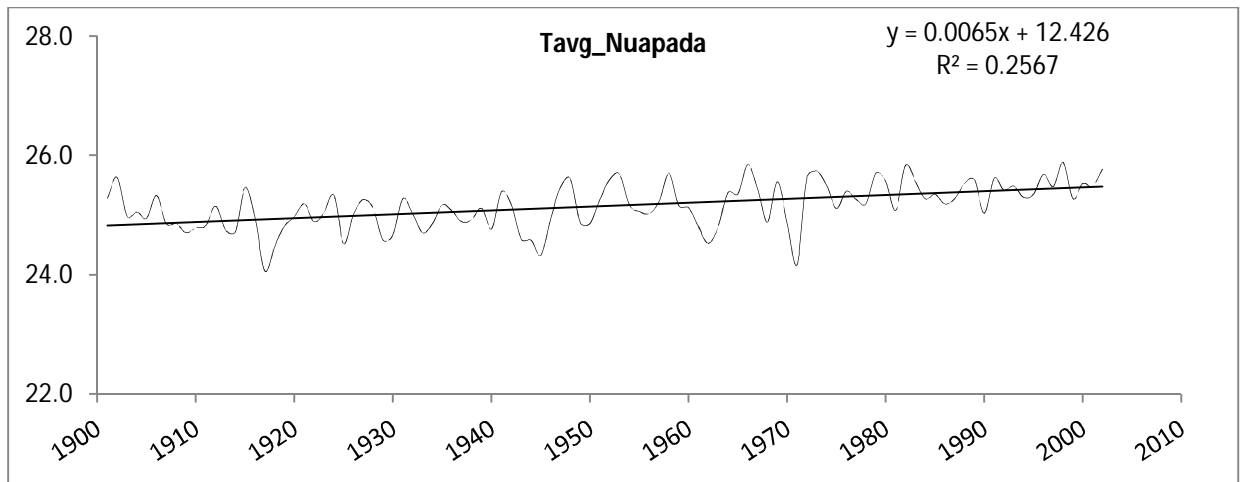
Fig. 3.19 Linear trend lines for the annual mean temperature (102 years) in Nuapada district
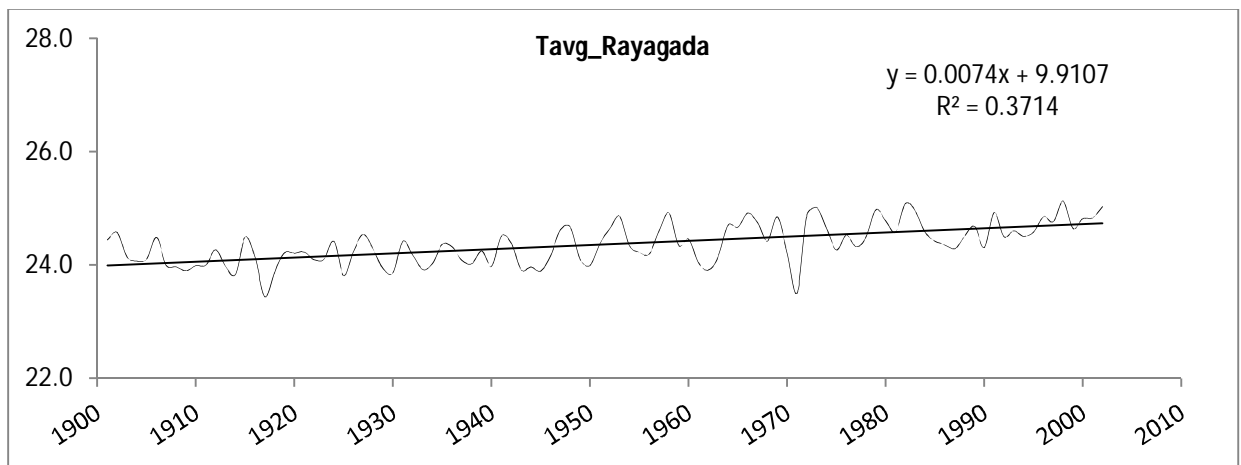
Fig. 3.20 Linear trend lines for the annual mean temperature (102 years) in Rayagada district
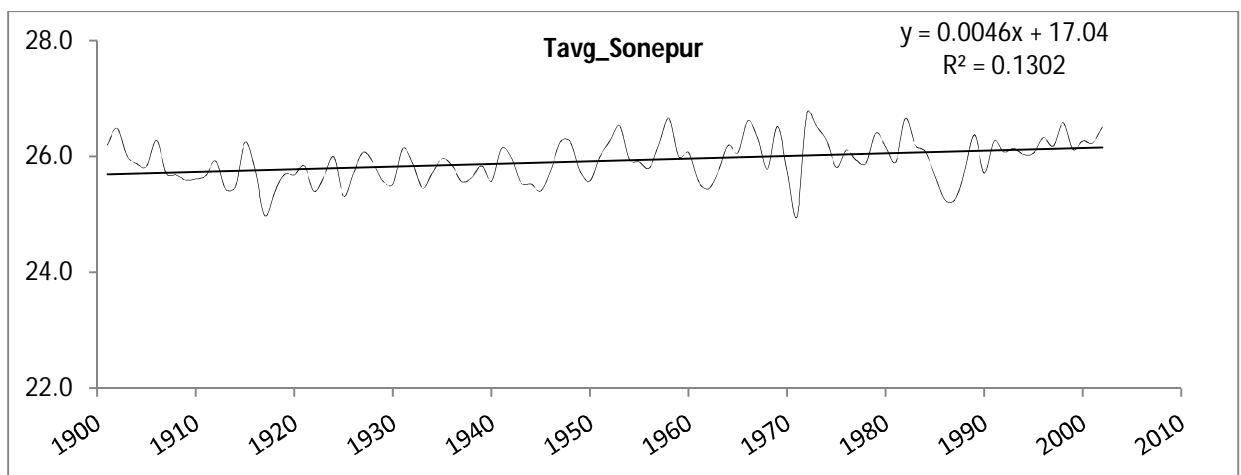
Fig. 3.21 Linear trend lines for the annual mean temperature (102 years) in Sonepur district

Table 3.10: Presence of outliers in the annual mean temperature series

Districts	Test of outliers				
	Max.	Min.	High	Low	Presence of outliers
Bolangir	26.45	24.68	26.86	24.61	No
Kalahandi	25.91	24.04	26.24	23.97	No
Koraput	25.97	24.10	26.30	23.92	No
Malkangiri	27.65	25.58	27.88	25.39	No
Nabarangpur	26.40	24.42	26.75	24.33	No
Nuapada	25.89	24.07	26.33	24.03	No
Rayagada	25.13	23.44	25.47	23.30	No
Sonepur	26.76	24.96	27.08	24.82	No
KBK region	26.25	24.41	26.57	24.34	No

Table 3.11: Mann-Kendall test statistics (Z value)

Districts	Mean temperature				
	Jan-Dec	Mar-May	Jun-Sep	Oct-Nov	Dec-Feb
Bolangir	3.267	1.741	1.660	2.967	3.932
Signific.	**	+	+	**	***
Kalahandi	3.568	3.013	2.660	3.117	3.632
Signific.	***	**	**	**	***
Koraput	3.689	4.325	4.083	3.290	3.285
Signific.	***	***	***	**	**
Malkangiri	3.660	4.291	3.834	3.233	3.111
Signific.	***	***	***	**	**
Nabarangpur	3.921	3.793	3.261	3.071	3.423
Signific.	***	***	**	**	***
Nuapada	3.643	2.527	1.978	3.071	4.054
Signific.	***	*	*	**	***
Rayagada	3.718	3.655	3.632	3.111	3.533
Signific.	***	***	***	**	***
Sonepur	2.741	0.544	1.047	2.729	3.718
Signific.	**			**	***
KBK region	3.689	3.406	2.995	3.209	3.643
Signific.	***	***	**	**	***

Level of significance
*** if trend at α = 0.001 level of significance; ** if trend at α = 0.01 level of significance; * if trend at α = 0.05 level of significance; + if trend at α = 0.1 level of significance.

Table 3.12: Sen's slope (β-value)

Districts	Mean temperature				
	Jan-Dec	Mar-May	Jun-Sep	Oct-Nov	Dec-Feb
Bolangir	0.004	0.004	0.003	0.008	0.008
Kalahandi	0.004	0.007	0.005	0.008	0.008
Koraput	0.004	0.010	0.007	0.008	0.007
Malkangiri	0.004	0.010	0.006	0.007	0.006
Nabarangpur	0.005	0.009	0.006	0.008	0.008
Nuapada	0.004	0.006	0.004	0.008	0.008
Rayagada	0.004	0.008	0.005	0.007	0.007
Sonepur	0.003	0.001	0.002	0.008	0.007
KBK region	0.004	0.008	0.005	0.008	0.007
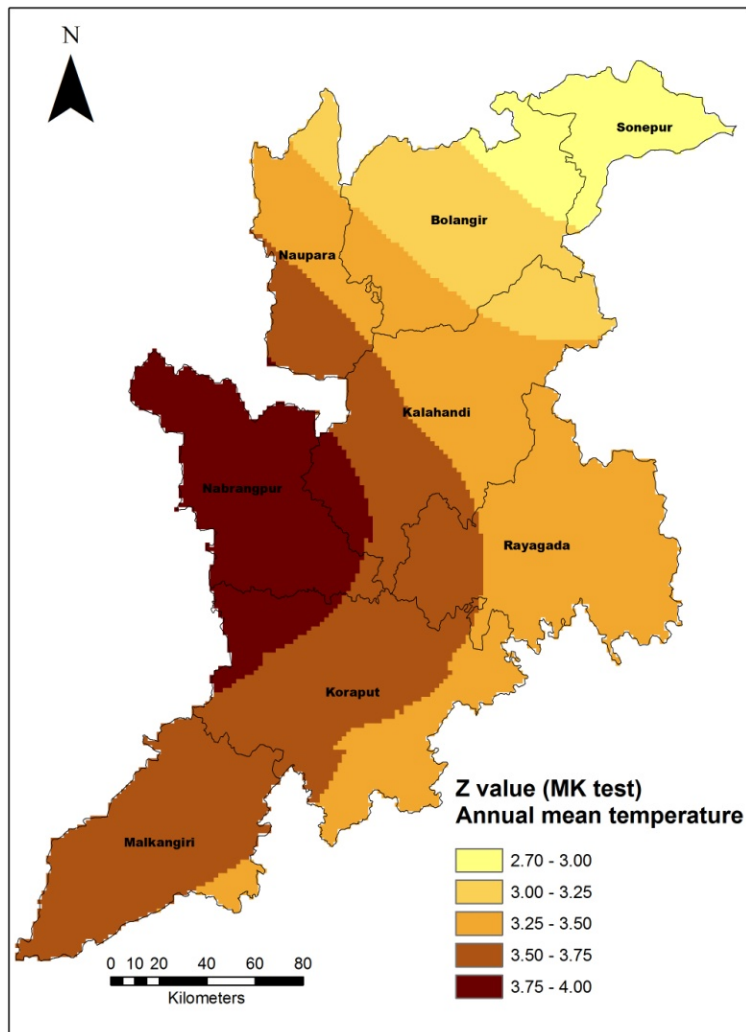
Fig. 3.22 Z value (MK test) for the annual mean temperature (102 years) of the KBK districts

3.4.2.2 Maximum temperature

It has been seen, particularly in KBK region, that the day temperature is reaching higher values surpassing the earlier records since last one decade. The summer temperature is becoming unbearable resulting in acute water shortage. Accordingly, monthly, annual and seasonal maximum temperature of KBK region for the period 1901 to 2002 (102 years) have been investigated for finding any trends existing or not. The basic statistics of the annual maximum temperature series is presented in Table 3.13. Regression lines using simple linear regression method have been detected for the entire KBK region as well as individual districts as shown in Figures 3.23 to 3.31. The monthly, seasonal and annual series are tested for existence of any outliers. The test indicates absence of outliers as presented in Table 3.14. Z statistics (MK test) and Sen's slope is presented in Table 3.15 and Table 3.16 respectively. Both regression method and MK test indicate a significant increasing temperature trend in the maximum series. The southern and western part of the KBK region, in particular, are experiencing increasing temperature trend at alpha = 0.001 level of significance. The spatial distribution of the Z value (Kriging interpolation) is shown in Fig. 3.32.

Table 3.13: Basic statistics of annual maximum temperature series for KBK region

Annual max. temperature series (°C)	Mean	Max	Min	Standard deviation	Coefficient of variation	Skewness	Kurtosis
Jan-Dec	31.00	31.77	29.97	0.37	0.01	-0.12	-0.16
Mar-May	35.80	37.56	34.11	0.67	0.02	-0.19	0.07
Jun-Sep	30.72	31.87	29.76	0.46	0.01	0.16	-0.61
Oct-Nov	29.08	30.50	27.54	0.69	0.02	0.07	-0.71
Dec-Feb	27.85	29.19	26.61	0.57	0.02	0.11	-0.63
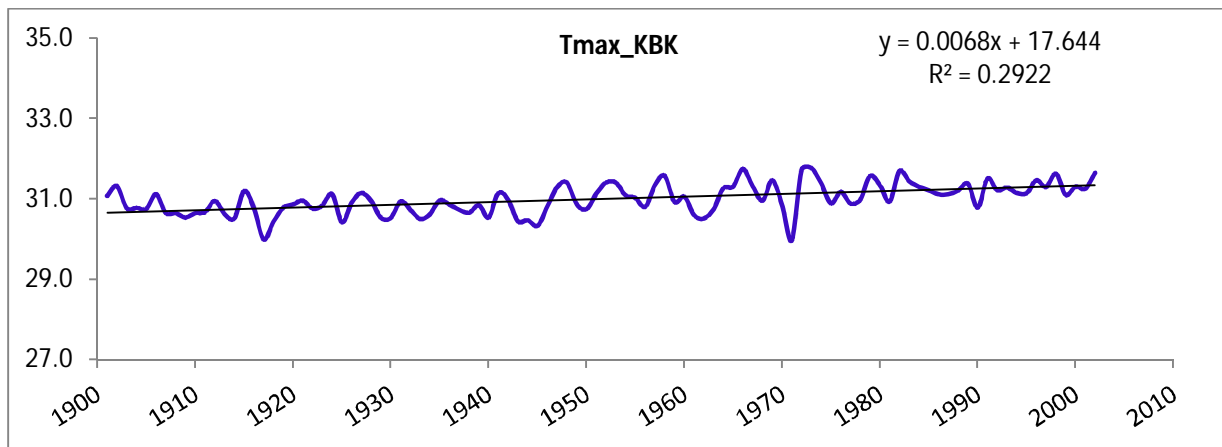
Fig. 3.23 Linear trend lines for the annual max. temperature (102 years) in whole KBK region
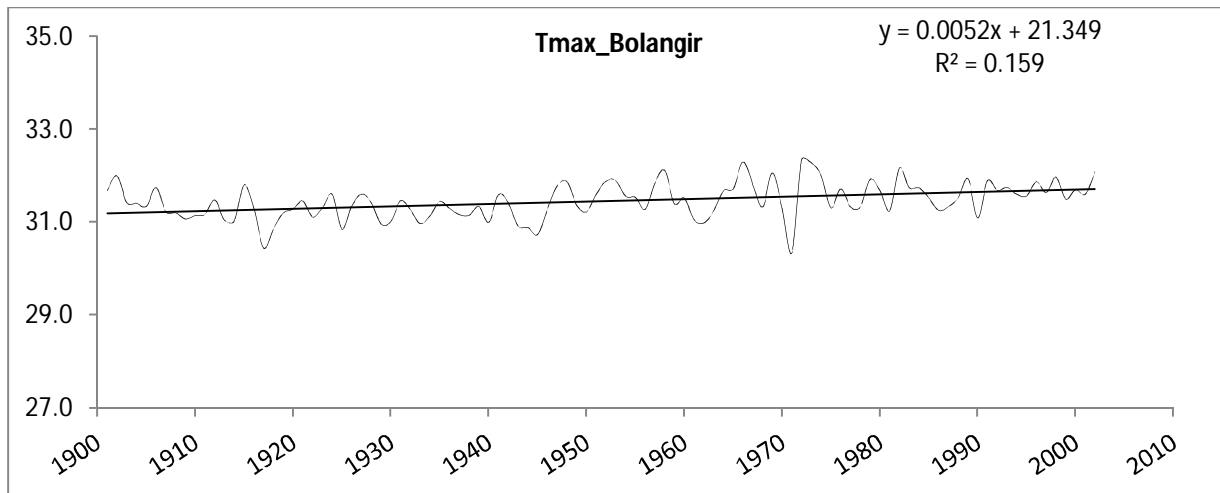
Fig. 3.24 Linear trend lines for the annual max. temperature (102 years) in Bolangir district
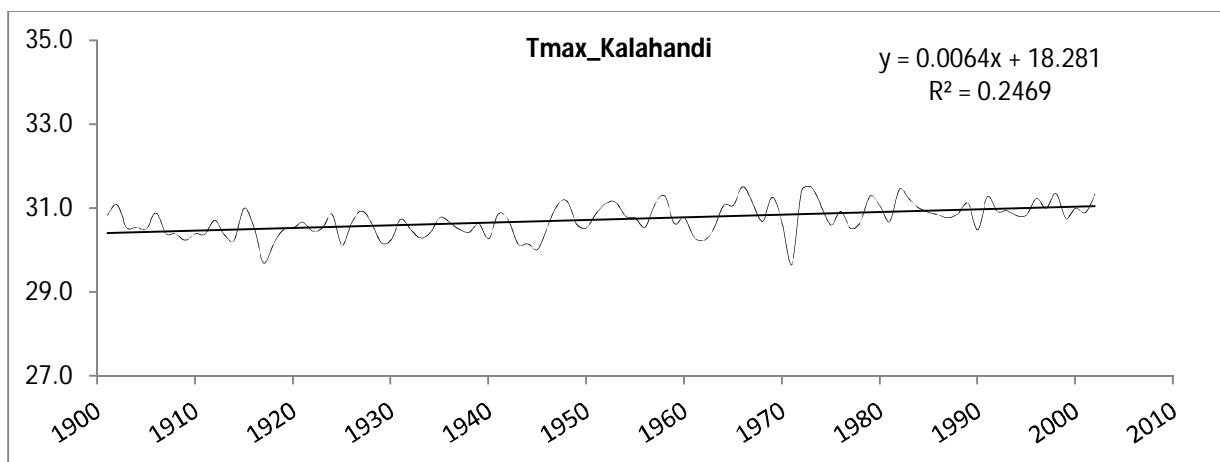
Fig. 3.25 Linear trend lines for the annual max. temperature (102 years) in Kalahandi district
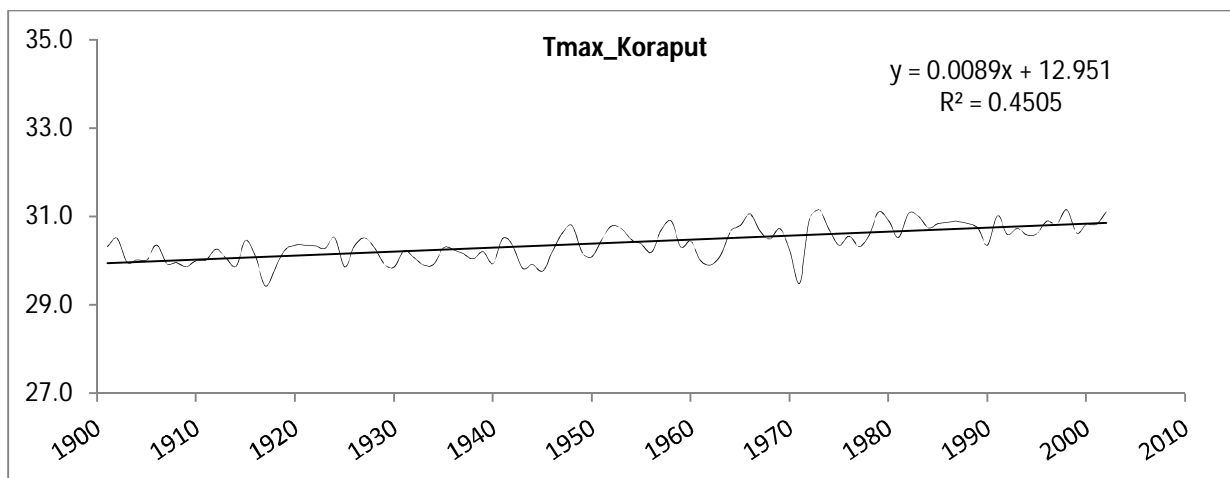
Fig. 3.26 Linear trend lines for the annual max. temperature (102 years) in Koraput district
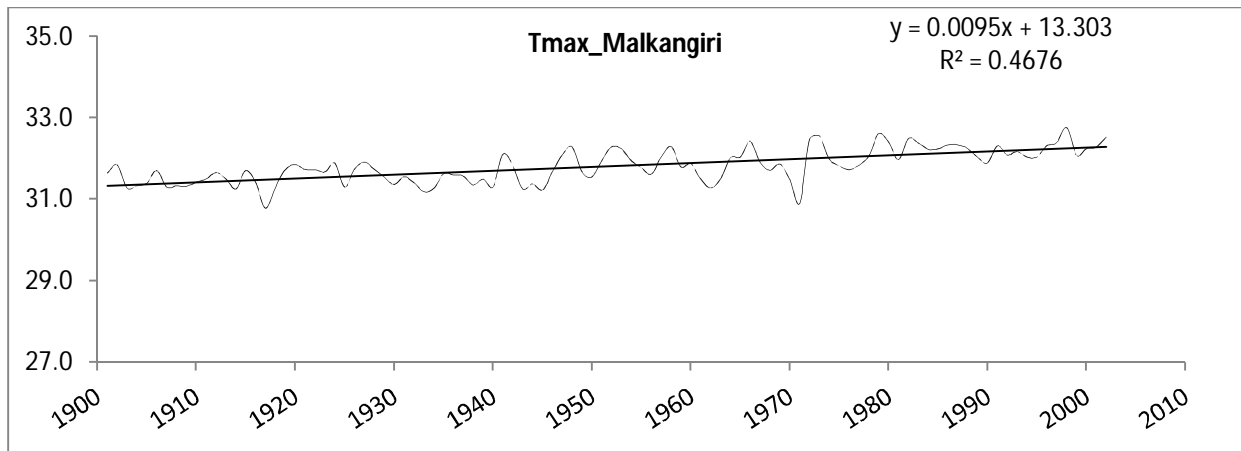
Fig. 3.27 Linear trend lines for the annual max. temperature (102 years) in Malkangiri district
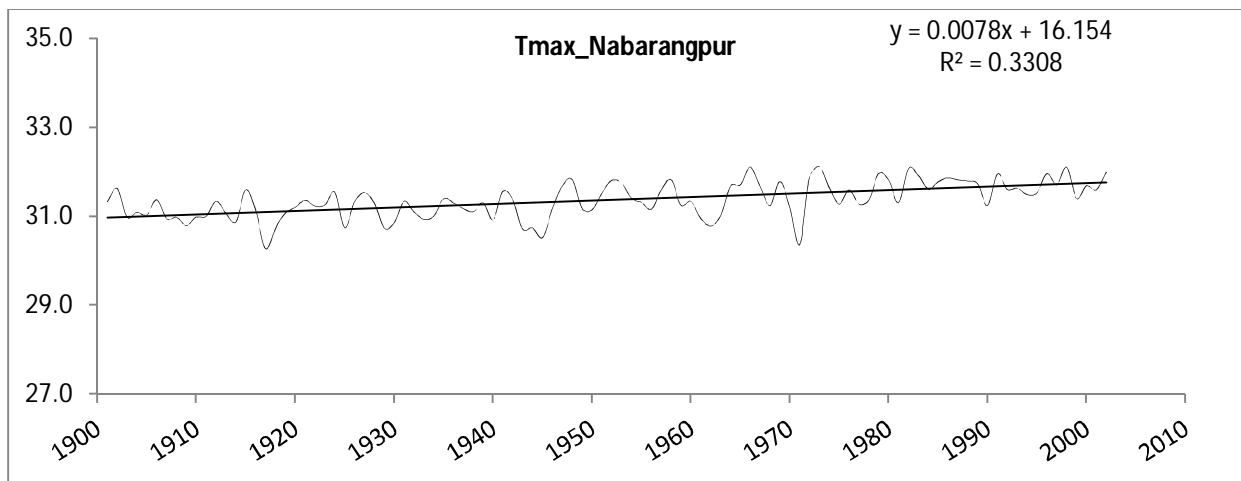
Fig. 3.28 Linear trend lines for the annual max. temperature (102 years) in Nabarangpur district
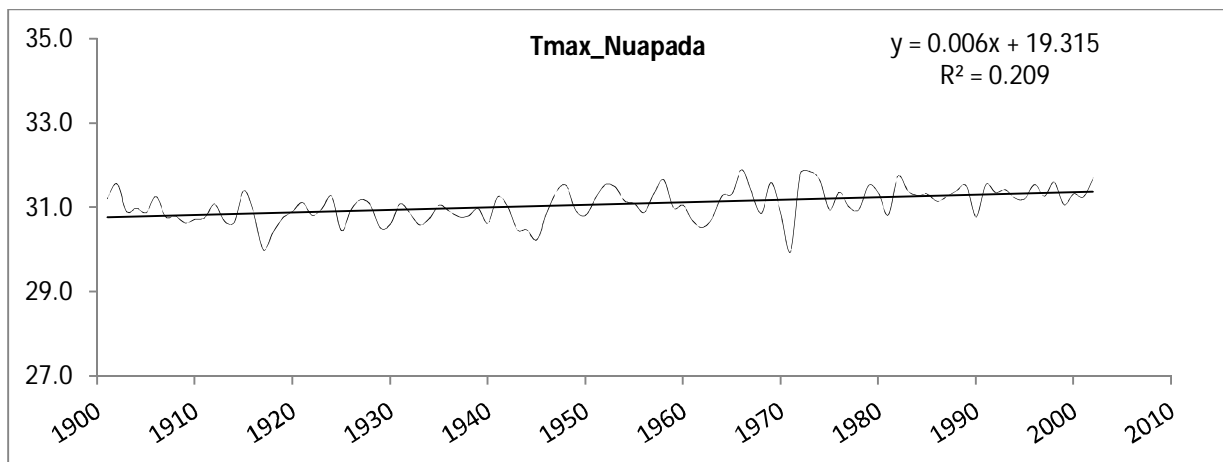
Fig. 3.29 Linear trend lines for the annual max. temperature (102 years) in Nuapada district
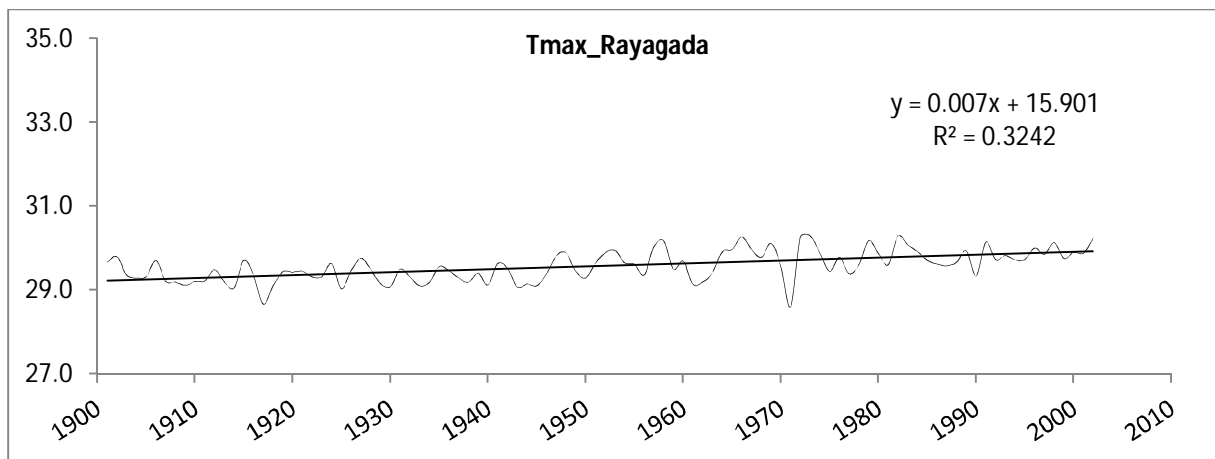
Fig. 3.30 Linear trend lines for the annual max. temperature (102 years) in Rayagada district
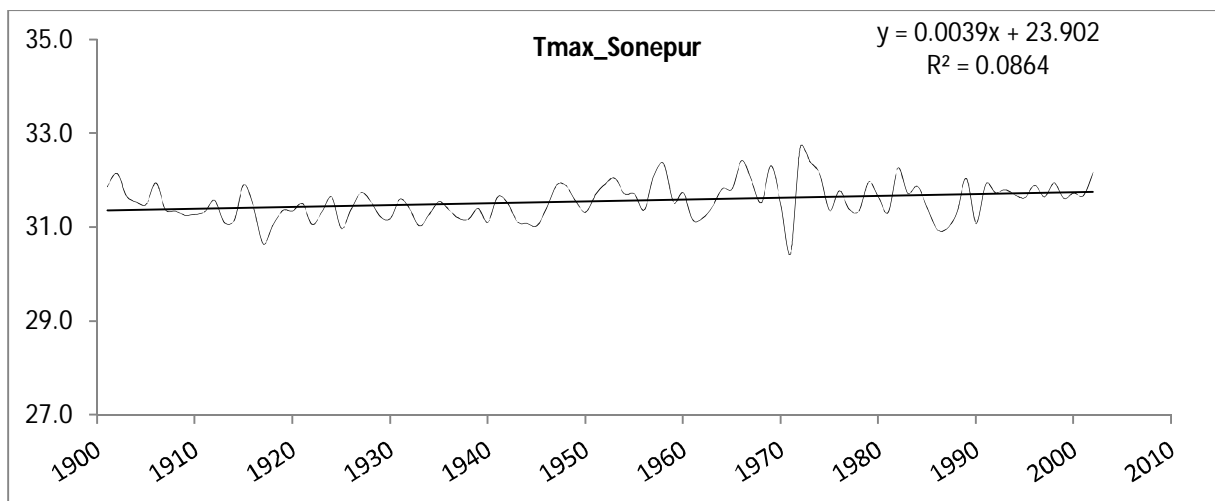
Fig. 3.31 Linear trend lines for the annual max. temperature (102 years) in Sonepur district

Table 3.14: Presence of outliers in the annual maximum temperature series

Districts	Test of outliers				
	Max.	Min.	High	Low	Presence of outliers
Bolangir	32.35	30.34	32.64	30.32	No
Kalahandi	31.52	29.67	31.90	29.60	No
Koraput	31.16	29.43	31.62	29.23	No
Malkangiri	32.76	30.78	33.07	30.59	No
Nabarangpur	32.13	30.28	32.60	30.17	No
Nuapada	31.90	29.96	32.27	29.91	No
Rayagada	30.30	28.59	30.69	28.49	No
Sonepur	32.71	30.44	32.77	30.39	No
KBK region	31.77	29.97	32.15	29.88	No

Table 3.15: Mann-Kendall test statistics (Z value)

Districts	Maximum temperature				
	Jan-Dec	Mar-May	Jun-Sep	Oct-Nov	Dec-Feb
Bolangir	3.319	1.492	1.584	3.169	3.840
Signific.	***			**	***
Kalahandi	3.736	3.001	2.544	3.186	3.672
Signific.	***	**	*	**	***
Koraput	3.973	4.337	3.944	3.591	3.383
Signific.	***	***	***	***	***
Malkangiri	3.793	4.273	3.938	3.406	3.209
Signific.	***	***	***	***	**
Nabarangpur	3.944	3.614	3.169	3.389	3.620
Signific.	***	***	**	***	***
Nuapada	3.660	2.255	1.879	3.244	3.979
Signific.	***	*	+	**	***
Rayagada	3.967	3.556	3.620	3.215	3.603
Signific.	***	***	***	**	***
Sonepur	2.440	0.411	0.937	2.828	3.597
Signific.	*			**	***
KBK region	3.788	3.215	2.891	3.180	3.788
Signific.	***	**	**	**	***

Table 3.16: Sen's slope (β-value)

Districts	Maximum temperature				
	Jan-Dec	Mar-May	Jun-Sep	Oct-Nov	Dec-Feb
Bolangir	0.004	0.004	0.003	0.009	0.008
Kalahandi	0.005	0.006	0.004	0.009	0.008
Koraput	0.004	0.010	0.007	0.008	0.007
Malkangiri	0.004	0.010	0.006	0.007	0.006
Nabarangpur	0.005	0.009	0.006	0.009	0.008
Nuapada	0.005	0.006	0.004	0.009	0.008
Rayagada	0.005	0.008	0.006	0.007	0.007
Sonepur	0.003	0.001	0.002	0.008	0.007
KBK region	0.005	0.007	0.005	0.008	0.007
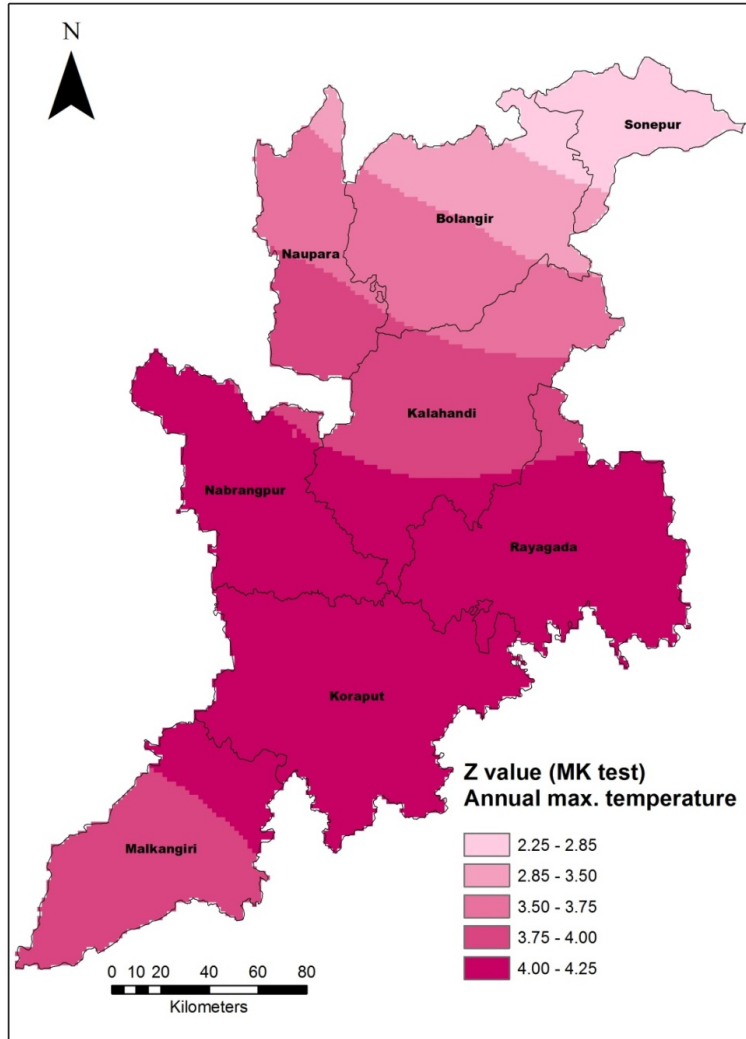
Fig. 3.32 Z value (MK test) for the annual max. temperature (102 years) of the KBK districts

3.4.2.3 Minimum temperature

Increase in mean temperature may be attributed to either increase in maximum temperature in a day and/ or increase in minimum day temperature. Already, the trend test for maximum temperature series in the region is indicating an increasing trend. Now, the study investigated the existence of any trend in the minimum temperature series. Accordingly, minimum series for 102 years (1901-2002) data were analyzed for trend detection. The basic statistics of the annual maximum temperature series is presented in Table 3.17. Regression lines using simple linear regression method have been detected for the entire KBK region as well as individual districts as shown in Figures 3.33 to 3.41. The monthly, seasonal and annual series are tested for existence of any outliers. The test indicates absence of outliers as presented in Table 3.18. Z statistics (MK test) and Sen's slope is presented in Table 3.19 and Table 3.20 respectively. Both linear and MK test indicates a significant increasing temperature trend in the minimum series in the KBK region. The spatial distribution of the Z value (Kriging interpolation) is shown in Fig. 3.42.

Table 3.17: Basic statistics of annual minimum temperature series for KBK region

Annual min. temperature series (°C)	Mean	Max	Min	Standard deviation	Coefficient of variation	Skewness	Kurtosis
Jan-Dec	19.91	20.91	18.88	0.38	0.02	0.00	-0.29
Mar-May	22.49	24.09	20.83	0.65	0.03	-0.15	-0.13
Jun-Sep	23.18	24.30	22.31	0.42	0.02	0.22	-0.54
Oct-Nov	18.30	20.19	16.59	0.74	0.04	0.33	0.05
Dec-Feb	14.03	15.39	12.76	0.60	0.04	0.08	-0.62
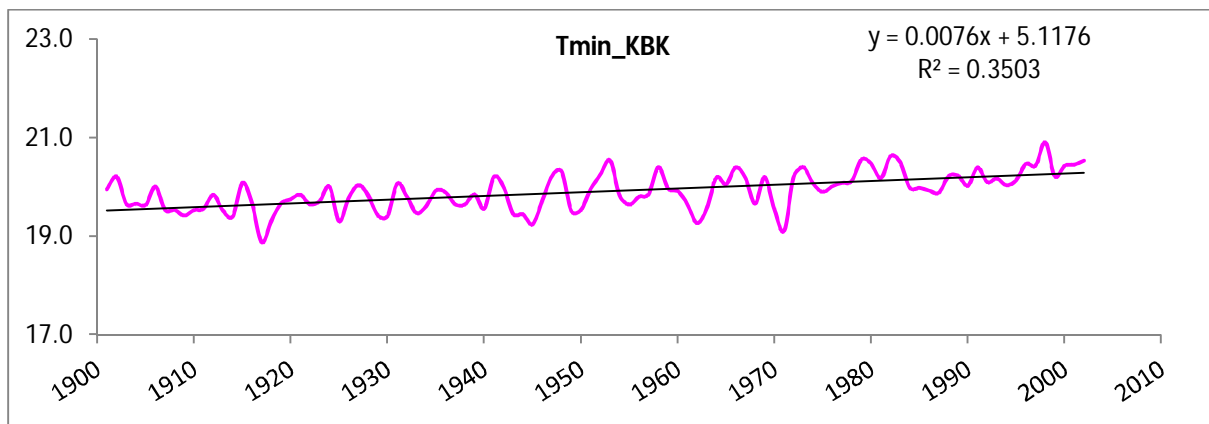
Fig. 3.33 Linear trend lines for the annual min. temperature (102 years) in whole KBK region
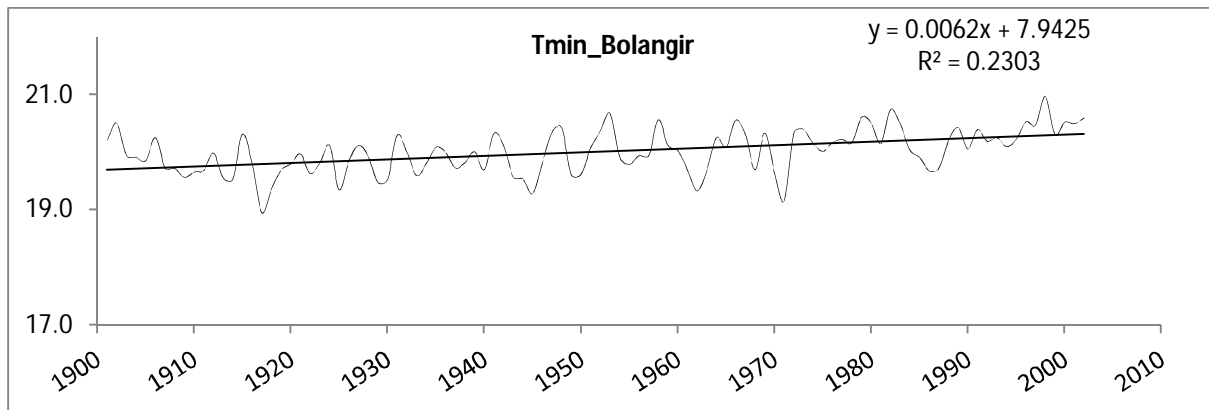
Fig. 3.34 Linear trend lines for the annual min. temperature (102 years) in Bolangir district
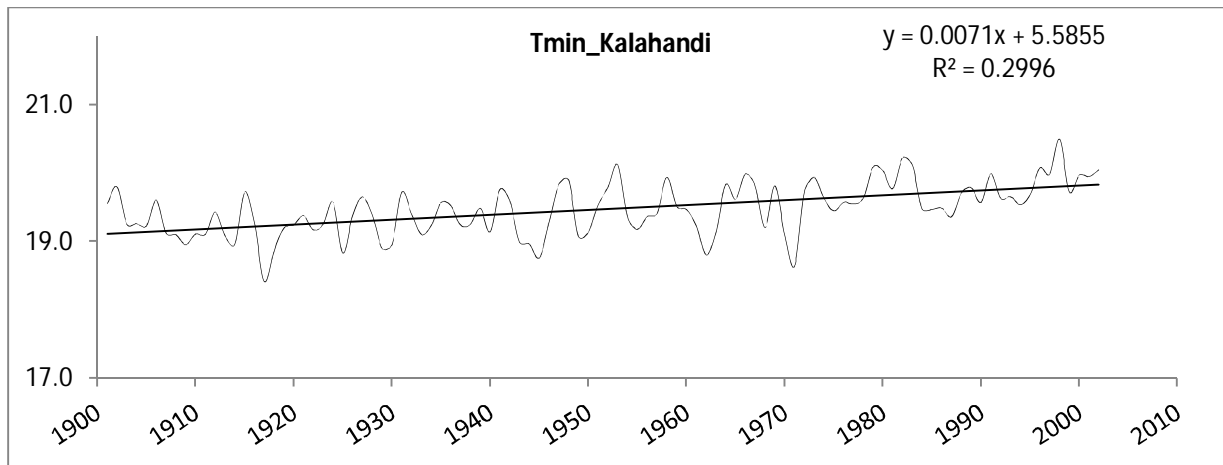
Fig. 3.35 Linear trend lines for the annual min. temperature (102 years) in Kalahandi district
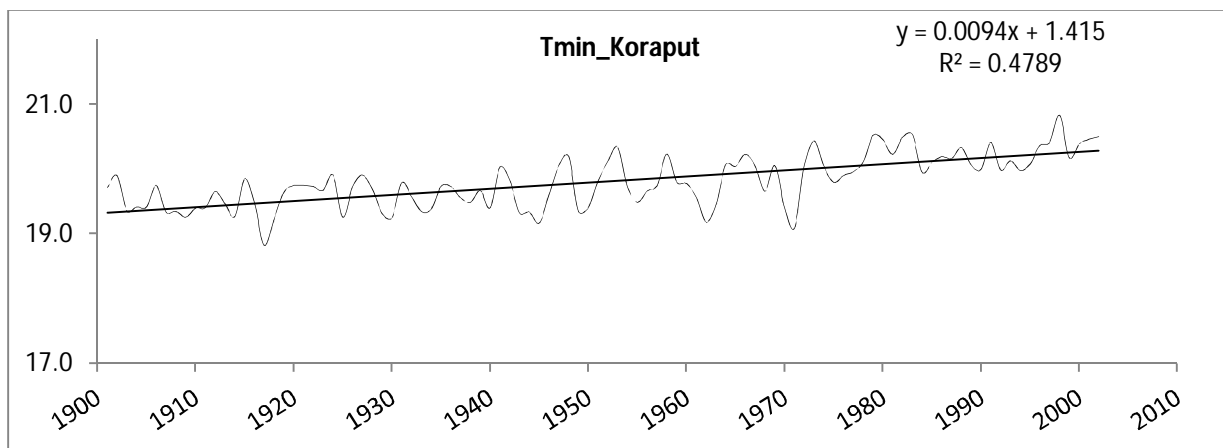
Fig. 3.36 Linear trend lines for the annual min. temperature (102 years) in Koraput district
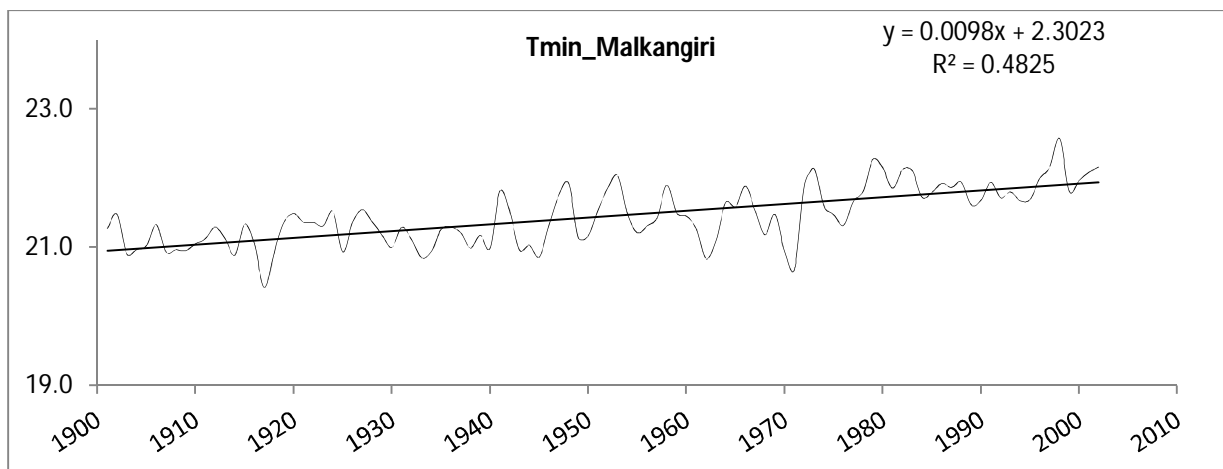
Fig. 3.37 Linear trend lines for the annual min. temperature (102 years) in Malkangiri district
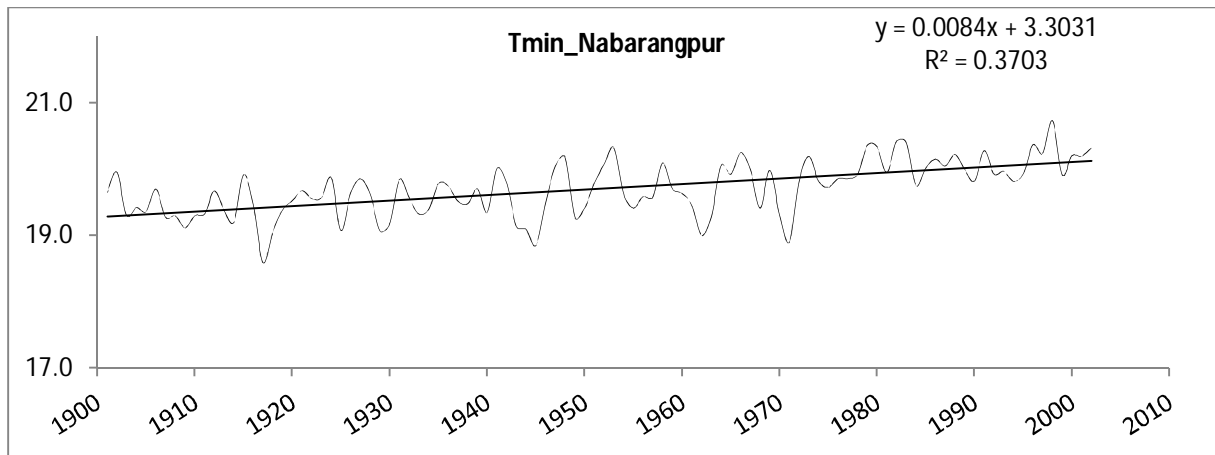
Fig. 3.38 Linear trend lines for the annual min. temperature (102 years) in Nabarangpur district
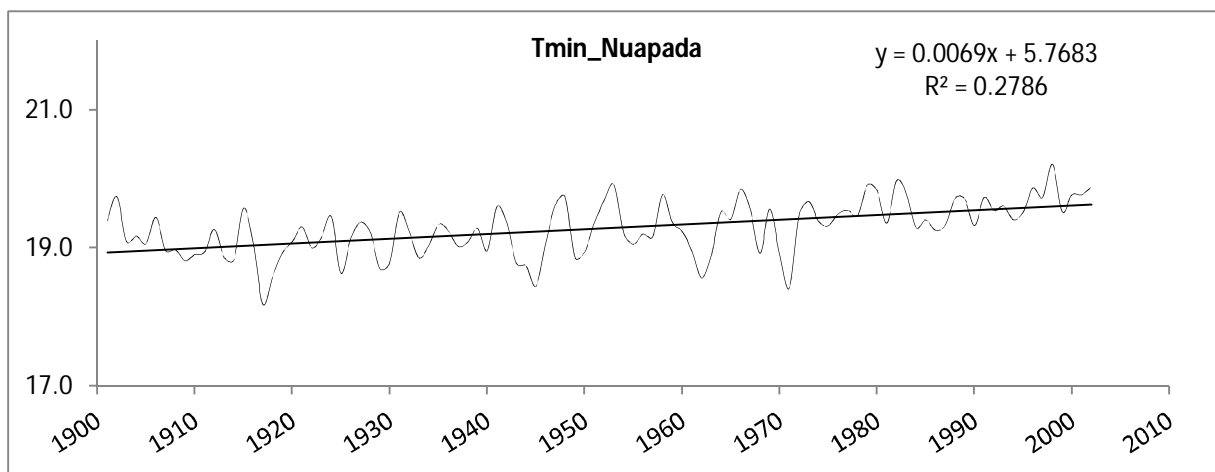
Fig. 3.39 Linear trend lines for the annual min. temperature (102 years) in Nuapada district
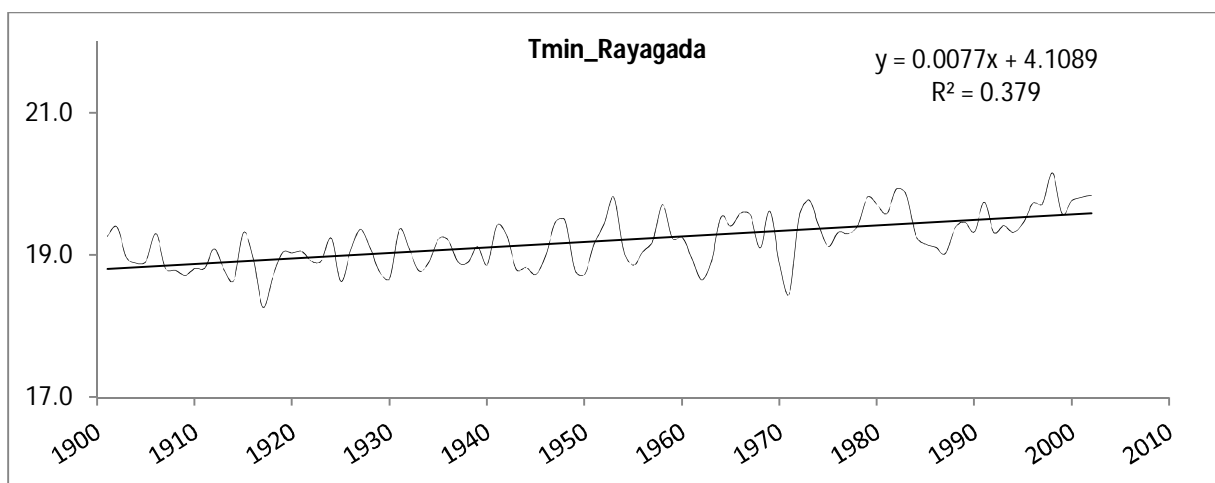
Fig. 3.40 Linear trend lines for the annual min. temperature (102 years) in Rayagada district
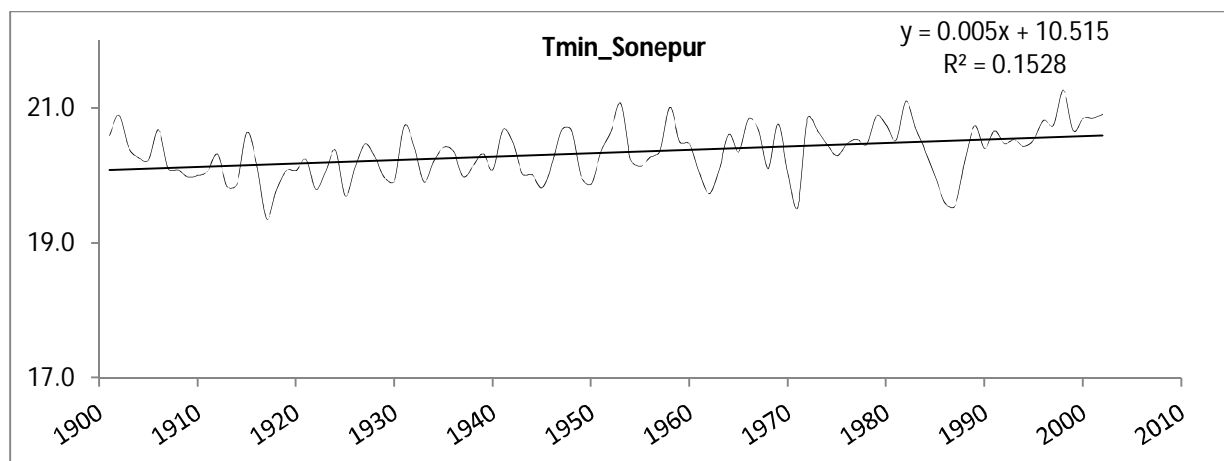
Fig. 3.41 Linear trend lines for the annual min. temperature (102 years) in Sonepur district

Table 3.18: Presence of outliers in the annual minimum temperature series

Districts	Test of outliers				
	Max.	Min.	High	Low	Presence of outliers
Bolangir	20.97	18.95	21.19	18.88	No
Kalahandi	20.50	18.41	20.66	18.34	No
Koraput	20.83	18.82	21.06	18.62	No
Malkangiri	22.57	20.42	22.74	20.22	No
Nabarangpur	20.73	18.59	20.98	18.50	No
Nuapada	20.21	18.18	20.49	18.14	No
Rayagada	20.16	18.27	20.35	18.10	No
Sonepur	21.27	19.36	21.52	19.21	No
KBK region	20.91	18.88	21.08	18.79	No

Table 3.19: Mann-Kendall test statistics (Z value)

Districts	Minimum temperature				
	Jan-Dec	Mar-May	Jun-Sep	Oct-Nov	Dec-Feb
Bolangir	3.123	2.128	1.764	2.770	3.770
Signific.	**	*	+	**	***
Kalahandi	3.366	3.186	2.614	2.926	3.730
Signific.	***	**	**	**	***
Koraput	3.371	4.245	3.961	2.972	3.377
Signific.	***	***	***	**	***
Malkangiri	3.406	4.331	3.770	3.047	3.134
Signific.	***	***	***	**	**
Nabarangpur	3.689	3.660	3.319	2.926	3.643

Signific.	***	***	***	**	***
Nuapada	3.377	2.822	2.012	2.868	3.961
Signific.	***	**	*	**	***
Rayagada	3.296	3.672	3.580	2.995	3.551
Signific.	***	***	***	**	***
Sonepur	2.758	0.977	1.087	2.695	3.684
Signific.	**			**	***
KBK region	3.383	3.574	3.007	3.042	3.701
Signific.	***	***	**	**	***

Table 3.20: Sen's slope (β-value)

Districts	Minimum temperature				
	Jan-Dec	Mar-May	Jun-Sep	Oct-Nov	Dec-Feb
Bolangir	0.004	0.004	0.003	0.008	0.008
Kalahandi	0.004	0.007	0.005	0.008	0.008
Koraput	0.004	0.010	0.006	0.007	0.007
Malkangiri	0.003	0.010	0.006	0.006	0.006
Nabarangpur	0.004	0.009	0.006	0.008	0.008
Nuapada	0.004	0.006	0.004	0.008	0.008
Rayagada	0.004	0.008	0.005	0.007	0.007
Sonepur	0.003	0.002	0.002	0.007	0.008
KBK region	0.004	0.008	0.005	0.007	0.008
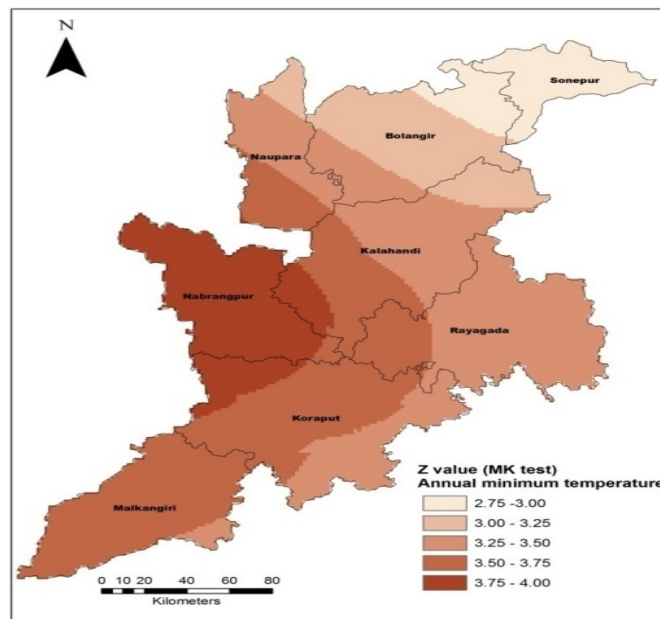
Fig. 3.42 Z value (MK test) for the annual min. temperature (102 years) of the KBK districts

3.4.3 Potential evapotranspiration trend

Recurring drought and water stress is a common scenario in the KBK region. Potential evapotranspiration is affected by many factors including the temperature of a region. A higher temperature coupled with dry atmosphere results in higher evaporation and transpiration loss by the plants. To sustain plant/ crop growth it is essential to meet the plant/ crop water requirement timely. With this in mind, the study investigated the trend in the potential evapotranspiration in the KBK districts as well as entire KBK region using 102 years data from 1901 to 2002. The basic statistics of the annual maximum temperature series is presented in Table 3.21. Regression lines using simple linear regression method have been detected for the entire KBK region as well as individual districts as shown in Figures 3.43 to 3.51. The monthly, seasonal and annual series are tested for existence of any outliers. The test indicates absence of outliers as presented in Table 3.22. Z statistics (MK test) and Sen's slope is presented in Table 3.23 and Table 3.24 respectively. The trend test indicates an increasing trend in the potential evapotranspiration series. This will result in higher crop water requirement in the region. The spatial distribution of the Z value (Kriging interpolation) is shown in Fig. 3.52.

Table 3.21: Basic statistics of potential evapotranspiration series for KBK region

Potential ET series (mm)	Mean	Max	Min	Standard deviation	Coefficient of variation	Skewness	Kurtosis
Jan-Dec	6.15	6.31	6.00	0.05	0.01	0.13	1.01
Mar-May	7.65	7.83	7.41	0.07	0.01	-0.20	1.73
Jun-Sep	5.54	5.82	5.24	0.09	0.02	-0.19	2.11
Oct-Nov	5.67	5.95	5.45	0.09	0.02	0.13	0.86
Dec-Feb	5.78	5.97	5.55	0.07	0.01	-0.01	1.47
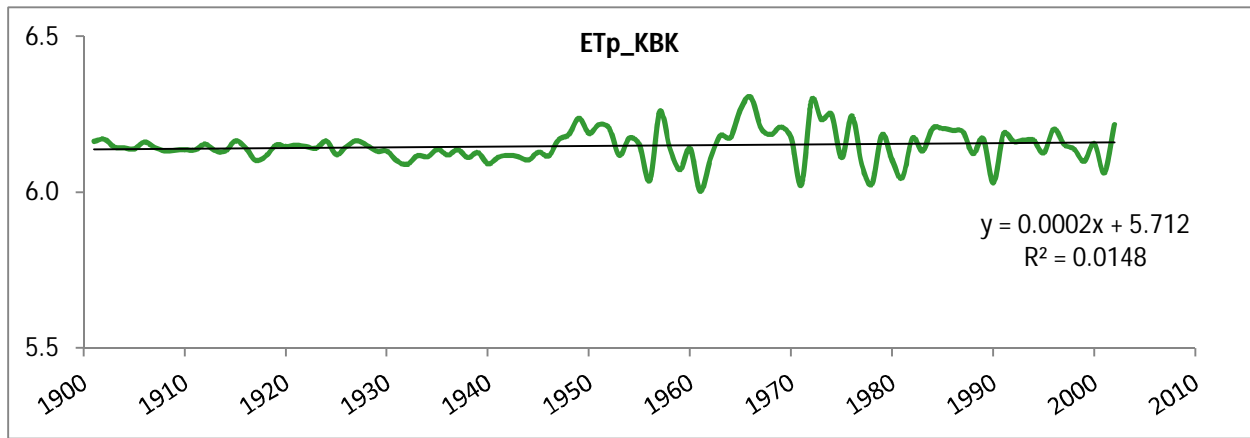
Fig. 3.43 Linear trend lines for the potential evapotranspiration (102 years) in whole KBK region
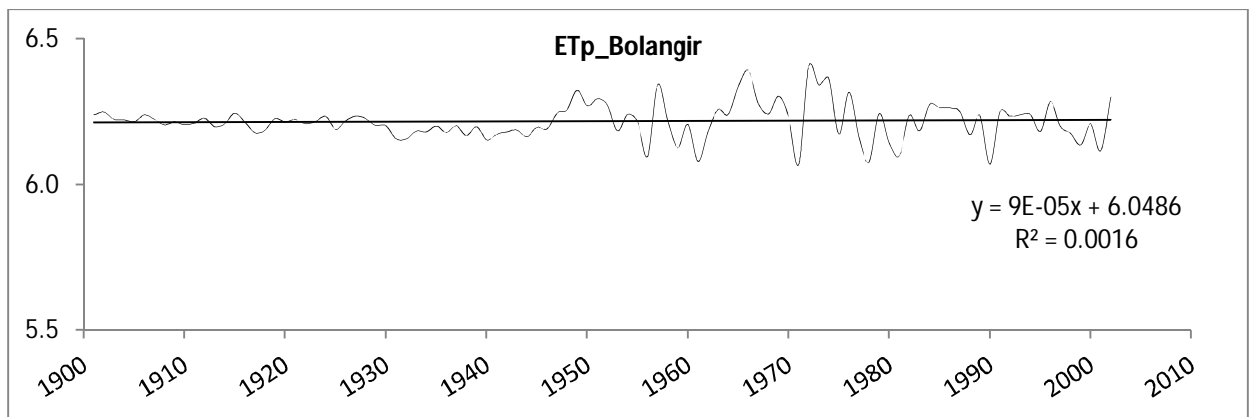
Fig. 3.44 Linear trend lines for the potential evapotranspiration (102 years) in Bolangir district
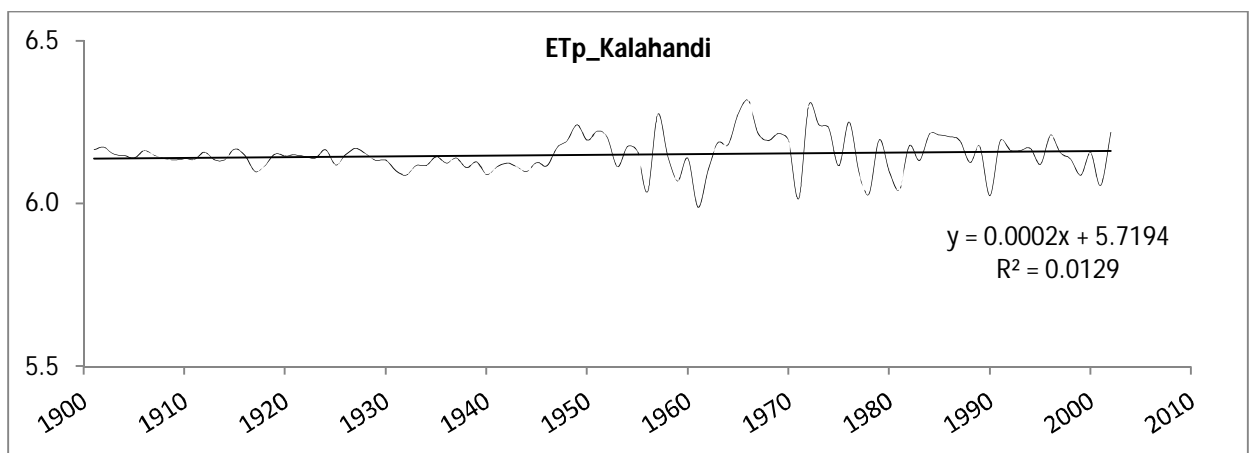
Fig. 3.45 Linear trend lines for the potential evapotranspiration (102 years) in Kalahandi district
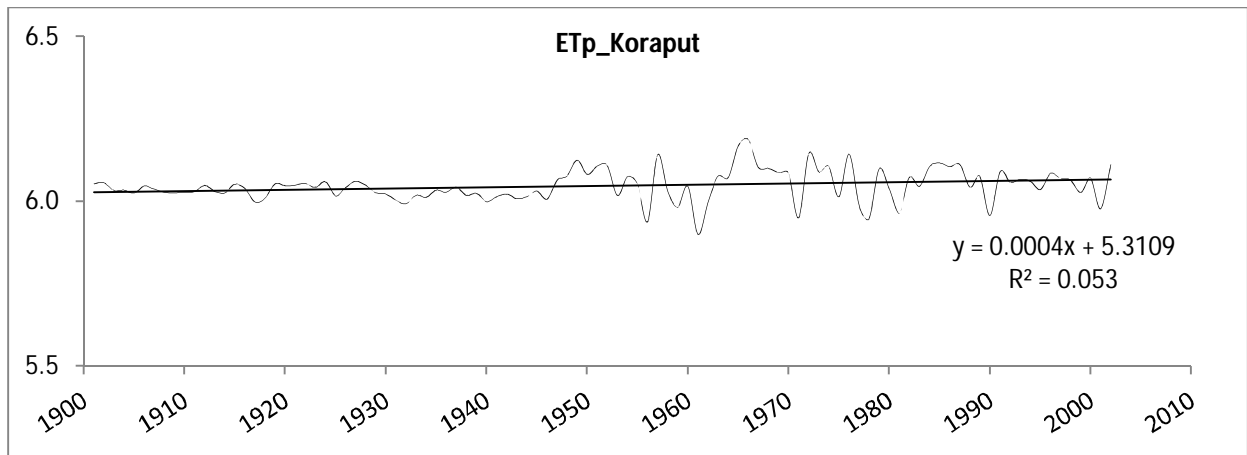
Fig. 3.46 Linear trend lines for the potential evapotranspiration (102 years) in Koraput district
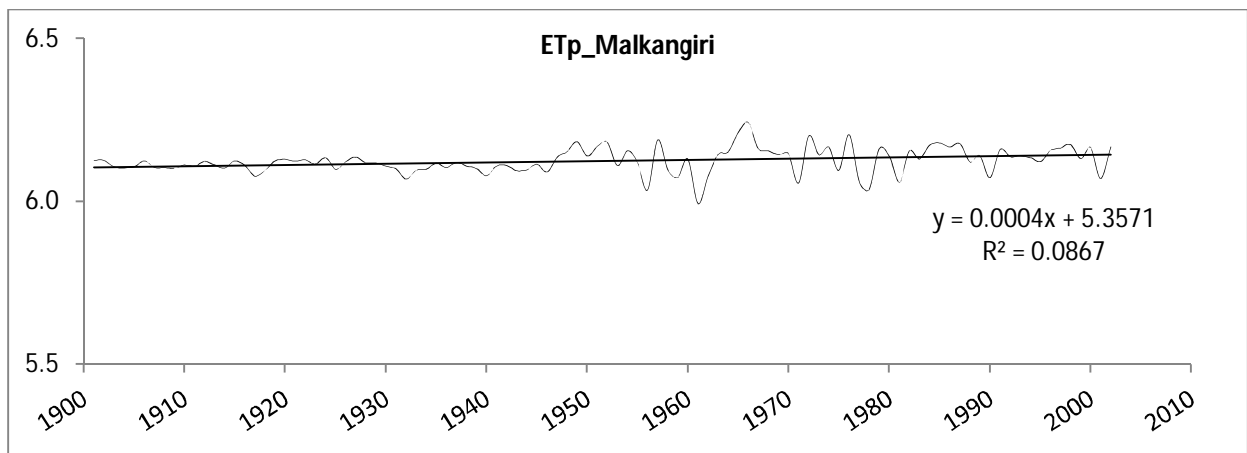
Fig. 3.47 Linear trend lines for the potential evapotranspiration (102 years) in Malkangiri district
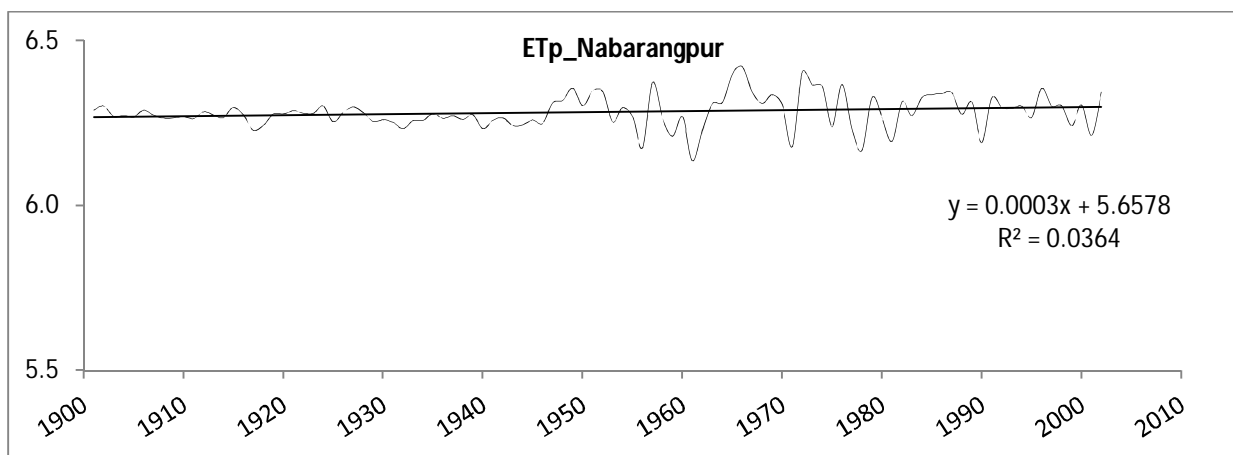
Fig. 3.48 Linear trend lines for the potential evapotranspiration (102 years) in Nabarangpur district
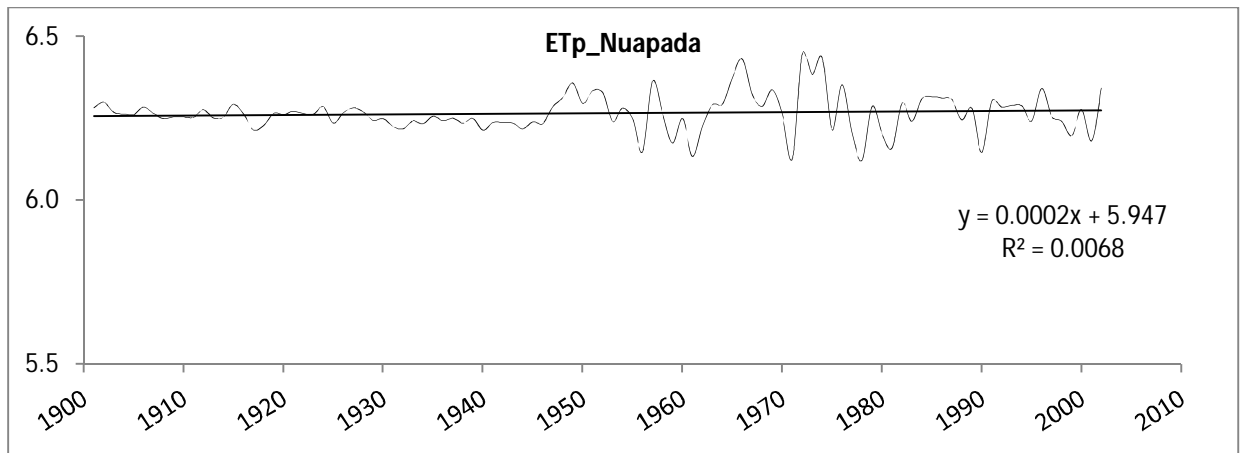
Fig. 3.49 Linear trend lines for the potential evapotranspiration (102 years) in Nuapada district
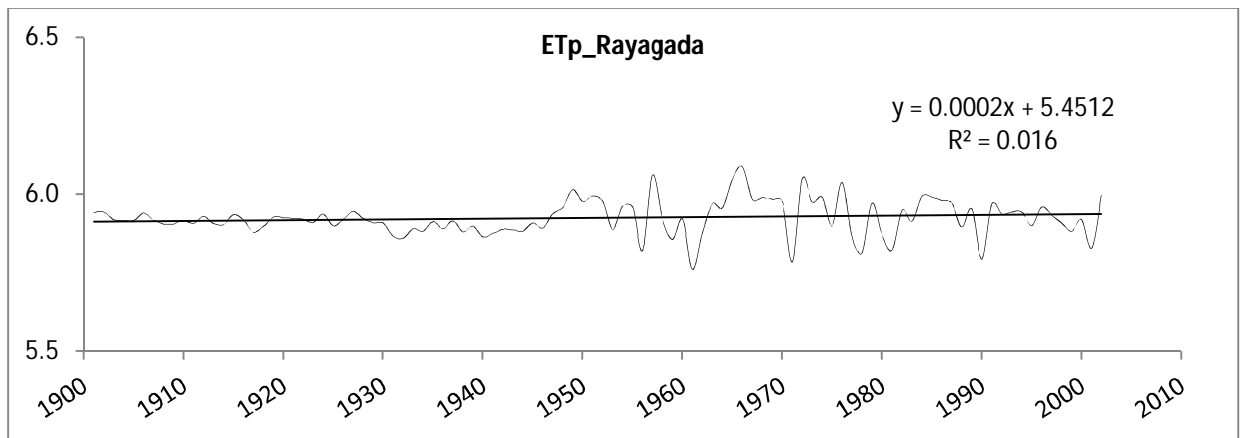
Fig. 3.50 Linear trend lines for the potential evapotranspiration (102 years) in Rayagada district
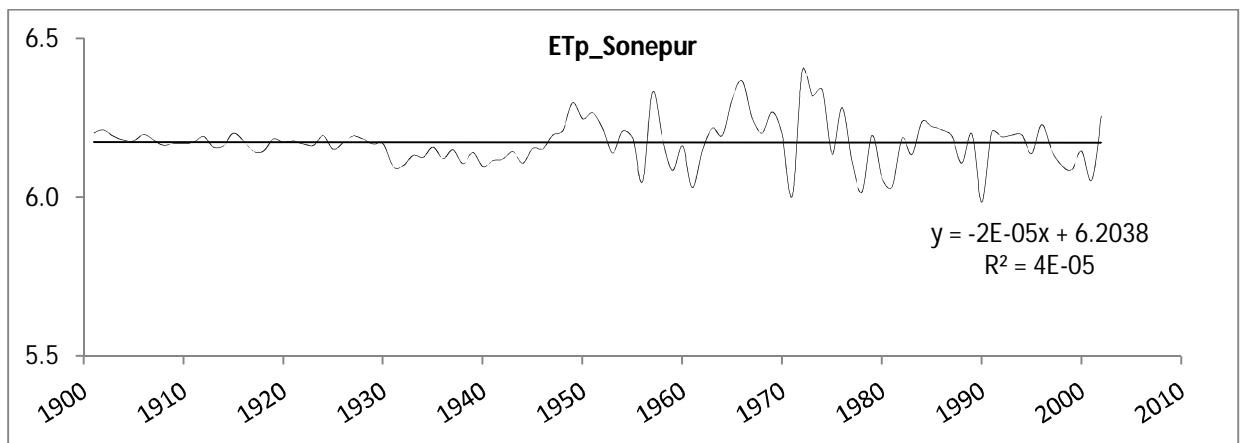
Fig. 3.51 Linear trend lines for the potential evapotranspiration (102 years) in Sonepur district

Table 3.22: Presence of outliers in the annual potential evapotranspiration series

Districts	Test of outliers				
	Max.	Min.	High	Low	Presence of outliers
Bolangir	6.41	6.07	6.41	6.03	No
Kalahandi	6.32	5.99	6.33	5.98	No
Koraput	6.19	5.90	6.20	5.90	No
Malkangiri	6.24	5.99	6.25	6.01	No
Nabarangpur	6.42	6.14	6.44	6.14	No
Nuapada	6.45	6.12	6.45	6.09	No
Rayagada	6.09	5.76	6.10	5.76	No
Sonepur	6.40	5.99	6.40	5.96	No
KBK region	6.31	6.00	6.31	5.99	No

Table 3.23: Mann-Kendall test statistics (Z value)

Districts	Potential evapotranspiration				
	Jan-Dec	Mar-May	Jun-Sep	Oct-Nov	Dec-Feb
Bolangir	1.157	1.295	0.353	0.257	1.460
Signific.					
Kalahandi	1.775	2.385	1.122	0.445	2.148
Signific.	+	*			*
Koraput	3.088	3.238	2.406	1.700	1.775
Signific.	**	**	*	+	+
Malkangiri	3.944	3.420	2.995	1.865	2.088
Signific.	***	***	**	+	*
Nabarangpur	2.764	2.912	1.576	1.671	1.770
Signific.	**	**		+	+
Nuapada	1.596	1.532	0.541	0.558	1.868
Signific.					+
Rayagada	1.891	2.556	1.434	0.801	1.492
Signific.	+	*			
Sonepur	0.758	0.824	0.197	-0.136	1.018
Signific.					
KBK region	1.937	2.325	1.209	0.648	1.399
Signific.	+	*			

Level of significance
*** if trend at $\alpha = 0.001$ level of significance; ** if trend at $\alpha = 0.01$ level of significance; * if trend at $\alpha = 0.05$ level of significance; + if trend at $\alpha = 0.1$ level of significance

Table 3.24: Sen's slope (β-value)

Districts	Potential evapotranspiration				
	Jan-Dec	Mar-May	Jun-Sep	Oct-Nov	Dec-Feb
Bolangir	0.0002	0.0003	0.0001	0.0001	0.0003
Kalahandi	0.0004	0.0005	0.0003	0.0001	0.0005
Koraput	0.0005	0.0006	0.0005	0.0004	0.0003
Malkangiri	0.0005	0.0006	0.0005	0.0003	0.0003
Nabarangpur	0.0004	0.0006	0.0004	0.0005	0.0004
Nuapada	0.0003	0.0004	0.0001	0.0002	0.0004
Rayagada	0.0004	0.0006	0.0004	0.0002	0.0004
Sonepur	0.0002	0.0002	0.0001	0.0000	0.0003
KBK region	0.0003	0.0005	0.0003	0.0001	0.0003
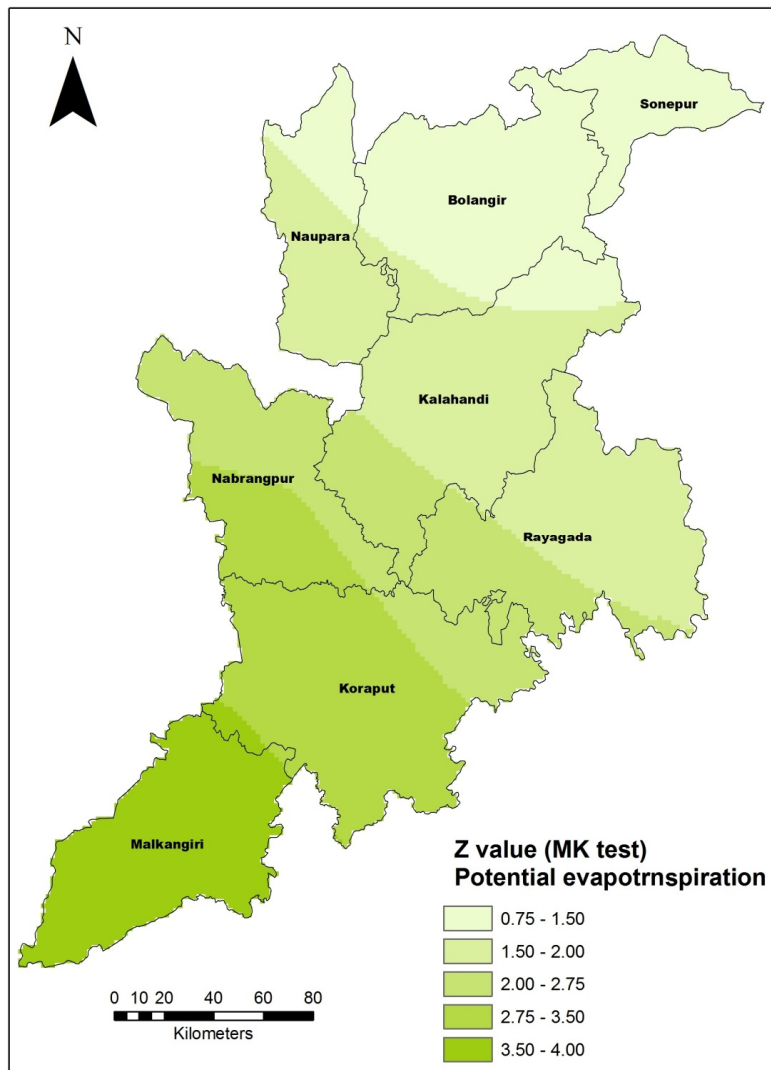
Fig. 3.52 Z value (MK test) for the annual mean potential evapotranspiration (102 years) of the KBK districts

3.4.4 Trend attribution

Finding attribute for the trend is as important as finding the existing trend of a climatic variable. Climatic variables are driven by several forces, primarily, land, ocean and atmosphere. The physiography of a location, demography, agriculture, source and type of irrigation, presence of industries are few human interventions that has significantly affecting the existing trend (Fig.3.53).

Following are few attributes that can be assigned for the existing trend in the KBK region:

❑ Northern districts are 'land-locked' with less coastal influence (about 300-350 km away) in comparison to South parts (100-150 km)

❑ South west high slope

❑ North comparatively plain and irrigated/ Hirakud command/ irrigated area

❑ High ridge line along North-South.

❑ Forest coverage high in South

❑ More industrial influence in North since 2003-04

❑ Soils in district of Nuapada and Kalahandi are mostly 'Black Cotton' with high Clay content.

❑ Area is surrounded by high slope

❑ One of the warmest region of Odisha with temperature reaching 50ºC (Titilagarh)

❑ These factors may be several reasons why the area is drought prone in spite of high rainfall.
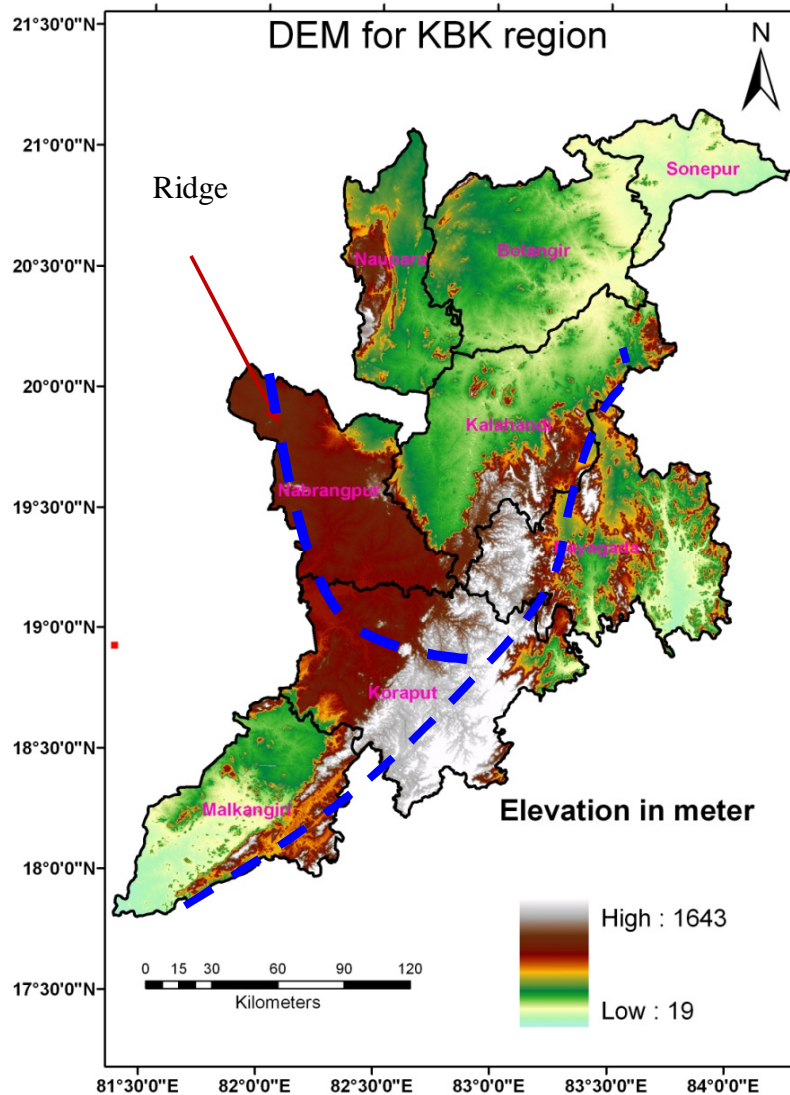
Fig. 3.53 Ridge line showing clear division of northern and southrern area

3.5 CONCLUSIONS

In this chapter, trends in long-term climatic data, i.e., rainfall (110 years), temperature (102 years), and potential evapotranspiration (102 years) have been investigated on monthly, seasonal and annual series in eight districts spread over in the KBK region in the western part of Odisha, India. The trends are generated using both parametric (linear regression method) and non-parametric (Mann-Kendall test and Sen's Slope estimates). Before analyzing for trend, outliers test and autocorrelation test were carried out to remove any unexpected high values and make the

series correlation free. However, it is not always advisable when the data length exceeds 70 years with low coefficient of variation.

3.5.1 Rainfall trend

The statistical analysis of the rainfall data indicates an annual average rainfall of 1297 mm with a standard deviation of 205 mm and coefficient of variation of 16%. The majority of the rainfall is received during June, July, August, and September due to monsoon front. Winter rainfall is insignificant in the KBK region. The region often witness pre-monsoon rainfall amounting to about 97 mm in the month of April and May. Often, cyclonic rainfall occurs during October and November due to low pressure created in the Bay of Bengal. The rainfall trend analysis indicates two districts with significant trend (Malkangiri with increasing and Nuapada with decreasing) in the annual rainfall at 95% significant level. The magnitude of the decreasing trends in the annual rainfall varies from 0.204 mm/ year (Kalahandi) to 1.419 mm/ year (Nuapada). The analysis also indicates a non-significant increasing trends in the annual rainfall in the districts of Koraput (+0.935 mm/ year) and Rayagada (+0.382 mm/ year). The annual rainfall series for the districts of Bolangir, Nabarangpur and Sonepur indicates non-significant decreasing trend. The winter series in the entire region showed a decreasing trend. Monsoon trend in the northern districts is showing decreasing trend in comparison to districts situated towards south of KBK region. The probable change years were mainly found prior to 1961 for annual rainfall series during the period 1901 to 2010 as per Pettitt's test, whereas SNHT indicates last decade (2005) when significant shift in rainfall pattern has occurred.

3.5.2 Temperature trend

Temperature is one of the important variables affecting the climate in a region. In the study monthly, annual and seasonal trend of mean, maximum and minimum temperature of KBK districts and entire KBK region has been investigated for the period 1901 to 2002 (102 years). Seasonal analysis has also been carried out for the annual mean temperature. The annual mean temperature in the region is 25.43°C. Summer mean temperature reaches up to 30.65°C, whereas it plunges less than 20°C during winter. Similarly, the statistical analysis of the maximum temperature series indicates an average maximum temperature of 31°C, reaches maximum of 35.80°C during summer. The mean maximum temperature in the region during winter hovers

around 28ºC. Annual minimum temperature series indicates a mean temperature of 19.91ºC ranging from 20.91ºC to 18.88ºC. Winter minimum temperature reaches up to 12ºC. In total the temperature variability across KBK region is significant. Both regression method and MK test indicate a significant increasing temperature trend in the mean annual series. The districts like Kalahandi, Koraput, Malkangiri, Nabarangpur, and Nuapada, the increasing temperature trend is significant at alpha = 0.001 level of significance. The seasonal mean temperature is also showing an increasing trend in the region. The northern part of the KBK region covering districts of Sonepur and Bolangir, showing increasing trend at alpha = 0.01 level of significance. The trend detection test for the maximum and minimum temperature series also indicate a significant increasing temperature trend. The Southern and Western part of the KBK region (Nabarangpur, Malkangiri), in particular, are experiencing significant increasing temperature trend at alpha = 0.001 level of significance in comparison to the Northern and Eastern part (Bolangir and Sonepur).

3.5.3 Potential evapotranspiration trend

On investigation of the potential evapotranspiration of the eight districts and whole KBK region, it has been found that the trend is upward in nature i.e. increasing. This indicates a higher crop water requirement in the region in the future.

Overall, the study concludes based on the trend analysis that the region is witnessing significant decreasing trends in annual rainfall in the northern parts covering the districts of Kalahandi, Nuapada and Sonepur which are already facing water scarcity. Southern districts like Koraput and Malkangiri with considerable forest coverage in comparison to other districts in the KBK region are showing increasing rainfall trend. The study also concludes a significant increasing trend in the temperature, both minimum and maximum, in future. This will result in higher crop water requirement by the crops to meet the high evaporation and transpiration losses. How far these trends sustain in long-run requires further investigations using data simulated from different global climate models before finalizing water resources availability, distribution and utilization to meet current and future need.

FUTURE CLIMATE PROJECTION

4.1 DOWNSCALING: CONCEPT AND TECHNIQUES

Climate is a complex system, and is very difficult to quantify its' variables. Precipitation and temperature are important parameters (variables) for climate change impact studies. A proper assessment for past events, and its' future scenarios of the variables are needed for water resources planning. Global Circulation Models (GCMs) are tools available to simulate the ongoing and future changes in climate at global scale. GCMs are numerical models representing the physical processes of the earth-atmosphere-ocean system (Robock et al., 1993; Hewitson and Crane, 1996; Wilby and Wigley, 1997; Prudhomme et al., 2003). These models are of coarse-grid resolution, and of high accuracy at large spatial scales (Bardossy, 1997; Ojha et al., 2010; Hassan and Harun, 2012). However, impact studies by hydrologists and water resources planner require local/ regional-scale hydrological variability to represent local climate phenomena. In climate change studies, the temporal scales could vary from a very short time interval (hourly) to an annual time scale. The spatial resolutions also vary from a few square kilometers (watershed) to several thousand square kilometers (large river basins). General Circulation Models or global climate models (GCMs) have been widely used to represent the global basic climate parameters, but these models are course in resolution and so far could not reproduce well details of regional climate conditions. Hence, there is a great need to develop techniques for downscaling GCM outputs to regional or station scales. By definition, downscaling is the process of transferring general circulation model (GCM) output to a finer spatial scale that is more meaningful for analyzing local and regional climate conditions (Brekke et al., 2009). Basically downscaling is a method to obtain high-resolution climate or climate change information from relatively coarse-resolution GCMs (Fig.4.1 & Fig.4.2). It is based on the view that regional climate is conditioned by climate on larger, for instance continental or even planetary, scales. Information is cascaded "down" from larger to smaller scales. The regional climate is the result of interplay of the overall atmospheric, or oceanic, circulation and of regional specifics, such as topography, land-sea distribution and land-use. As such, empirical/statistical downscaling seeks to derive the local

scale information from the larger scale through inference from the cross-scale relationships, using a random or deterministic function as given:

$$L_c = f(G_c, H_i) \qquad \qquad ...(4.1)$$

Where,

L_c is the local climate response;

G_c is the external large scale natural forcing; and

H_i is the large scale non-natural forcing

Formally, the concept of regional climate being conditioned by the large-scale state may be written as:

$$R = F(L) \qquad \qquad ...(4.2)$$

Where,

R represents the predictand (a set of regional climate variables), L is the predictor (a set of large-scale variables), and F a stochastic and/or deterministic function conditioned by L. In general, F is unknown and is modeled dynamically (i.e., through regional climate models) or empirically from observational (or modeled) data sets. In some cases R and L are the same variables but on different spatial scales.

4.2 ASSUMPTIONS IN DOWNSCALING

When using downscaling for assessing regional climate change, three implicit assumptions are made:

(1) The predictors are variables of relevance and are realistically modeled by the AOGCM.

(2) The transfer function is valid also under altered climatic conditions. This is an assumption that in principle cannot be proven in advance. The observational record should cover a wide range of variations in the past; ideally, all expected future realizations of the predictors should be contained in the observational record.

(3) The predictors employed fully represent the climate change signal. In the following, an overview of statistical and dynamic downscaling is provided.

In recent years, different downscaling methods have been proposed in a number of studies around the world. Hence, different approaches are evolved to downscale the coarse-grid scale GCM data to finer scale surface variables in last few decades. Such methods include canonical correlation analysis, multiple linear regressions, artificial neural networks and support vector machines (Aksornsingchai and Srinilta, 2011; Ghosh and Mujumdar, 2006; Raje and Mujumdar, 2009). Recently, downscaling of precipitation has found wide utility for scenario generation on different time scales. Statistical Downscaling Model (SDSM) is one of the statistical downscaling tools that implement the multiple linear regression model, and provides scenario of daily surface weather variables under the present and future climate forcing. The tool also performs ancillary tasks of data quality control and transformation, pre-screening of predictor variables, model calibration and validation, scenario generation, statistical analysis and its representation of climate data (Wilby and Dawson, 2007).
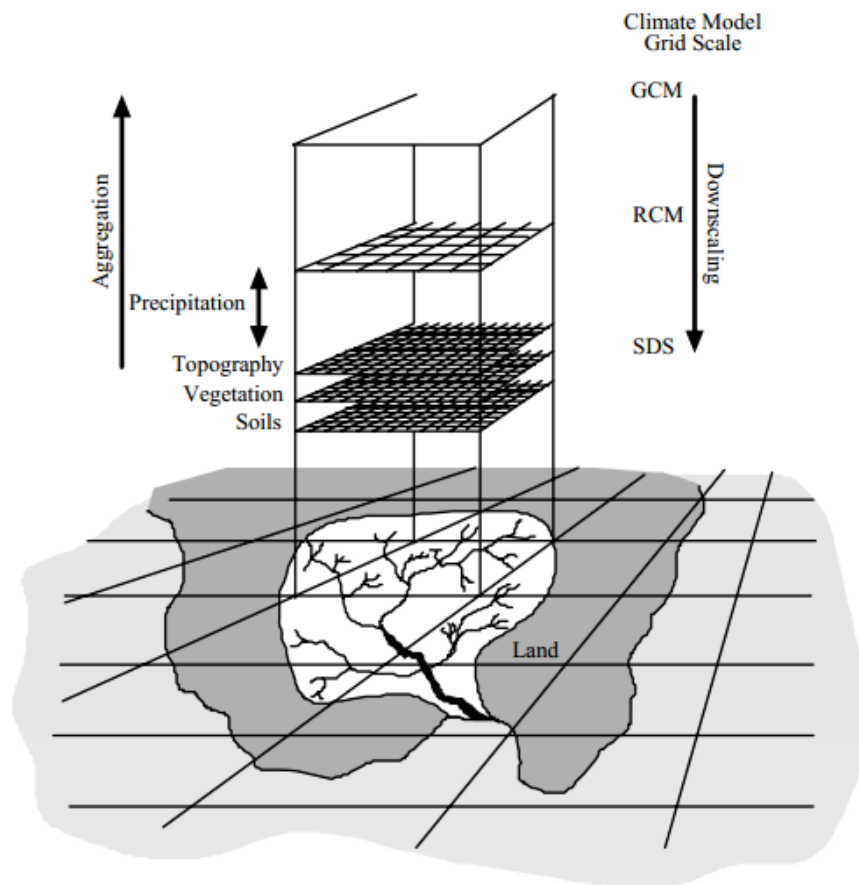
Fig.4.1. Schematic showing downscaling concept
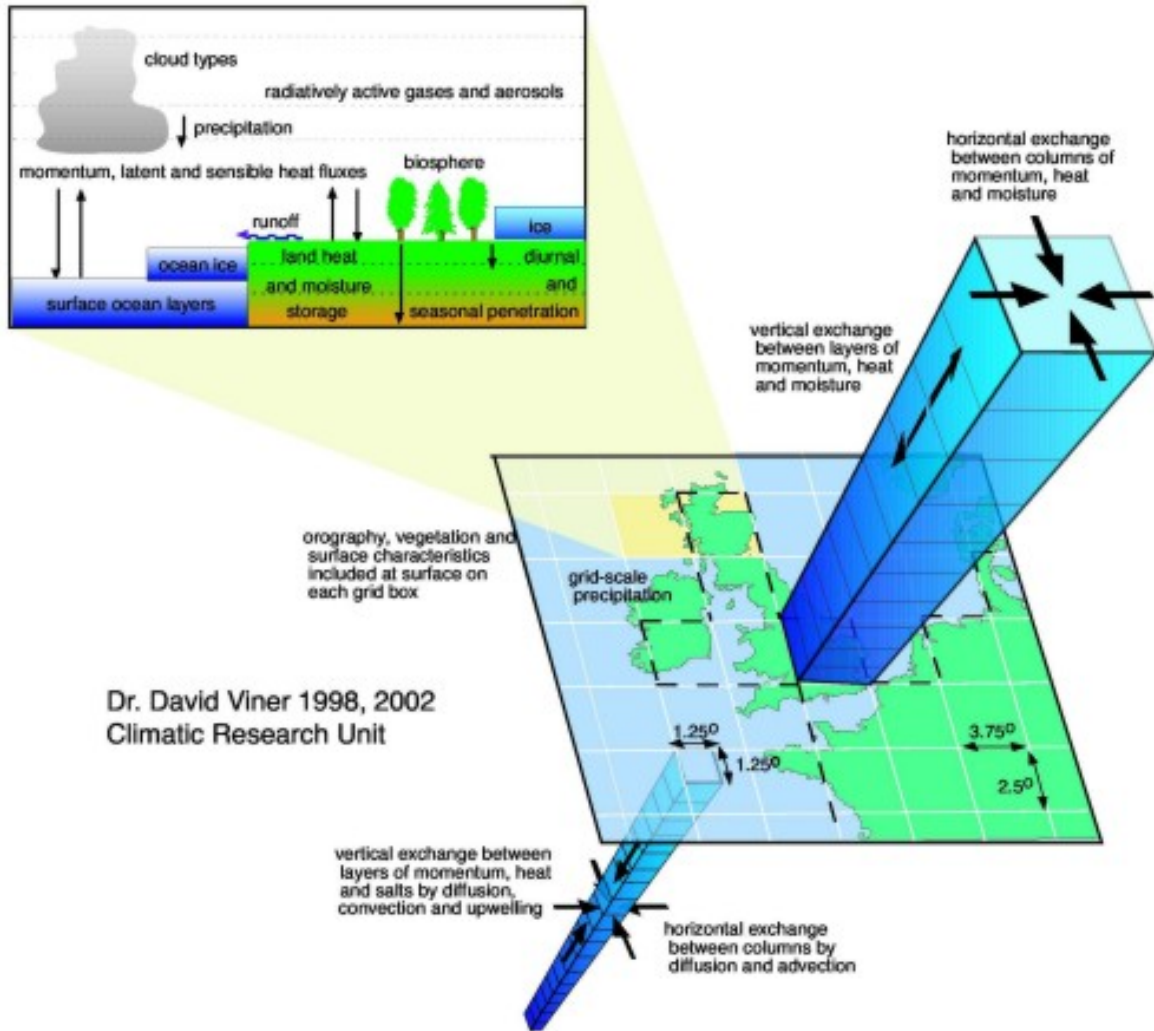
Fig.4.2. Schematic showing climatic modelling

4.3. DOWNSCALING TYPES

Downscaling, or translation across scales, is a term adopted in recent years to describe a set of techniques that relate local- and regional-scale climate variables to the larger scale atmospheric forcing. Conceptually, this is a direct evolution of more traditional techniques in synoptic climatology; however, the downscaling approach was developed specifically to address present needs in global environmental change research, and the need for more detailed temporal and spatial information from Global Climate Models (GCMs). Two general categories exist for downscaling techniques: process based techniques focused on nested models, and empirical techniques using one form or another of transfer function between scales. While in the long term nested models hold the greatest promise for regional-scale analysis, this approach is still in development, requires detailed

surface climate data, and is dependent on high end computer availability. Conversely, empirical relationships offer a more immediate solution and significantly lower computing requirements, consequently offering an approach that can be rapidly adopted by a wider community of scientists (Hewitson and Crane, 1996).

There are two broad categories of downscaling procedures:

i. Dynamical downscaling:

    It involves extraction of regional scale information from large-scale GCM data based on the modeling of regional climate dynamical processes; and

ii. Statistical (or empirical) downscaling:

    It rely on the empirical relationships between modelled large-scale atmospheric variables (predictors) and observed surface climatic variables (predictand).

It has been found that two methods reproduce general features of the basin climatology, but both displayed systematic biases with respect to observations. Between these two techniques, statistical downscaling methods offer several practical advantages over dynamic downscaling methods, especially in terms of flexible adaptation to specific study purposes, and inexpensive computing resource requirements. Several SD techniques have been developed to establish relationships between local weather variables and the large-scale GCMs' results. Amongst statistical downscaling techniques, Statistical Downscaling Model (SDSM) and the stochastic weather generator LARS-WG are widely used tools for generating climate change scenarios for daily precipitations and temperature at local level using GCM modelled data.

4.3.1 SDSM

SDSM is a multi linear regression based spatial downscaling model of daily predictor-predictand relationships. The predictor variables provide daily information concerning the large-scale state of the atmosphere, whilst the predictand describes conditions at the site scale. The SDSM tool (software) reduces the task of statistically downscaling daily weather series into a number of discrete processes:

1. Preliminary screening of potential downscaling predictor variables

   In this step, the model identifies large-scale predictor variables which are significantly correlated with observed station (predictand) data. A number of variables derived from mean sea level pressure fields are included, e.g. air flow strength, meridional and zonal components of air flow, vorticity etc. There are 26 predictor variables.

2. Assembly and calibration of statistical downscaling model(s)

   Here the large-scale predictor variables identified instep 1 are used in the determination of multiple linear regression relationships between these variables and the local station data. Statistical models may be built on a monthly, seasonal or annual basis. Information regarding the amount of variance explained by the model(s) and the standard error is given in order to determine the viability of spatial downscaling for the variable and site in question;

3. Synthesis of ensembles of current weather data using observed predictor variables

   In this process, once the statistical downscaling models have been determined they can be verified by using an independent data set of observed predictors. The stochastic component of SDSM allows the generation of up to 100 ensembles of data which have the same statistical characteristics but which vary on a day-to-day basis;

4. Generation of ensembles of future weather data using GCM

   In this step the derived predictor variables - provision of the appropriate GCM-derived predictor variables allows the generation of ensembles of future weather data by using the statistical relationships calculated in step 2;

5. Diagnostic testing/analysis of observed data and climate change scenarios

   In this step calculation of the statistical characteristics of both the observed and synthetic data in order for easy comparison and thus determination of the effect of spatial downscaling.

4.3.2 LARSWG

LARSWG is also a standard user-friendly downscaling tool (software) consisting of three main sections:

1. Analysis:

   The first step in the weather generation process is the analysis of the observed station data in order to calculate the weather generator parameters, i.e. the statistical characteristics of the data. LARS-WG requires observations for precipitation and one or all of maximum and minimum temperature and sunshine hours or solar radiation. The analysis process uses semi-empirical distributions, i.e. frequency distributions calculated from the observed data, for wet and dry series duration, precipitation amount and solar radiation. Maximum and minimum temperature are described using Fourier series. The resulting parameter file is then used in the generation process.

2. Generator:

   LARS-WG generates synthetic weather data by combining a scenario file containing information about changes in precipitation amount, wet and dry series duration, mean temperature, temperature variability and solar radiation with the parameter files generated in step 1. If LARS-WG is being used to generate synthetic data in order to determine how well the model is simulating observed conditions, or to simulate a longer time series of data for a station with only a short observational record, then the scenario file contains no changes. However, if LARS-WG is being used to generate daily data for a particular scenario of climate change, then the scenario file will contain the appropriate monthly changes.

3. Qtest:

   LARS-WG simplifies the procedure for determining how well it is simulating observed conditions by providing the Qtest option. In this step, the statistical characteristics of the observed data are compared with those of synthetic data generated using the parameters derived from the observed station data. A number of statistical tests, the chi-squared test,

Student's t-test and the F-test, are used to determine whether the distributions, mean values and standard deviations, respectively, of the synthetic data are significantly different from those of the original observed data set.

4.4 SCENARIOS IN DOWNSCALING

4.4.1 SRES Scenarios

Future climate has been modeled through conceptualizing different scenarios based on Future greenhouse gas (GHG) emission. GHG emissions are the product of very complex dynamic systems, determined by driving forces such as demographic development, socio-economic development, and technological change. Their future evolution is highly uncertain. Scenarios are alternative images of how the future might unfold and are an appropriate tool with which to analyze how driving forces may influence future emission outcomes and to assess the associated uncertainties. They assist in climate change analysis, including climate modeling and the assessment of impacts, adaptation, and mitigation. A set of scenarios was developed to represent the range of driving forces and emissions in the scenario literature so as to reflect current understanding and knowledge about underlying uncertainties. They exclude only outlying "surprise" or "disaster" scenarios in the literature. Any scenario necessarily includes subjective elements and is open to various interpretations (Special Report on Emissions Scenarios, SRES, IPCC, 2000). Four different narrative storylines were developed to describe consistently the relationships between emission driving forces and their evolution and add context for the scenario quantification. Each storyline represents different demographic, social, economic, technological, and environmental developments, which may be viewed positively by some people and negatively by others. The scenarios cover a wide range of the main demographic, economic, and technological driving forces of GHG and sulfur emissions2 and are representative of the literature. Each scenario represents a specific quantitative interpretation of one of four storylines. All the scenarios based on the same storyline constitute a scenario "family". For each storyline several different scenarios were developed using different modeling approaches to examine the range of outcomes arising from a range of models that use similar assumptions about driving forces (Fig.4.3). Six models were used which are representative of integrated assessment frameworks in the literature. One advantage of a multi-model approach is that the resultant 40 SRES scenarios together encompass the current range of uncertainties of future

GHG emissions arising from different characteristics of these models, in addition to the current knowledge of and uncertainties that arise from scenario driving forces such as demographic, social and economic, and broad technological developments that drive the models, as described in the storylines. Thirteen of these 40 scenarios explore variations in energy technology assumptions. They cover a wide range of key "future" characteristics such as demographic change, economic development, and technological change. These are described as storyline and scenario.

- The A1 storyline and scenario family
  - This scenario describes a future world of very rapid economic growth, global population that peaks in mid-century and declines thereafter, and the rapid introduction of new and more efficient technologies. Major underlying themes are convergence among regions, capacity building, and increased cultural and social interactions, with a substantial reduction in regional differences in per capita income. The A1 scenario family develops into three groups that describe alternative directions of technological change in the energy system. The three A1 groups are distinguished by their technological emphasis: fossil intensive (A1FI), non-fossil energy sources (A1T), or a balance across all sources (A1B).

The main characteristics of the four SRES storylines and scenario families

Figure 1: Schematic illustration of SRES scenarios. Four qualitative storylines yield four sets of scenarios called "families": A1, A2, B1, and B2. Altogether 40 SRES scenarios have been developed by six modeling teams. All are equally valid with no assigned probabilities of occurrence. The set of scenarios consists of six scenario groups drawn from the four families: one group each in A2, B1, B2, and three groups within the A1 family, characterizing alternative developments of energy technologies: A1FI (fossil fuel intensive), A1B (balanced), and A1T (predominantly non-fossil fuel). Within each family and group of scenarios, some share "harmonized" assumptions on global population, gross world product, and final energy. These are marked as "HS" for harmonized scenarios. "OS" denotes scenarios that explore uncertainties in driving forces beyond those of the harmonized scenarios. The number of scenarios developed within each category is shown. For each of the six scenario groups an illustrative scenario (which is always harmonized) is provided. Four illustrative marker scenarios, one for each scenario family, were used in draft form in the 1998 SRES open process and are included in revised form in this Report. Two additional illustrative scenarios for the groups A1FI and A1T are also provided and complete a set of six that illustrates all scenario groups. All are equally sound.

Fig.4.3 Schematic showing scenarios

➢ The A2 scenario family

    o It is based on a high population growth scenario of 15 billion by 2100 that assumes a significant decline in fertility for most regions and stabilization at above replacement levels. The A2 storyline and scenario family describes a very heterogeneous world. The underlying theme is self-reliance and preservation of local identities. Fertility patterns across regions converge very slowly, which results in continuously increasing global population. Economic development is primarily regionally oriented and per capita economic growth and technological change are more fragmented and slower than in other storylines.

- The B1 storyline and scenario family
  - describes a convergent world with the same global population that peaks in midcentury and declines thereafter, as in the A1 storyline, but with rapid changes in economic structures toward a service and information economy, with reductions in material intensity, and the introduction of clean and resource-efficient technologies. The emphasis is on global solutions to economic, social, and environmental sustainability, including improved equity, but without additional climate initiatives.
- The B2 storyline and scenario family
  - describes a world in which the emphasis is on local solutions to economic, social, and environmental sustainability. It is a world with continuously increasing global population at a rate lower than A2, intermediate levels of economic development, and less rapid and more diverse technological change than in the B1 and A1 storylines.

4.4.2 Representative Concentration Pathways (RCPs)

The Representative Concentration Pathways (RCP) is the latest generation of scenarios that provide input to climate models. Scenarios have long been used by planners and decision makers to analyze situations in which outcomes are uncertain. In climate research, emissions scenarios are used to explore how much humans could contribute to future climate change given uncertainties in factors such as population growth, economic development, and development of new technologies. Projections and scenarios of future social and

> **Gases and Pollutants included in RCPs**
>
> Greenhouse gases: CO_2, methane, nitrous oxide, several groups of fluorocarbons and sulphur hexafluoride.
> Aerosols and chemically active gasses: Sulphur dioxide, soot, organic carbon, carbon monoxide, nitrogen oxides, volatile organic compounds, ammonia

environmental conditions are also used to explore how much impact lesser or greater amounts of climate change would have on different possible states of the world, for example futures with greater or lesser amounts of poverty. The purpose of using scenarios is not to predict the future, but to explore both the scientific and real-world implications of different plausible futures. Over

time, a variety of approaches to scenarios in climate research have been used. An overview of several of the most prominent sets of emissions scenarios is provided in Table 4.1.

Table 4.1: History of scenarios

Year	Name	Used in
1990	SA90	First Assessment Report
1992	IS92	Second Assessment Report
2000	SRES – Special Report on Emissions and Scenarios	Third and Fourth Assessment Report
2009	RCP – Representative Concentration Pathways	Fifth Assessment Report

RCPs are time and space dependent trajectories of concentrations of greenhouse gases and pollutants resulting from human activities, including changes in land use. RCPs provide a quantitative description of concentrations of the climate change pollutants in the atmosphere over time, as well as their radiative forcing in 2100 (for example, RCP 6 achieves an overall impact of 6 watts per square metre by 2100). The word "representative" signifies that each

Radiative forcing, expressed as Watts per square metre, is the additional energy taken up by the Earth system due to the enhanced greenhouse effect. More precisely, it can be defined as the difference in the balance of energy that enters the atmosphere and the amount that is returned to space compared to the pre-industrial situation. Total radiative forcing is determined by both positive forcing from greenhouse gases and negative forcing from aerosols. The dominant factor by far is the positive forcing from CO_2. As the radiative forcing increases, the global temperature rises. However, the precise relationship between these factors is not fully

RCP provides only one of many possible scenarios that would lead to the specific radiative forcing pathway. Radiative forcing is a measure of the additional energy taken up by the Earth system due to increases in climate change pollution (Fig.4.4). A key difference between the new RCPs and the previous scenarios is that there are no fixed sets of assumptions related to population growth, economic development, or technology associated with any RCP. Many different socio-economic futures are possible leading to the same level of radiative forcing. This enables researchers to test various permutations of climate policies and social, technological, and economic circumstances. Another key difference is that the RCPs are spatially explicit and provide information a global grid at a resolution of approximately 60 kilometres. This gives the spatial and temporal information about the location of various emissions and land use changes.

This is an important improvement as the location of some emissions affects their warming potential. The four RCPs are consistent with certain socio-economic assumptions. Those are:

- RCP 8.5 – High emissions

  This RCP is consistent with a future with no policy changes to reduce emissions. It was developed by the International Institute for Applied System Analysis in Austria and is characterized by increasing greenhouse gas emissions that lead to high greenhouse gas concentrations over time. This scenario is comparable to scenario A1 F1.

  This future is consistent with:

  - Three times today's CO_2 emissions by 2100
  - Rapid increase in methane emissions
  - Increased use of croplands and grassland which is driven by an increase in population
  - A world population of 12 billion by 2100
  - Lower rate of technology development
  - Heavy reliance on fossil fuels
  - High energy intensity
  - No implementation of climate policies

- RCP 6 – High emissions

  This RCP is developed by the National Institute for Environmental Studies in Japan. Radiative forcing is stabilised shortly after year 2100, which is consistent with the application of a range of technologies and strategies for reducing greenhouse gas emissions. It is comparable to SRES scenario: B2.

  This future is consistent with:

  - Heavy reliance on fossil fuels
  - Intermediate energy intensity
  - Increasing use of croplands and declining use of grasslands
  - Stable methane emissions
  - CO_2 emissions peak in 2060 at 75 per cent above today's levels, then decline to 25 per cent above today

- RCP 4.5 – Intermediate emissions

This RCP is developed by the Pacific Northwest National Laboratory in the US. Here radiative forcing is stabilised shortly after year 2100, consistent with a future with relatively ambitious emissions reductions. This scenario is comparable SRES scenario: B1.

This future is consistent with:

- o Lower energy intensity
- o Strong reforestation programmes
- o Decreasing use of croplands and grasslands due to yield increases and dietary changes
- o Stringent climate policies
- o Stable methane emissions
- o CO_2 emissions increase only slightly before decline commences around 2040

- RCP 2.6 – Low emissions

This RCP is developed by PBL Netherlands Environmental Assessment Agency. Here radiative forcing reaches 3.1 W/m2 before it returns to 2.6 W/m2 by 2100. In order to reach such forcing levels, ambitious greenhouse gas emissions reductions would be required over time. There is no comparable SRES scenario.

This future would require:

- o Declining use of oil
- o Low energy intensity
- o A world population of 9 billion by year 2100
- o Use of croplands increase due to bio-energy production
- o More intensive animal husbandry
- o Methane emissions reduced by 40 per cent
- o CO_2 emissions stay at today's level until 2020, then decline and become negative in 2100
- o CO_2 concentrations peak around 2050, followed by a modest decline to around 400 ppm by 2100
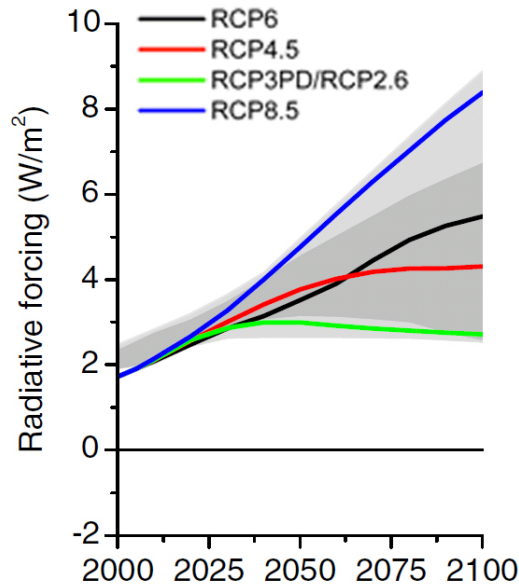
Fig. 4.4. Schematic showing RCPs

4.5 DYNAMIC DOWNSCALING TECHNIQUES

Dynamic downscaling techniques consist of using the outputs of a global climate model as lateral boundary conditions for more sophisticated models of a limited geographic area and with a higher resolution in space. Dynamical downscaling uses regional climate models (RCMs) to simulate finer-scale physical processes consistent with the large scale weather evolution prescribed from a GCM. In dynamical downscaling, a regional climate model (RCM) uses GCM output as initial and lateral boundary conditions over a region of interest. A RCM is a downscaling tool that adds fine scale (high resolution) information to the large-scale projections of a global general circulation model (GCM). According to IPCC, GCMs representing physical processes in the atmosphere, ocean, cryosphere and land surface, are the most advanced tools currently available for simulating the response of the global climate system to increasing GHG concentrations. While simpler models have also been used to provide globally- or regionally-averaged estimates of the climate response, only GCMs, possibly in conjunction with nested regional models, have the potential to provide geographically and physically consistent estimates of regional climate change which are required in impact analysis. GCMs depict the climate using a three dimensional grid over the globe, typically having a horizontal resolution of between 250 and 600 km, 10 to 20 vertical layers in the atmosphere and sometimes as many as 30 layers in the oceans. Their resolution is thus quite coarse relative to the scale of exposure units in most impact

assessments. Moreover, many physical processes, such as those related to clouds, also occur at smaller scales and cannot be properly modeled. Instead, their known properties must be averaged over the larger scale in a technique known as parameterization. This is one source of uncertainty in GCM-based simulations of future climate. Others relate to the simulation of various feedback mechanisms in models concerning, for example, water vapour and warming, clouds and radiation, ocean circulation and ice and snow albedo. For this reason, GCMs may simulate quite different responses to the same forcing, simply because of the way certain processes and feedbacks are modeled. GCMs can provide predictions of changes in climate down to scales of a few hundred kilometers or so at best. Currently the resolution of the atmospheric part of a typical GCM is about 250 km in the horizontal with 20 levels in the vertical. The resolution of a typical ocean model is 125 km to 250 km, with, again, 20 levels from the sea surface to the ocean floor. Hence GCMs make projections at a relatively coarse resolution and cannot represent the fine-scale detail that characterizes the climate in many regions of the world, especially in regions with complex orography or heterogeneous land surface cover or coastlines. As a result, "GCMs cannot access the spatial scales that are required for climate impact and adaptation studies" (WMO, 2002). Historically, GCMs have been the primary source of information for constructing climate scenarios and will always provide the basis of comprehensive assessments of climate change at all scales from local to global. GCMs predictions may be adequate where the terrain is reasonably flat and uniform, and away from coasts. However, in areas where coasts and mountains have a significant effect on weather (and this will be true for most parts of the world), scenarios based on global models will fail to capture the local detail needed for impacts assessments at a national and regional level. Also, at such coarse resolutions, extreme events such as cyclones or heavy rainfall are either not captured or their intensity is unrealistically low. The best method for adding this detail to global predictions is to use a regional climate model (RCM). GCMs are typically run with horizontal scales of 300km; regional models can resolve features down to 50km or less. This makes for a more accurate representation of many surface features, such as complex mountain topographies and coastlines. It also allows small islands and peninsulas to be represented realistically, whereas in a global model their size (relative to the model gridbox) would mean their climate would be that of the surrounding ocean. RCMs are full climate models, and as such are physically based. They represent most if not all of the processes, interactions and feedbacks between climate system components represented in GCMs. They

produce a comprehensive set of output data over the model domain. A regional climate model (RCM) has a high resolution (typically 50 km) and covers a limited area of the globe (typically 5,000 km x 5,000 km). It is a comprehensive physical model, usually of the atmosphere and land surface, containing representations of the important processes in the climate system (e.g. clouds, radiation, rainfall, soil hydrology) as are found in a GCM. A RCM does not generally include an ocean component; this would increase complexity and need more computing power; in any case, most applications for impacts' assessments require only land surface or atmospheric data. Given that RCMs are limited area models they need to be driven at their boundaries by time-dependent large scale fields (e.g., wind, temperature, water vapour and surface pressure). These fields are provided either by analyses of observations or by GCM integrations in a buffer area that is not considered when analyzing the results of the RCM. RCM predictions of ideally 30 years (e.g. the period 2071-2100) are needed to provide robust climate statistics, e.g. distributions of daily rainfall or intra-seasonal variability. There are many different RCMs currently available, for various regions, developed at different modeling centers around the world. The different RCMs produce different high resolution scenarios for a given boundary forcing, due to differences in model formulation, but also due to small-scale internal variability generated by the RCM. There has been considerable international effort recently to quantify uncertainty in regional climate change through the inter-comparison of multiple RCMs. The typical grid size of RCM simulations to date has been 25 km or 50 km. However, recently RCM simulations with grid scales below 20 km have become available for Europe and RCMs with grid sizes of 5km or less are being developed at several modeling centers. For example a 5 km RCM has been developed over Japan.

4.5.1 HadCM3

HadCM3 (*Hadley Centre Coupled Model, version 3*) is a coupled atmosphere-ocean general circulation model (AOGCM) developed at the Hadley Centre in the United Kingdom. It was one of the major models used by the IPCC. HadCM3 does not need flux adjustment (additional "artificial" heat and freshwater fluxes at the ocean surface) to produce a good simulation. The higher ocean resolution of HadCM3 is a major factor in this; other factors include a good match between the atmospheric and oceanic components; and an improved ocean mixing scheme. HadCM3 is composed of two components: the atmospheric model HadAM3 and the ocean model (which includes a sea ice model). The atmospheric component of the model has 19 levels

with a horizontal resolution of 2.5 degrees of latitude by 3.75 degrees of longitude, which produces a global grid of 96 x 73 grid cells. This is equivalent to a surface resolution of about 417 km x 278 km at the Equator, reducing to 295 km x 278 km at 45 degrees of latitude. The atmosphere component of the model also optionally allows the transport, oxidation and removal by physical deposition and rain out of anthropogenic sulphur emissions to be included interactively. This permits the direct and indirect forcing effects of sulphate aerosols to be modeled given scenarios for sulphur emissions and oxidants. The oceanic component of the model has 20 levels with a horizontal resolution of 1.25 x 1.25 degrees. At this resolution it is possible to represent important details in oceanic current structures.

4.5.2 HadRM3

The third generation Hadley Centre RCM (HadRM3) is based on the latest GCM, HadCM3. It has a horizontal resolution of 50 km with 19 levels in the atmosphere (from the surface to 30 km in the stratosphere) and four levels in the soil. In addition to a comprehensive representation of the physical processes in the atmosphere and land-surface, it also includes the sulphur cycle. This enables it to estimate the concentration of sulphate aerosol particles produced from SO2 emissions. These have a cooling effect as they scatter back sunlight and also produce brighter clouds by allowing smaller water droplets to form. The IPCC SRES emission scenarios show substantial changes in SO2 emissions in the future, so it is important that the RCM can calculate their effect.

Developing, setting up and using a regional model over a specific area of the globe requires a considerable amount of effort from an experienced climate modeler. In addition, RCMs (like GCMs) are usually run on large computing installations. Both these factors effectively exclude many developing countries from producing climate change predictions and scenarios. The Hadley Centre has configured its third-generation Hadley Centre RCM to PRECIS so that it is easy to set up and can be run over any area of the globe on a relatively inexpensive fast PC.

4.5.3 PRECIS

PRECIS (*Providing Regional Climates for Impacts Studies)* is a regional modelling system that can be run over any area of the globe on a relatively inexpensive, fast PC to provide regional climate information for impacts studies. The PRECIS climate model is an atmospheric and land surface model of limited area and high resolution which is locatable over any part of the globe. Dynamical flow, the atmospheric sulphur cycle, clouds and precipitation, radiative processes, the

land surface and the deep soil are all described. The model requires prescribed surface and lateral boundary conditions. Surface boundary conditions are only required over water, where the model needs time series of surface temperatures (sea-surface temperatures, SSTs) and ice extents. If this information is taken directly from a coupled GCM then its coarse resolution means that there could be quite large regional errors in the data, and for coastal points and inland seas they may have to be interpolated or extrapolated which could lead to even larger errors locally. An alternative is to use observed values (at higher resolution) for the GCM and RCM simulations of present day climate and then obtain values for the future by adding on changes in the SSTs and sea ice extent and thickness from a coupled GCM. The Hadley Centre has used the second of the above approaches. Observed SSTs and sea-ice (on a 1° grid) are used with an atmosphere-only GCM for the present-day simulation (which then provides lateral boundary conditions for the RCM present-day simulation). Lateral boundary conditions provide dynamical atmospheric information at the latitudinal and longitudinal edges of the model domain. There is no prescribed constraint at the upper boundary of the model. The lateral boundary conditions comprise the standard atmospheric variables of surface pressure, horizontal wind components and measures of atmospheric temperature and humidity. Also, as certain configurations of the PRECIS RCM contain a full representation of the sulphur cycle, a set of boundary conditions (including sulphur dioxide, sulphate aerosols and associated chemical species) are also required for this. These lateral boundary conditions are updated every six hours; surface boundary conditions are updated every day.

Application of the PRECIS is essentially a three-stage process comprising:

1) Running the PRECIS RCM over the area of interest to provide simulations of a recent climate period (e.g. 1961-90), and comparing these with observations, to validate the model;

2) Running the PRECIS RCM to provide climate change projections for the region of interest; the regional model is supplied with GCM fields from the Hadley Centre, although the system is being developed to use fields from other climate models; and

3) Deriving relevant climate information from these projections guided by an understanding of the needs of the impacts models and an assessment of the climate models' performance and projections.

An assessment of impact of climate change in 2030s on four key sectors of the Indian economy, namely Agriculture, Water, Natural Ecosystems & Biodiversity and Health in four climate

sensitive regions of India, namely the Himalayan region, the Western Ghats, the Coastal Area and the North-East Region has been carried out by the Ministry of Environment and Forest (MOEF 2010). The work was undertaken by the Indian Network for Climate Change Assessment (INCCA), a network-based programme that brings together over 120 institutions and over 220 scientists from across the country to undertake scientific assessments of different aspects of climate change. The 4x4 Assessment examines the implications of climate change for India in 2030s deduced from a Regional Climate Model HadRM3 (Hadley Centre Regional Model Version 3) run for A1B scenario PRECIS was used as the regional climate model.

4.6 STATISTICAL DOWNSCALING METHODS

Statistical (or empirical) downscaling methodologies can be classified into three categories according to the computational techniques used:

i.   Weather typing approaches;

ii.   Regression methods; and

iii.   Stochastic weather generators.

In general, statistical (or empirical) downscaling methods require three common assumptions:

(i) the surface local-scale parameters are a function of synoptic forcing; (ii) the GCM used for deriving downscaled relationships is valid at the scale considered; and (iii) the derived relationships remain valid under changing climate conditions.

4.7 COMPARISON OF DYNAMICAL AND STATISTICAL DOWNSCALING METHODS

Few formal comparative studies of different regionalization techniques have been carried out. To date, published work mostly focused on the comparison between regional climate model and statistical downscaling techniques. General advantages and disadvantages associated with statistical and dynamical classes of downscaling methods have been listed in Table 4.2.

Table 4.2: General advantages and disadvantages associated with statistical and dynamical classes of downscaling methods

	Statistical	**Dynamical**
Advantages	• Comparatively cheap and computationally efficient • Can provide point-scale climatic variables from GCM-scale output • Able to directly incorporate observations into method	• Produces responses based on physically consistent processes • Produces finer-resolution information from GCM-scale output that can resolve atmospheric processes on a smaller scale (for example, orographic and rain shadow effects in mountainous areas)
Disadvantages	• Does not account for non-stationarity in the predictor-predictand relationship • Climate system feedbacks not included • Dependent on GCM boundary forcing; affected by biases in underlying GCM • Dependent on statistical or empirical model structure and associated parameters; different models will give different results	• Computationally intensive • Limited number of scenario ensembles available • Dependent on GCM boundary forcing; affected by biases in underlying GCM • Dependent on RCM parameterizations; different RCMs will give different results

4.8 UNCERTAINTY IN DOWNSCALING

There are several levels of uncertainty in the generation of regional climate change information. The first level is associated with emission scenarios. The second level of uncertainty is related to the simulation of the transient climate response by coupled AOGCMs for a given emission scenario. This uncertainty is important both, when coupled AOGCM information is used for impact work without the intermediate step of a regionalization tool, and when AOGCM fields are used to drive a regionalization technique. The final level of uncertainty occurs when the coupled AOGCM data are processed through a regionalization method. Overall, the natural variability of the climate system adds a further level of uncertainty in the evaluation of a climate change simulation.

4.9 APPROACH AND METHODOLOGY

4.9.1 General

Climate models are essentially computer programs which describe the most important components, processes and interactions in the climate system, such as the frequency and magnitude of monsoons, El Niños and other climate modes. In order to calculate how human activities could affect the climate system, scientists insert greenhouse gas concentrations, pollution, and changes in land use and land cover to their models. These factors influence the Earth's climate. How much emissions and land use change scientists should add depends on future social and economic development, including economic growth, technological change, innovation, population growth and urbanization. This information is provided by scenarios produced by the integrated assessment models.

In the present research work, the water resources in the KBK region requires to be assessed in the future climate. Alternatively, this can be explained that future impact of climate change on the water resources in the KBK region to be assessed. In this situation, one has to project the climate in future. A climate projection is usually a statement about the likelihood that something will happen several decades to centuries in the future if certain influential conditions develop. Scenarios however, are not projections or predictions, but rather represent alternative, possible ways in which the future may unfold. In the study, GCM HadCM A2 and B2 scenarios have been utilized to downscale the large scale predictors with local predictant (observed variable). Both rainfall and temperature (max) have been downscaled using Statistical Downscaling Model (SDSM). The Statistical Downscaling Model (SDSM) is a multiple regression-based tool, introduced by Wilby et al. (2002), for generating future scenarios to assess the impact of climate change. It has the ability to capture the inter-annual variability better than other statistical downscaling approaches, e.g. weather generators, weather typing. The model requires two types of daily data, the first type corresponds to local data known as 'Predictand' (Precipitation, temperature) and the second type corresponds to large-scale data of different atmospheric variables known as 'Predictors'(NCEP reanalysis data and simulated GCM based data), for downscaling. Formulating an empirical relationship between predictand and predictors is central to the downscaling technique. This can be achieved by methods, both parametric (Multiple

Linear Regression) and non-parametric (Artificial Neural Network; Support Vector Machine). The study has been carried out using SDSM tool version 4.2.9 (Fig.4.5).

4.9.2 SDSM Tool

The SDSM tool (software) reduces the task of statistically downscaling daily weather series into a number of discrete processes:

1. Preliminary screening of potential downscaling predictor variables

   In this step, the model identifies large-scale predictor variables which are significantly correlated with observed station (predictand) data. A number of variables derived from mean sea level pressure fields are included, e.g. air flow strength, meridional and zonal components of air flow, vorticity etc. There are 26 predictor variables.

2. Assembly and calibration of statistical downscaling model(s)

   Here the large-scale predictor variables identified instep 1 are used in the determination of multiple linear regression relationships between these variables and the local station data. Statistical models may be built on a monthly, seasonal or annual basis. Information regarding the amount of variance explained by the model(s) and the standard error is given in order to determine the viability of spatial downscaling for the variable and site in question;

3. Synthesis of ensembles of current weather data using observed predictor variables

   In this process, once the statistical downscaling models have been determined they can be verified by using an independent data set of observed predictors. The stochastic component of SDSM allows the generation of up to 100 ensembles of data which have the same statistical characteristics but which vary on a day-to-day basis;

4. Generation of ensembles of future weather data using GCM

   In this step the derived predictor variables - provision of the appropriate GCM-derived predictor variables allows the generation of ensembles of future weather data by using the statistical relationships calculated in step 2;

5. Diagnostic testing/analysis of observed data and climate change scenarios

In this step calculation of the statistical characteristics of both the observed and synthetic data in order for easy comparison and thus determination of the effect of spatial downscaling.

Fig. 4.5 Window showing SDSM model

4.9.3 Procedure adopted in SDSM

4.9.3.1 Selection of predictors

For downscaling predictand, the selection of suitable predictors is one of the most important and time consuming steps during downscaling. The appropriate predictor variables are selected

through scatter plots, correlation and partial correlation analysis performed between the predictand of interest and predictors. The observed daily NCEP reanalysis data set for the periods 1961-2001 was used to identify the predictors (Fig. 4.6).

4.9.3.2 Model calibration and validation

Model calibration involves development of an empirical relationship, here multiple linear regression, between the predictand of interest and identified daily observed predictors. Part of the NCEP reanalysis data for the period 1961-1991 is used for model calibration, and remaining data between 1992-2001 for validation. Validation process enables to produce synthetic daily data based on inputs of the data not considered during model calibration and the formulated regression model. The model performance was evaluated based on the coefficient of correlation (R), defined as:

$$R = \frac{\sum \left(X_{obs} - \overline{X}_{obs}\right)\left(X_{mod} - \overline{X}_{mod}\right)}{\sqrt{\sum \left(X_{obs} - \overline{X}_{obs}\right)^2 \sum \left(X_{obs} - \overline{X}_{obs}\right)^2}} \qquad (4.1)$$

Where,

X_{obs} = Observed value; $\overline{X}_{obs}$ = Mean observed value; X_{mod} = Modelled value; $\overline{X}_{mod}$ = Mean modelled value.

4.9.3.3 Scenario generation

The validated regression model is applied to generate future scenario for the region utilizing the simulated HadCM3 A2 GCMs data. The study assumes that the relationship between predictor and predictand remains valid under the future climate conditions. Twenty ensembles of daily synthetic precipitation for a period of 139 years (1961-2099) have been generated. The ensemble values are averaged and divided into three separate time period viz. 2020s (2011-2040), 2050s (2041-2070) and 2080s (2071-2099).
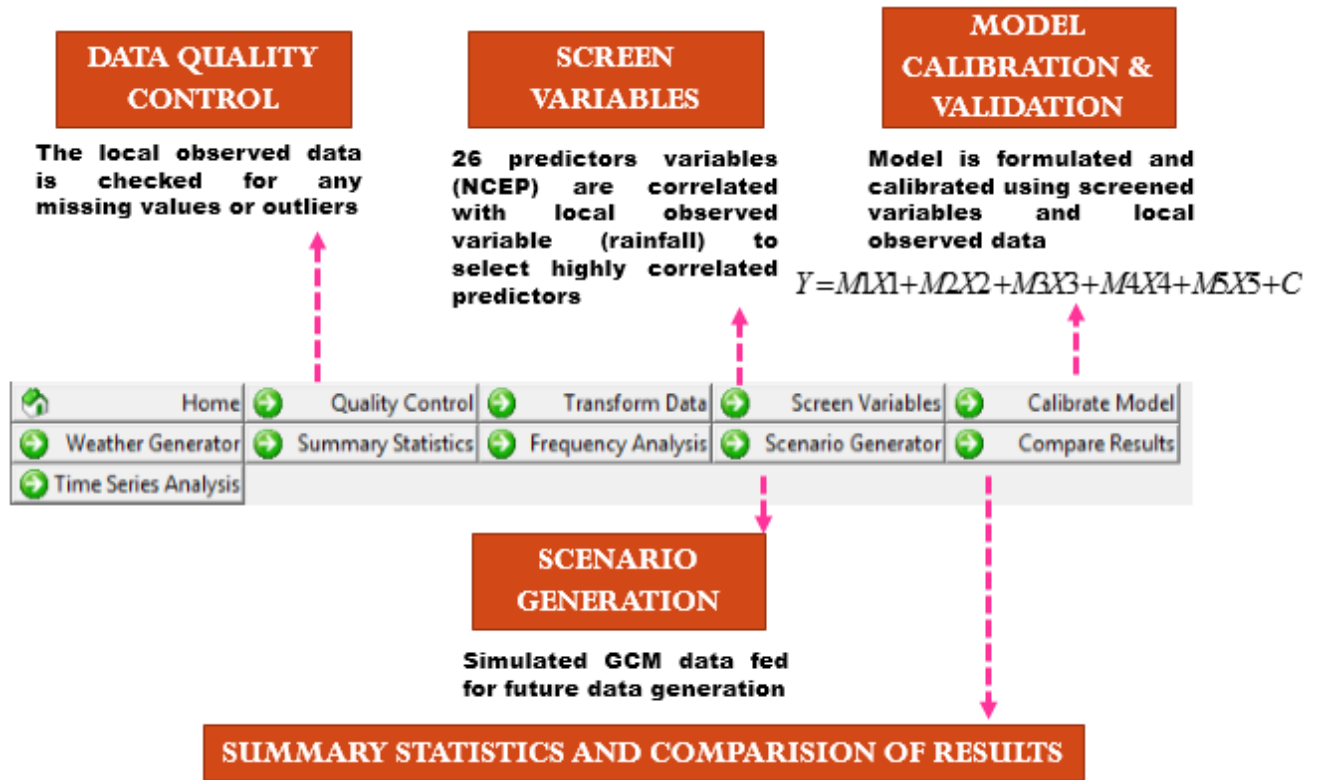
Fig. 4.6 Schematic showing steps in SDSM model

4.9.4 Data used

4.9.4.1 Meteorological data

The daily precipitation data were collected from India Meteorological Department (IMD), Pune for the periods 1961 to 2001. The daily data were converted to monthly, seasonal and annual time scale before analysis is done.

4.9.4.2 Reanalysis data

The daily observed predictor data (re-analysis data) of atmospheric variables, derived from the National Center of Environmental Prediction (NCEP) on 2.50 latitude x 2.50 longitude grid-scale for 41 years (1961–2001) are obtained from the Canadian Climate Impacts Scenarios (CCIS) website (http://www.cics.uvic.ca/scenarios/sdsm/select.cgi).

4.9.4.3 GCM data

The large-scale daily predictors of Hadley Center's GCM (HadCM3) for HadCM3 A2 future scenarios for 139 years (1961–2099) on 3.750 latitude x 3.750 longitude grid-scale are obtained from the Canadian Climate Impacts Scenarios (CCIS) website (http://www.cics.uvic.ca/scenarios/sdsm/select.cgi). Among the SRES scenarios A2, being the worst case scenario with high emission projection in future, was considered. HadCM3 is a coupled atmosphere-ocean GCM developed at the Hadley Centre of the United Kingdom's National Meteorological Service. HadCM3 has been chosen because of its' wider acceptance in many climate change impact studies. Further, it provides daily predictor variables, which can be exclusively used for the SDSM model.

4.10 RESULTS AND DISCUSSION
4.10.1 Downscaling daily precipitation
4.10.1.1 Selection of predictor variables

The selection of predictor variables is the most significant and time consuming step in statistical downscaling. A list of predictor variables (NCEP and GCM) of a grid-box closest to the KBK region is presented in Table 4.3. A total of 26 large-scale predictor variables have been considered in the initial screening process. These are categorized into six types based on the atmospheric pressure level. The predictors are selected based on correlation and partial

correlation analysis of NCEP predictors and observed weather variables for the period 1961-2003 in SDSM. Variables with higher correlation coefficients between precitand (precipitation) and predictors (NCEP) are chosen for model formulation for scenario generation. The selected predictors with their corresponding correlation coefficients, partial correlation and p value are given in Table 4.4. The scatter plot between selected predictors and observed variable are shown in Fig.4.7. These statistics help to identify the amount of explanatory power that is unique to each predictor. A 5% significance level ($p<0.05$) is used to test the significance of predictor-predictand correlation. 5 predictor variables are choosen based on correlation. Those are: ncepmslpas; ncepp5_zas; ncepp850as; ncepr500as; ncepshumas.

Table 4.3: Name and description of all NCEP and GCM predictors

Sl. No.	Atmospheric pressure level	NCEP Variables	Name	Unit
A.	1013.25 hPa (1)	MSL pressure	mslp	Pa
B.	1000 hPa (6)	Wind speed (Geostrophic)	p_f	m/s
		Zonal (Eastward) velocity (U-component)	p_u	m/s
		Meridional (Northward) velocity (V-component)	p_v	m/s
		Vorticity	p_z	s^{-1}
		Wind direction	p_th	Degree
		Divergence	p_zh	s^{-1}
C	850 hPa (8)	Wind speed (Geostrophic)	p8_f	m/s
		Zonal (Eastward) velocity (U-component)	p8_u	m/s
		Meridional (Northward) velocity (V-component)	p8_v	m/s
		Vorticity	p8_z	s^{-1}
		Wind direction	p8_th	Degree
		Divergence	p8_zh	s^{-1}
		Geopotential height	p850	M
		Relative humidity	r850	%
D	500 hPa (8)	Wind speed (Geostrophic)	p5_f	m/s
		Zonal (Eastward) velocity (U-component)	p5_u	m/s
		Meridional (Northward) velocity (V-component)	p5_v	m/s
		Vorticity	p5_z	s^{-1}
		Wind direction	p5_th	
		Divergence	p5_zh	s^{-1}
		Geopotential height	p500	M

		Relative humidity	r500	%
E	Near surface (3)	Specific humidity	shum	g/kg
		Mean temperature	temp	^0C
		Relative humidity	rhum	%

Table 4.4: Selected NCEP predictors with correlation coefficient, partial correlation and p value

Sl No.	Selected Predictors	Correlation coefficients	Partial correlation	P value
1	ncepmslpas	0.374	0.128	0.0001
2	ncepp5_zas	0.320	0.089	0.0001
3	ncepp850as	0.344	0.062	0.0006
4	ncepr500as	-0.214	-0.058	0.0013
5	ncepshumas	-0.239	0.056	0.0022
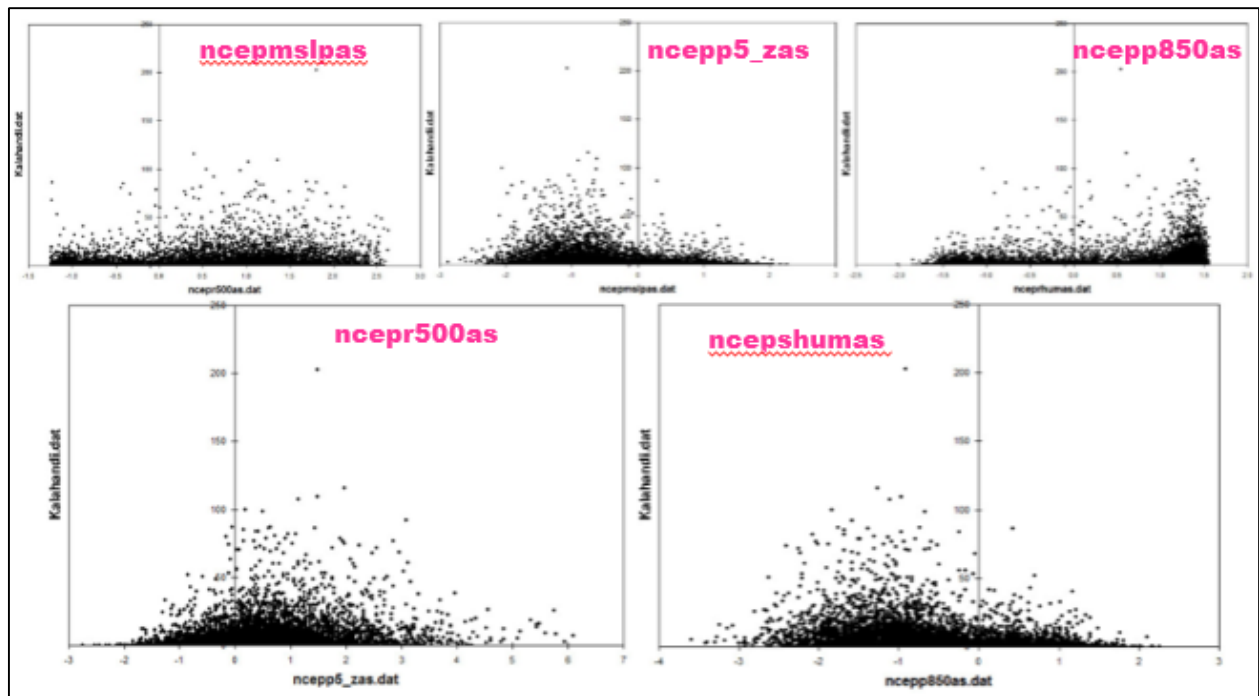
Fig.4.7. Scatter plots between predictand and selected NCEP predictors

4.10.1.2 Model Calibration and Validation

The model calibration process formulates downscaling model based on multiple regressions between the predictand (observed precipitation) and selected NCEP predictors. Since the predictand-predictor relationship is governed by wet-day occurrence, an intermediate process

in the case of precipitation, a threshold value of 0.3 mm rainfall is considered during model calibration. Calibration (1961-1991) and validation (1992-2001) result of the model downscaling (1961-1991) of daily rainfall is presented in Table 4.5. It can be seen that the SDSM model shows a good agreement between the observed and computed mean daily rainfall, standard deviation and variance with correlation coefficient of 0.51 and 0.47 during calibration and validation respectively.

Table 4.5: Comparison between Daily Precipitation (Observed) and Daily Precipitation (Computed) during Model Calibration and Validation

Type	Period	Mean	SD	Var	Correlation, r
Model Calibration	Precp_61-91_Observed	3.02	11.70	136.88	0.51
	Precp_61-91_Computed	3.59	7.24	52.47	
Model Validation	Precp_92-01_Observed	3.31	14.46	209.01	0.47
	Precp_92-01_Computed	3.44	6.69	44.81	

4.10.1.3 Future scenario generation

The validated Multiple Linear Regression models between the predictand and large-scale predictors are used to generate the future downscaled data using the HadCM3 GCM data for A2 scenario and B2 scenarios. The annual precipitation corresponding to future emission is presented in Table 4.6. The result clearly indicates an increase in trend of annual precipitation for successive scenarios. In the 2020s, the simulated annual precipitation is about 200 mm higher than the mean annual precipitation for the present scenario which stands at 1129 mm. Similarly for 2050s and 2080s, the annual mean precipitations are 1515.92 mm and 1692.70 mm respectively. The result of the downscaled daily rainfall for different periods is shown in Fig.4.8. The figure indicates an increasing rainfall trend in the future for different periods.

Table 4.6: Annual average precipitation for present and downscaled precipitation corresponding to HadCM3 A2 & B2 scenario

Scenario	Annual average precipitation (mm)
Present	1129.58
HadCM3 A2 scenario **(Worst case scenario with high future emission)**	
2020s	1327.17
2050s	1515.92
2080s	1692.70
HadCM3 B2 scenario	
2020s	1277.37
2050s	1457.02
2080s	1503.10
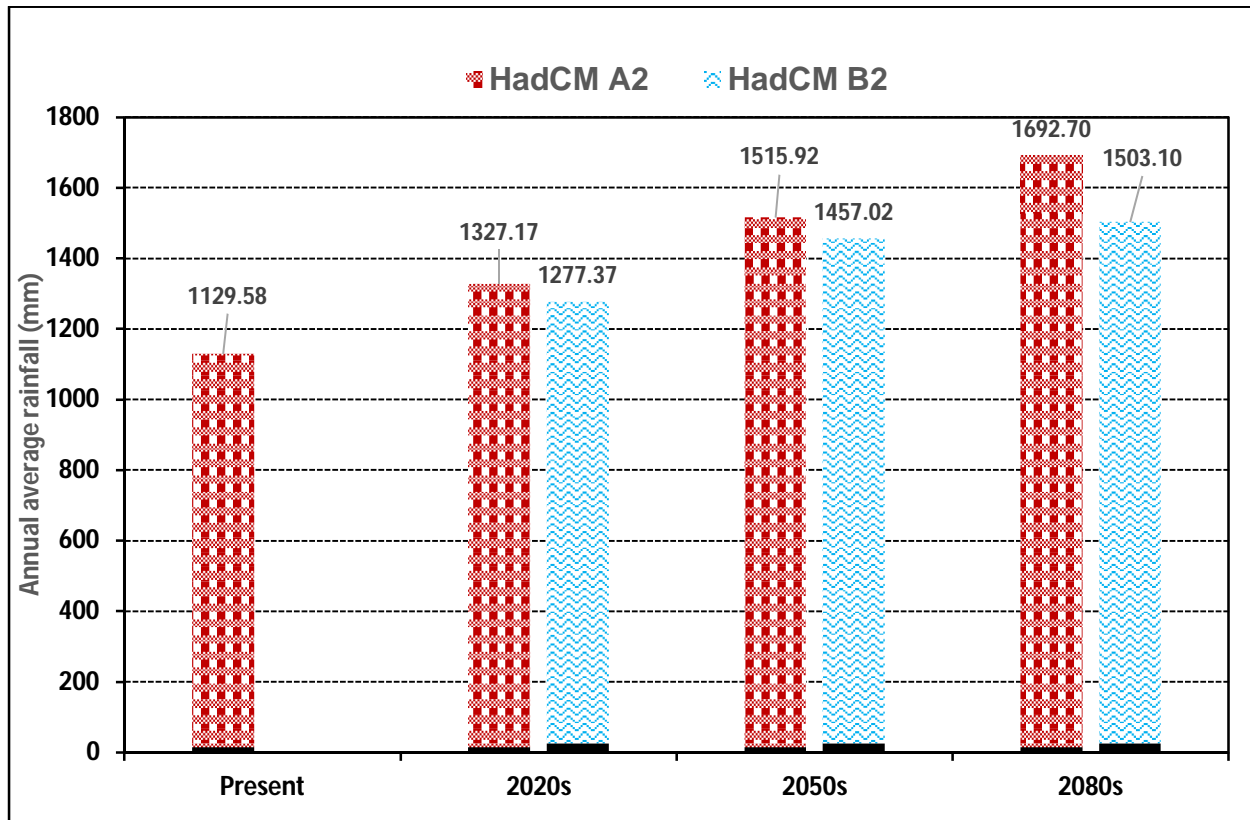
Fig.4.8. Downscaled annual mean rainfall for different periods using HadCM A2 & B2 scenarios

4.10.2 Downscaling daily maximum temperature

4.10.2.1 Selection of predictor variables

Already discussions have been made in the previous section on selection of large scale predictors. The scatter plot between selected predictors and observed variable are shown in Fig.4.9. 5 predictor variables are chosen based on correlation. Those are: ncepmslpas; ncepp_uas; ncepp_zhas; ncepshumas; nceptempas.
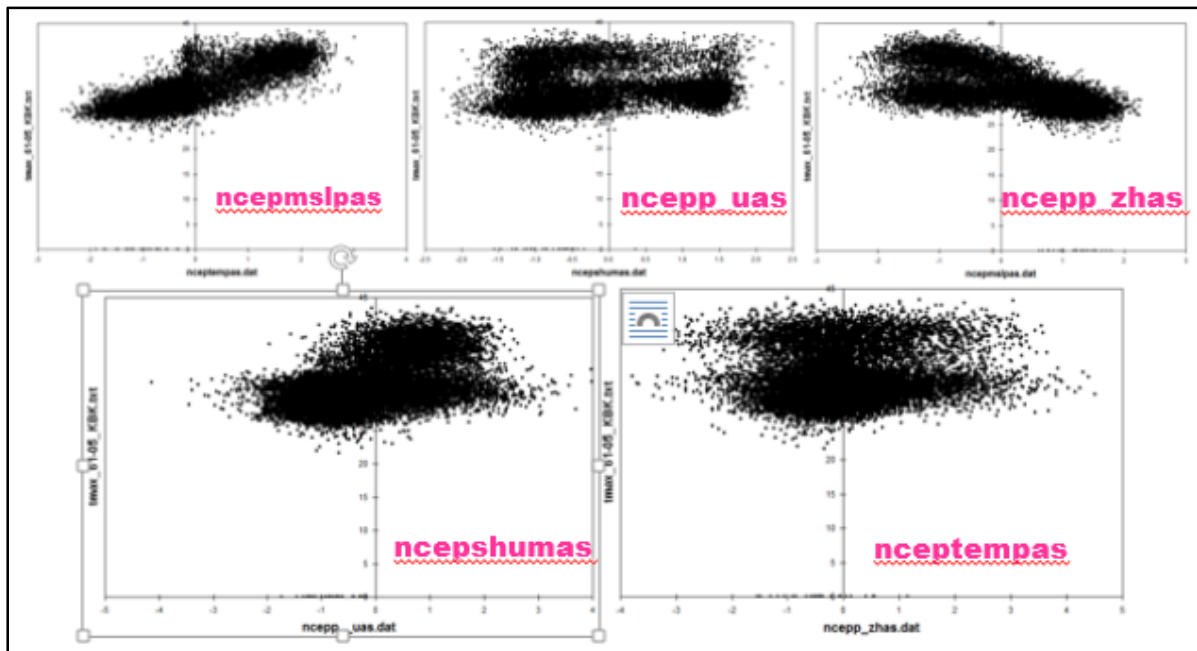
Fig.4.9. Scatter plots between predictand and selected NCEP predictors

4.10.2.2 Model Calibration and Validation

The model calibration process formulates downscaling model based on multiple regressions between the predictand (observed precipitation) and selected NCEP predictors. Since the predictand-predictor relationship. Calibration (1961-1991) and validation (1992-2001) result of the model downscaling (1961-1991) of daily maximum temperature is presented in Table 4.7. It can be seen that the SDSM model shows an excellent agreement between the observed and computed mean daily rainfall, standard deviation and variance with correlation coefficient of 0.87 and 0.91 during calibration and validation respectively.

Table 4.7: Comparison between Daily Maximum Temperature (Observed) and Daily Maximum Temperature (Computed) during Model Calibration and Validation

Type	Period	Mean	SD	Var	Correlation, r
Model Calibration	Tmax_61-91_Observed	32.42	49.58	24.56	0.87
	Tmax_61-91_Computed	32.12	43.16	16.59	
Model Validation	Tmax_92-01_Observed	33.35	58.95	209.01	0.91
	Tmax_92-01_Computed	33.78	66.9	111.2	

4.10.2.3 Future scenario generation

The validated Multiple Linear Regression models between the predictand and large-scale predictors are used to generate the future downscaled data using the HadCM3 GCM data for A2 and B2 scenarios. The annual average maximum temperature corresponding to future emission is presented in Table 4.8. The result clearly indicates an increase in trend of annual precipitation for successive scenarios. In the 2020s, the simulated annual precipitation is about 200 mm higher than the mean annual precipitation for the present scenario which stands at 1129 mm. Similarly for 2050s and 2080s, the annual mean precipitations are 1515.92 mm and 1692.70 mm respectively. The result of the downscaled daily maximum temperature for different periods is shown in Fig.4.10. The figure indicates an increasing temperature trend in the future for different periods.

Table 4.8: Annual average max. temperature (^{0}C) for present and downscaled temperature corresponding to HadCM3 A2 & B2 scenarios

Scenario	Annual average max. temperature (^{0}C)
Present	32.12
HadCM3 A2 scenario **(Worst case scenario with high future emission)**	
2020s	34.15
2050s	34.89
2080s	35.10
HadCM3 B2 scenario	
2020s	33.31
2050s	33.88
2080s	33.99
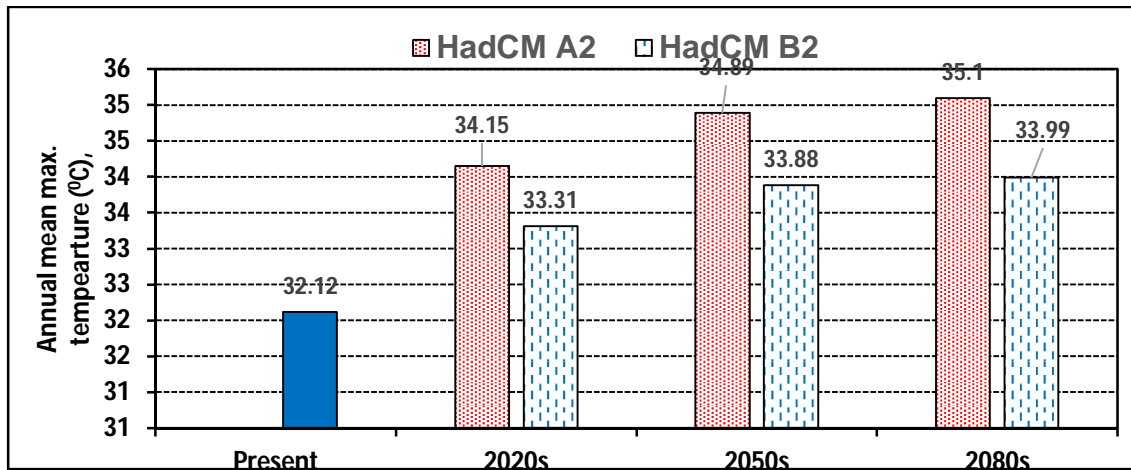
Fig.4.10. Downscaled annual average maximum temperature for different periods using HadCM A2 & B2 scenarios

4.11 CONCLUSIONS

SDSM is one of the downscaling tools widely used to downscale simulated GCM data into local fine-scale data. In the present study, multiple linear regression based SDSM model has been used to downscale daily precipitation data corresponding to HadCM3 A2 GCM (1961-2099) and HadCM3 B2 GCM (1961-2099). The model calibration and validation has been performed using NCEP reanalysis data for the duration 1961-91 and 1992-2001 respectively. The calibration and validation results indicate that the probability of future maximum temperature for occurrence is more with high correlation coefficient than the daily precipitation. SDSM model can be used in the KBK region to downscale temperature at different temporal and spatial scale. However, for downscaling daily precipitation other robust downscaling techniques such as RCM, SVM, ANN, etc. should be explored. The study indicates an increasing mean daily, monthly and annual precipitation suggesting a wetter climate in the future. This also holds similar for temperature which will be increasing in future. To summarize, the precipitation is likely to increase in future as per HadCM3 A2 and B2 scenarios. The temperature (max) will also aggravate in future as per HadCM3 A2 and B2 scenarios.

WATER AVAILABILITY AND UTILIZATION

5.1 GENERAL

Planning for water resources development in a basin requires careful assessment of the available water resources and utilization for various purposes such as drinking, irrigation, hydro-power, industries, navigation etc. This chapter deals with the assessment of water availability in the Tel basin. The water availability for the entire KBK region is difficult to estimate, reason being several basins exist in the region draining into the Bay of Bengal and Godavari basin. Based on the data availability Tel basin has been considered as a representative basin for water availability and utilizations under different stake-holders. In the study, dependable water yield from Tel river has been assessed based on the daily gauge data from the Kantamal G&D site. It has been found that there are no major/ medium structures for water abstraction in the Tel basin, hence water utilizations is estimated based on the existing cropped area & population/ livestock (districts-wise). Further, SWAT model has been set-up for the Tel basin, to find the different water balance component.

5.2 TEL BASIN

5.2.1 Physiography and climate:

The total basin area is about 22,818 km^2, and lies between 19°16'1.039"N and 20°44'40.452"N latitude and 82°3'4.813"E and 84°18'5.929"E longitude. About 94% of the basin area is falling in Odisha, remaining 6% in the State of Chhatisgarh. The major districts encompassing the basin are Kalahandi, Bolangir, Nuapada, Sonepur and Kandhmal. The Tel river, a tributary to Mahandi river, flows in the districts of Nabarangpur, Kalahandi, Balangir, and Sonepur. Before joining Mahanadi at Sonepur, river Suktel joins Tel river downstream of Kantamal G&D site. There are two G&D sites in the basin viz. Kantamal G&D site and Kesinga G&D site. The general physiography of the basin is undulating with forest coverage in the Southern-Western part of the basin.

The study area experiences tropical wet and dry climate. The average annual rainfall is around 1150 mm, mainly receives rainfall in the months of June, July, August, and September. Sometimes increased flow during monsoon could lead to flood and waterlog situation in rainy season, remaining months are generally dry. The average maximum temperature which is felt in May of around 39°c and an average minimum temperature of around 13°c during the month of December. The summer temperature reaches maximum in the month of May before arrival of Monsoon. Titilagarh, a small town in the Tel basin often discussed for its peak temperature crossing more than 50^0C. The winter period is mild in nature. Agriculture is the main source of income for the people in the basin. The soils in the Tel basin can be broadly classified as clayey and loamy soil. Some parts of the region are erosion prone with poor drainage quality. The soil of center part of basin has loamy soil and sandy-loam with well drain characteristics. Paddy is the principal crop grown in the Tel basin. The major crops grown in the area are rice, cotton, sugarcane, and groundnut. Fig.5.1(a) and 5.1(b) illustrates the basin location. The district-wise geographical coverage of the basin is given in Table 5.1. The digital elevation of the Tel basin is presented in Fig. 5.2. The elevation map indicates that the elevation ranges between 1315 m to 91 m.
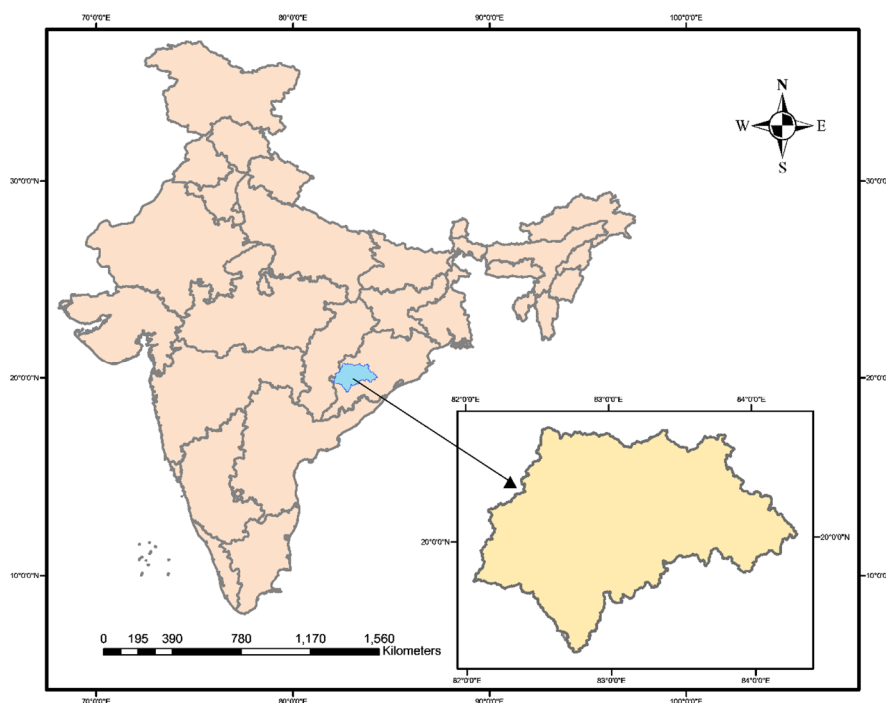
Fig. 5.1(a): Index map of Tel basin
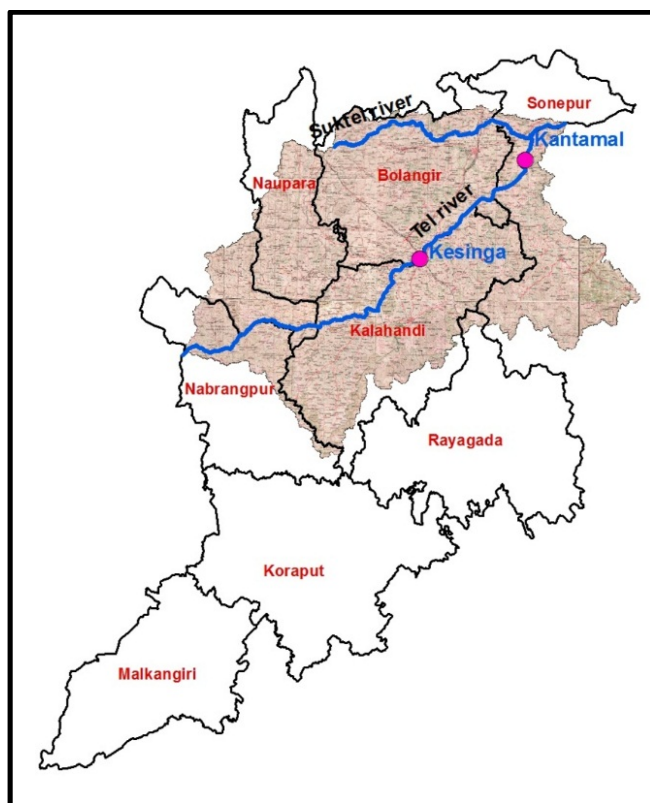
Fig.5.1 (b): Tel basin overlaid on KBK region

Table 5.1: District-wise geographical area of the Tel basin

Sl. No.	Districts (State)	Administrative district area (Km^2)	% area of the district in the basin out of total area	Area of the district falling in Tel basin (Km^2)	% district area in the basin
1	Raipur (Chhatisgarh)	13083	10.6	1385	6.1
2	Kandhamal	8021	34.5	2765	12.1
3	Boudh	3098	31.5	975	4.3
4	Bolangir	6575	82.5	5425	23.8
5	Sonepur	2284	47.5	1085	4.8
6	Kalahandi	7920	86.7	6867	30.1
7	Nuapada	3408	75.0	2556	11.2
8	Nabarangpur (Koraput)	5294	32.9	1740	7.6
9	Bargarh (Sambalpur)	5837	0.3	20	0.1
	Total			**22818**	**100**
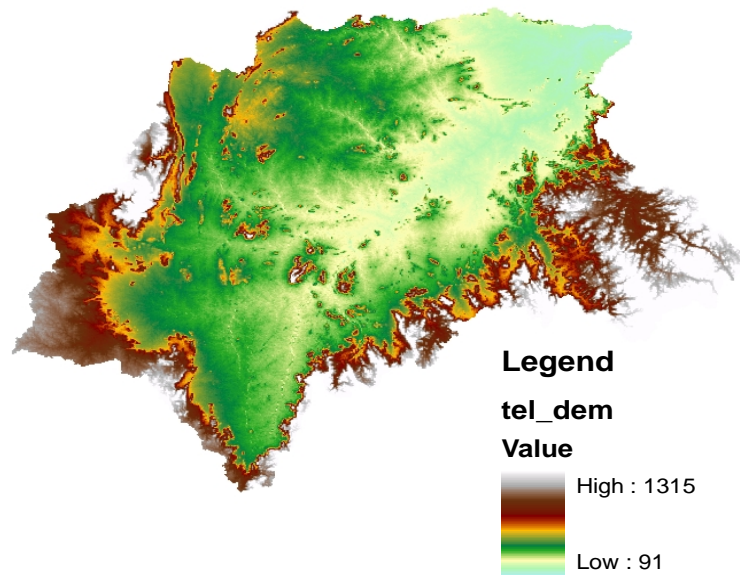
Fig.5.2: Digital elevation map of the Tel basin
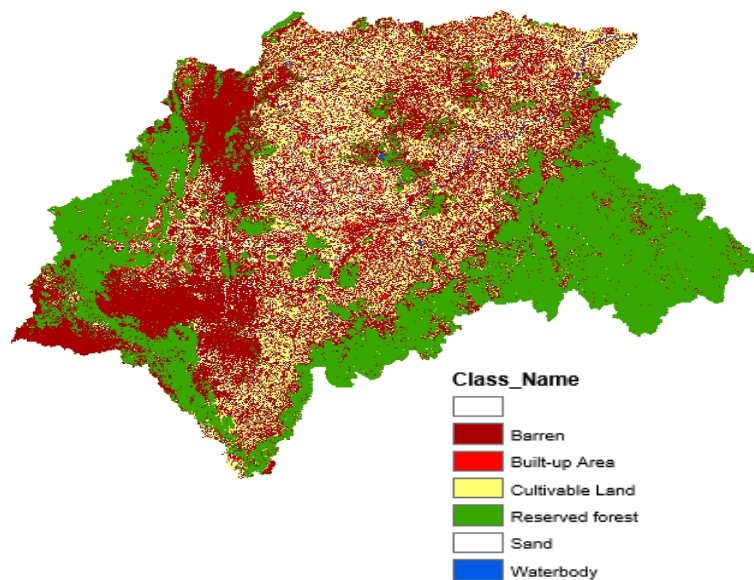
Fig.5.3: LULC map of the Tel basin

5.3 METHODOLOGY

5.3.1 Surface water availability

The observed flow data at the Kantamal G&D site (Catchment area = 19600 km^2), for the period 1972-2102 were collected from IndiaWRIS. Since the upstream utilization is less (no major abstractions except few LI points, these observed flows, are considered as virgin

yields. Monsoon and non-monsson yields were separately estimated prior to adding the two for arriving at total yield for Tel basin. The annual total yields thus arrived are arranged in descending order, from which 50% and 75% dependable annual yields were estimated.

5.3.2 Surface water utilization

The surface water is mainly used for irrigation, and domestic consumption. There are no hydropower schemes or major industries in the Tel basin. The surface water utilizations is estimated based on the existing cropped area & population/ livestock (districts-wise).

5.3.3 Application of SWAT model

SWAT model for the basin was setup, especially to find the recharge component, and other water balance components. The Soil and Water Assessment Tool (SWAT) model is physical based semi-distributed model which has the provision of point as well as spatial input data. SWAT includes a hydrological model which is better utilized with different components of water balance in a particular basin. Though several rainfall-runoff models are available, selection of suitable model for a given watershed is very difficult for efficient planning and management of watershed. Numerous models as mentioned earlier have been developed by various researchers for rainfall-runoff modelling (Chaubey et al., 2012; Nayak et al., 2014). However, SWAT model results have been found to be more acceptable and widely used than any other hydrologic models. Water balance equation used by SWAT model is as follows:

$$SW_t = SW_0 + \sum_{t-1}^{t} \left(R_{day} - Q_{surf} - ET_a - W_{seep} - Q_{gw} \right)$$

(5.1)

where,

SW_t = Final soil water content (mm); SW_0 = Initial water content (mm); T = Time (day), R_{day} = Amount of precipitation (mm); Q_{surf} = Amount of surface runoff (mm); ET_a = Amount of Evapotranspiration (mm); W_{seep} = Amount of water entering the vadose zone from the soil profile (mm); Q_{gw} = Amount of return flow (mm)

SWAT is a semi-distributed, continuous-time step model that operates on a daily time step and is designed to predict the impact of management on water, sediment, and agricultural chemical yields in watersheds. The model is physically based, computationally efficient, and capable of continuous simulation over long time periods. Major components in SWAT model

includes weather, hydrology, soil properties, plant-growth, nutrients, pesticides, bacteria and pathogens, and land management practices. In SWAT model, a watershed is divided into multiple sub-watersheds, which are further subdivided into different hydrologic response units (HRUs) that consist of homogeneous land use, slope, and soil characteristics. The general objective of SWAT model is to estimate the impact of agriculture or land management on water and sediment, and agricultural chemical yields in a basin. It has option of high level of spatial and point source data as input, and simulation may be run on daily, monthly, or yearly time steps. However, the model components includes weather condition, soil properties, hydrology, erosion, plant growth, land management, nutrients, pesticides, and stream routing etc. In this study, SWAT is used for hydrological analysis of the watershed. The entire process has been completed through six major steps, which are:

(i) **Watershed delineation module:** This module involves the information related to Digital Elevation Model (DEM) of the watershed, which in turn provides the morphometry of the watershed, i.e., steam delineation, stream definition, flow direction and accumulation, inlet and outlet definition etc.;

(ii) **Hydrological Response Unit (HRU):** HRUs analysis involves the three sub-parts, i.e., Satellite imagery analysis, soil map and the slope information. These sub-modules provide information related to LULC, soil map and slope definition in different layers;

(iii) **Hydro Meteorological data:** In this module, various hydro-meteorological data at various locations (point locations),i.e., precipitation, minimum/ maximum temperature, relative humidity, solar radiation, wind speed, dew point and its location and elevation, etc. are provided;

(iv) **Define Weather Station**: In this step, weather stations location (latitude/ longitude) with its elevation details and other geographical as well as other statistical details of various parameters discussed in step (iii) are provided;

(v) **Edit database (optional):** In this module, one can add or edit other point source information such as point source discharge, inlet discharge, reservoir, sub-basin or watershed discharge, etc.;

(vi) **Run swat model**, in this step the model is run after inputting all the required data as mentioned in steps (1) to (v). The general framework of the SWAT model is shown in Fig.5.4

PROCESS FLOW CHART OF SWAT MODEL

1 | **Watershed Delineation**

Digital Elevation Model
↓
Pre-Process
↓
Watershed Delineation
↓
Masking According to Catchment Area
↓
Stream
↓
Stream
↓
Flow Direction and
↓
Outlet & Inlet Definition (Automatic/Manual)

2 | **Hydrological Response Unit (HRU)**

Satellite Image	Soil Map	Slope Definition
↓	↓	↓
Geo-referencing	Geo-referencing	Slope Discretization
↓	↓	↓
LULC Map	Create Polygons	Multiple Slope classes
↓	↓	↓
Raster LULC (Gridded)	Convert Vector to Raster	Reclassify
↓	↓	
Lookup Table	Lookup Table	
↓	↓	
Reclassify	Reclassify	

Overlay

3 | **Hydro Meteorological**

Precipitation	Min/Max Temperature
Relative Humidity	Solar Radiation
Wind Speed	Dew Point

4 | **Define Weather Stations**

Weather Stations Locations and Data Time Series

5 | **Edit SWAT Database (if required)**

Define Weather Scenario	Define PET Calculation
Specify Simulation Period	Setup Management files

6 | **Setup/Run SWAT Model**

Tentative Result
↓
Sensitivity Analysis
↓
Calibration/Validation
↓
Final Results and Model Parameters

Figure 5.4 Methodology of SWAT model

5.3.4 Basic Equations used in SWAT

SWAT uses **climate** data from the *station nearest to the centroid* of each sub-basin. **Surface runoff** is estimated by using modified *soil conservation service (SCS) curve number* (CN) method or the Green & Ampt infiltration method. In the SCS-CN, which is used in this study, the runoff is estimated using the following equations (USDA, 1972; Bhadra et al., 2010):

$$Q = \frac{(R - 0.2s)}{R + 0.8s}, \qquad R \geq 0.2s$$
$$Q = 0, \qquad\qquad R \leq 0.2s \tag{5.2}$$

where, Q is the daily runoff; R is daily rainfall, and s is a retention parameter. The retention parameter, s varies (a) among sub-basin because of variation in soil, landuse, management, and slope (b) with time because of change in soil water content. The parameter s is related to curve number (CN) by the SCS equation (USDA, 1972).

$$s = 254\left(\frac{100}{CN} - 1\right) \tag{5.3}$$

The constant, 254 in the above equation gives s in mm. Thus, R and Q are also expressed in mm. CN is the curve number for antecedent moisture content (AMC-II). The value of curve number for different landuse conditions and hydrological soil group are applied to AMC-II only i.e., for average condition. The equation gives the value of runoff (Q) depth. In this study, runoff curve number (AMC-II) values for the Indian condition are adopted.

5.3.4.1 Potential evapotranspiration

Potential evapotranspiration (PET) can be estimated by any of the three methods, i.e., *Penman-Monteith* method (Monteith 1965), the *Priestley- Taylor method* (Priestley and Taylor 1972), and the *Hargreaves method* (Hargreaves and Samani 1985) depending on data availability. It may be noticed that Priestley-Taylor method requires solar radiation and air temperature as input, while the Hargreaves method requires air temperature only. If wind speed, relative humidity, and solar radiation data are not available, the Hargreaves method is more acceptable in most cases (Arnold et al., 1998). In this study Penman-Monteith method is used for estimation of potential evapotranspiration.

The Penman-Monteith equation combines components the account for energy needed to sustain evaporation, the strength of the mechanism requires to remove the water vapour and aerodynamic and surface resistance terms. The Penman-Monteith equation as follows:

$$\lambda E = \frac{\Delta \cdot (H_{net} - G) + \rho_{air} \cdot c_p \cdot \left[e_z^o - e_z\right]/r_a}{\Delta + \gamma \cdot (1 + r_c/r_a)}$$

(5.4)

where, λE is the latent heat flux density (MJ m^{-2} d^{-1}), E is the depth rate evaporation (mm d^{-1}), Δ is the slope of the saturation vapour pressure-temperature curve, de/dT (kPa °C^{-1}), H_{net} is the net radiation (MJ m^{-2} d^{-1}), ρ_{air} is the air density (kg m^{-3}), c_p is the specific heat at constant pressure (MJ kg^{-1} °C^{-1}), e_z^o is the saturation vapor pressure of air at height z (kPa), γ is the psychometric constant (kPa °C^{-1}), r_c is the plant canopy resistance (s m^{-1}), and r_a is the diffusion resistance of the air layer (aerodynamic resistance) (s m^{-1})

For well-watered plants under neutral atmospheric stability and assuming logarithmic wind profiles, the Penman-Monteith equation may be written (Jensen et al., 1990):

$$\lambda E_t = \frac{\Delta \cdot (H_{net} - G) + \gamma \cdot K_1 \cdot (0.622 \cdot \lambda \cdot \rho_{air}/P) \cdot \left(e_z^o - e_z\right)/r_a}{\Delta + \gamma \cdot (1 + r_c/r_a)}$$

(5.5)

where, λ is the latent heat of vaporization (MJ kg^{-1}), E_t is the maximum transpiration rate (mm d^{-1}), K_1 is the dimension coefficient needed to ensure the two terms in the numerator have the same unit (for u_z in m s^{-1}, K_1=8.64 x 10^4), and P is atmospheric pressure (kPa). The calculation of net radiation, H_{net}, is discussed in previously. The remaining undefined term are the soil heat flux, G, the combined term $K_1 0.622\lambda\rho/P$, the aerodynamic resistance, r_a, and the canopy resistance, r_c.

5.3.4.2 Lateral sub-surface flow

Lateral subsurface flow in the soil profile (0-2 m) is calculated simultaneously with percolation. A kinematic storage model (Sloan et al., 1984) is used to predict lateral flow in each soil layer.

$$q_{lat} = 0.024 \frac{(2s\,SC\sin(\alpha))}{\theta_d\,L}$$

(5.6)

where, q_{lat} is lateral flow (mm/d), S is drainable volume of soil water (mh^{-1}), α is slope (m/m), θ_d is drainable porosity (mm^{-1} and L is flow length (m). If the saturated zone rises above the soil layer, water is allowed to flow to the layer above (back to the surface for the upper soil layer), to account for multiple layers, the model is applied to each soil layer independently, starting at the upper layer.

5.3.4.3 Percolation

The percolation component of the SWAT uses a storage routing technique combined with a crack-flow model to predict flow through each soil layer. Once water percolates below the root zone, it is lost from the watershed (becomes groundwater or appears as return flow in downstream basins). The storage routing technique is based on the following equation:

$$SW_i = SW_{oi} \exp\left(\frac{-\Delta t}{TT_i}\right)$$ (5.7)

where, SW_i and SW_{oi} are the soil water contents at the beginning and end of the day in mm, Δt is the time interval (24 h), and TT_i is the travel time through layer i. Thus, subtracting SW_{oi} from SW_i can compute the percolation

$$O_i = SW_{oi}\left[1 - \exp\left(\frac{-\Delta t}{TT_i}\right)\right]$$ (5.8)

Where, O_i is the percolation rate in mm/day.

The travel time, TT_i is computed for each soil layer with the linear storage equation

$$TT_i = \frac{(SW_i - FC_i)}{H_i}$$ (5.9)

where H_i is the hydraulic conductivity in mm/h and FC is the field capacity minus wilting point water content for layer i in mm. The hydraulic conductivity varies from the saturated conductivity value at saturation to near zero at field capacity.

$$H_i = SC_i\left(\frac{SW_i}{UL_i}\right)^{\beta_i}$$ (5.10)

where SC_i is the saturated conductivity for layer i in mm/h, UL_i is soil water content at saturation in mm/mm. β_i is a parameter that causes H_i to approach zero as SW_i approaches FC_i The equation for estimating β is

$$\beta_i = \frac{-2.655}{\log_{10}\left(\frac{FC_i}{UL_i}\right)}$$ (5.11)

The constant (-2.655) in equation (5.11) was set to assure $H_i = 0.002SC_i$ at field capacity. Upward flow may occur when a lower layer exceeds field capacity. The soil water to field capacity ratios of the two layers regulates movement from a lower layer to an adjoining upper

50 layer. Percolation is also affected by the soil temperature. If the temperature in a particular layer is at 0°C or below, no percolation is allowed from that layer.

5.3.4.4 Ground water flow

Ground water flow contribution to total stream flow is simulated by creating shallow aquifer storage. The water balance for the shallow aquifer is

$$Vsa_i = Vsa_{i-1} + Rc - revap - rf - perc_{gw} - WU_{SA} \qquad (5.12)$$

where Vsa is the shallow aquifer storage (mm), Rc is recharge (percolate from the bottom of the soil profile) (mm), revap is root uptake from the shallow aquifer (mm), rf is the return flow (mm), $perc_{gw}$ is the percolation to the deep aquifer (mm), WUSA is the water use (withdrawal) from the shallow aquifer (mm), and i is the day. Return flow from the shallow aquifer to the stream is estimated with the equation (Arnold et al., 1993):

$$rf_i = rf_{i-1} e^{-\alpha\Delta t} + Rc\left(1 - e^{-\alpha\Delta t}\right) \qquad (5.13)$$

where, α is the constant of proportionality or the reaction factor.

The relationship for water table height is h_i (Arnold et al., 1993):

$$h_i = h_{i-1} e^{-\alpha\Delta t} + \frac{Rc}{0.8\mu\alpha}\left(10 - e^{-\alpha\Delta t}\right) \qquad (5.14)$$

where, h is the water table height, (m above stream bottom), and μ is the specific yield.

The data used in the SWAT model setup, calibration and validation is described in Table 5.2.

Table 5.2: Data used and its sources in the SWAT model setup

Data	Source(s)
DEM	Aster Digital Elevation Model (ASTER-DEM) (Resolution of 30m) Source: http://gdem.ersdac.jspacesystems.or.jp/
Imageries	Landsat-5 TM and Landsat-7 ETM+ (Resolution of 30m) Source: http://glovis.usgs.gov/
Soil Series Map	National Bureau of Soil Survey and Land Use Planning (NBSS-LUP), Nagpur, India
Rainfall	Indian Meteorological Department (IMD), Pune (India) (Grid Resolution of 0.25°x0.25°) National Innovations on Climate Resilient Agriculture (NICRA), Indian Council of Agricultural Research (ICAR) *Source: http://www.nicra-icar.in/nicrarevised/index.php/tools-services*
Minimum/ Maximum Temperature	Indian Meteorological Department (IMD), Pune NASA Prediction of Worldwide Energy Resource (POWER) *Source:http://power.larc.nasa.gov/cgi-*

	bin/cgiwrap/solar/agro.cgi?email=agroclim@larc.nasa.gov
Relative Humidity	NASA Prediction of Worldwide Energy Resource (POWER) *Source:http://power.larc.nasa.gov/cgi-bin/cgiwrap/solar/agro.cgi?email=agroclim@larc.nasa.gov*
Solar Radiation	
Wind Speed	
Dew Point	
Discharge Data	IndiaWRIS (Mahanadi basin) India-Water Resources Information System (India-WRIS$_{webGIS}$) *http://www.india-wris.nrsc.gov.in/wris.html*

Software and hardware used

Workstation (Xeon processor), ArcSWAT (Ver. 2009.93.7a), ERDAS/IMAGIN 2013, ArcGIS (Ver. 9.3), Contex FSS (Full scale scanner) 8000, and laser printer has been utilized at National Institute of Hydrology, Roorkee.

5.4 RESULTS AND DISCUSSION

5.4.1 Surface water availability

The observed flow data at the Kantamal G&D site (Catchment area = 19600 km^2), for the period 2003-04 to 2012-13 is given in Table 5.3.

Table 5.3: Annual average runoff

Year	Avg. Non-monsoon flow (Nov-May) (Cumec)	Avg. monsoon flow (Jul-Oct) (Cumec)	Avg. Annual runoff (Cumec)
2003-2004	126.64	1066.75	452.52
2004-2005	105.85	678.97	316.32
2005-2006	101.19	490.33	175.41
2006-2007	98.96	1346.25	580.33
2007-2008	91.78	1023.52	507.51
2008-2009	73.92	1343.79	517.20
2009-2010	78.49	863.23	327.96
2010-2011	101.12	542.85	376.99
2011-2012	19.07	454.68	190.57
2012-2013	59.31	510.52	272.31

The purpose of developing any model is to replicate the behaviour of physical system. Model is acceptable provided that the results obtained from the model matches with the observed values. If the outcome of model does not matches with the observed values, parameters of the model are adjusted so as to match with the observed values. This process is known as the calibration process. Once the model is calibrated, it is validated through another set of observed values. Further, once the model is calibrated and validated then the model is ready for the use with future data.

In SWAT model, two options are available for calibration i.e., manual as well as automatic. Both the calibration techniques are widely used. Manual calibration, though, is tedious and time consuming approach and the success depends on the experience of modeller and knowledge about the watershed being modelled, still, it is preferred to automatic calibration because of its advantages. Therefore, in this study also manual calibration process is adopted. During the calibration process, it is desired to know the tuned values of the parameters. Visual examine of simulated and observed hydrograph is also an important activity for improvement of results during the calibration process. In the SWAT model, parameters such as curve number, soil available water content, effective hydraulic conductivity, soil bulk density, threshold depth of water in shallow aquifer, groundwater "revap" coefficient, soil evaporation compensation factor, average slope steepness, manning's "n", average slope length, base-flow alpha factor, ground water delay, plant uptake compensation factor etc. are taken into consideration for calibration of model regarding runoff estimation. These parameters varies between its upper and lower limits. The process of calibration has been adopted after sensitivity analysis in SWAT model. Since many of the input parameters were available for the basin, they are not calibrated. In present study, calibration process is carried out using the observed discharge at the outlet of Katamal G&D site on monthly basis with the simulated values. The period (1972-2000) data is taken for calibration and remaining years (1999-2012) data is considered for validation purpose. The list of parameters and as per the rank (on the basis of sensitivity to output) and its range is shown in Table 5.4.

Table 5.4: List of SWAT parameters with respective range and values for the case study

Rank	Name	Description	Lower Bound	Upper Bound	Process	Default	Calibrated
1	**CN**	**SCS runoff CN for moisture condition II**	**35**	**98**	**Runoff**	**83**	**74.7**
2	**ESCO**	**Soil evaporation compensation factor**	**0**	**1**	**Evaporation**	**0.95**	**0.8**
3	**GWQMN**	**Threshold depth of water in the shallow aquifer required for return flow to occur (mm)**	**0**	**5000**	**Groundwater**	**0**	**207**
4	SOL_Z	Soil depth (mm)	0	3000	Soil	-	-
5	REVAPMN	Threshold depth of water in the shallow aquifer for revap to occur (mm)	0	500	Groundwater	-	-
6	**SOL_AWC**	**Available water capacity of the soil layer (mm/mm soil)**	**0**	**1**	**Soil**	**0.096**	**0.114**
7	CANMX	Maximum canopy storage (mm)	0	10	Soil	-	-
8	BLAI	Maximum potential leaf area index	0	1	Crop	-	-
9	SOL_K	Soil conductivity (mm hr)	0	100	Soil	-	-
11	**GW_REVAP**	**Groundwater -revap coefficient**	**0.02**	**0.2**	**Groundwater**	**0.02**	**0**
12	EPCO	Plant evaporation compensation factor	0	1	Evaporation	-	-
13	CH_K2	Hydraulic conductivity in main channel (mm hrs)	-0.01	150	Channel	-	-
14	SLOPE	Average slope steepness (m/m)	0.0001	0.6	Geomorphology	-	-
15	GW_DELAY	Groundwater delay (days)	0	50	Groundwater	-	-
16	SURLAG	Surface runoff lag coefficient	0	10	Runoff	-	-
17	**CH_N**	**Manning coefficient for main channel**	**0.01**	**0.5**	**Channel**	**0.014**	**0.017**
18	BIOMIX	Biological mixing efficiency	0	1	Management	-	-
19	SLSUBBSN	Average slope length (m)	10	150	Geomorphology	-	-
20	SOL_ALB	Soil albedo	0	0.1	Evaporation	-	-
27	SFTMP	Snowfall temperature (°C)	0	5	Basin	-	-
27	SMFMN	Melt factor for snow on December 21 (mm water °C-day)	0	10	Basin	-	-
27	SMFMX	Melt factor for snow on June 21 (mm water °C-day)	0	10	Basin	-	-
27	SMTMP	Snow melt base temperature (°C)	0	5	Basin	-	-
27	TIMP	Snow pack temperature lag factor	0.01	1	Basin	-	-
27	TLAPS	Temperature lapse rate (°C km)	0	50	Sub Basin	-	-

Source: Van et al. (2006)

Parameter values are calibrated (in terms of multiplication/ addition/ subtraction) on the basis of its impact on the result. However, a parameter is never allowed to go beyond the predefined parameter range during the calibration.

In order to calibrate the model, Katamal G&D site is identified where the observed flow is available. After running the model with initial model parameters values (default), the monthly discharge is estimated. The observed and estimated (pre-calibrated) monthly discharge values during the calibration period (1972-2000) is plotted and is shown in Fig. 5.5. It has been noticed that the pre-calibrated discharge values continuously over-estimate the discharge in most of the years. Therefore, the parameters of the model are revised so as to improve the performance of the model. The parameters are revised on the basis of its impact and its ranking in its role on output. Table 5.4 shows the initial as well as the revised parameters of the model during the calibration period. The observed and estimated discharge values before and after calibration are shown in Fig. 5.6.
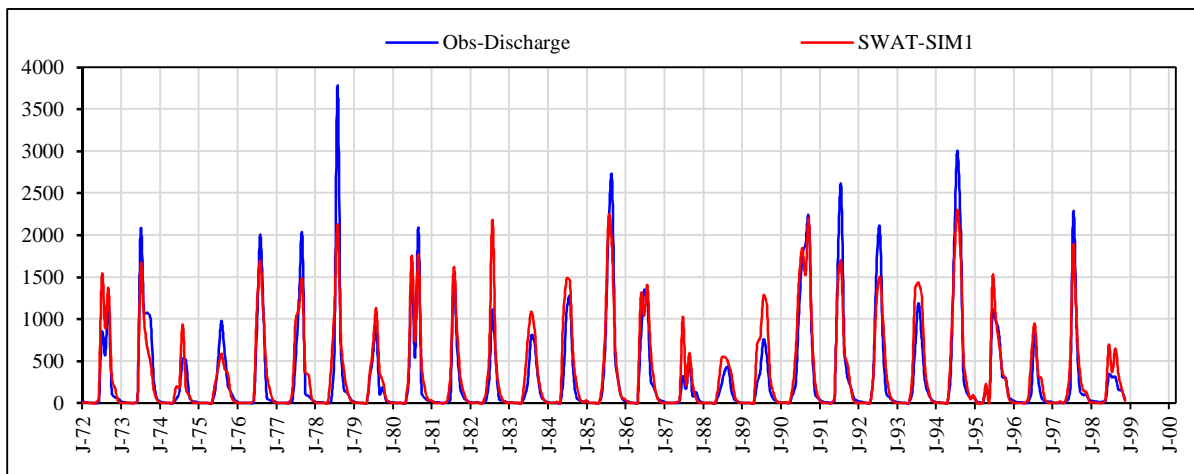
Fig. 5.5 Pre-calibrated observed and simulated discharge of the Tel basin;
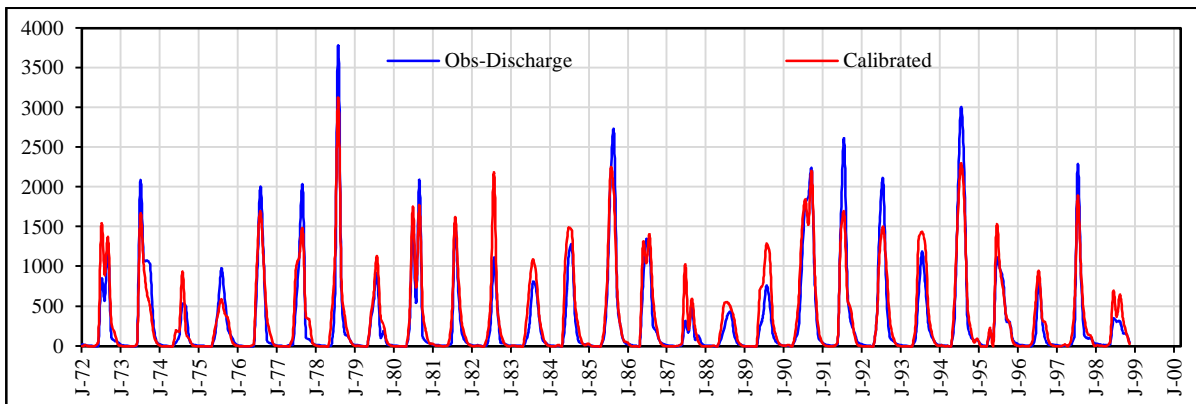
Fig. 5.6 Calibrated observed and simulated discharge of the Tel basin

Besides the comparison of rising and recession curves, it is important to examine the variation of estimated discharge from the observed values. For this purpose, a scatter graph is plotted between the observed and estimated flow values as shown in Figs. 5.7 & 5.8 respectively for un-calibrated and calibrated conditions. A 45° line is marked which represents the perfect estimation. From Figs. 5.7 & 5.8 it may be observed that even the calibrated model is over estimating the monthly discharge. This is perhaps because of the reasons that the AMC conditions are not incorporated correctly or the temporary small storages in the fields are not depicted correctly in the model. For accurate depiction of the area, extensive survey is needed which could not be accomplished in this study.
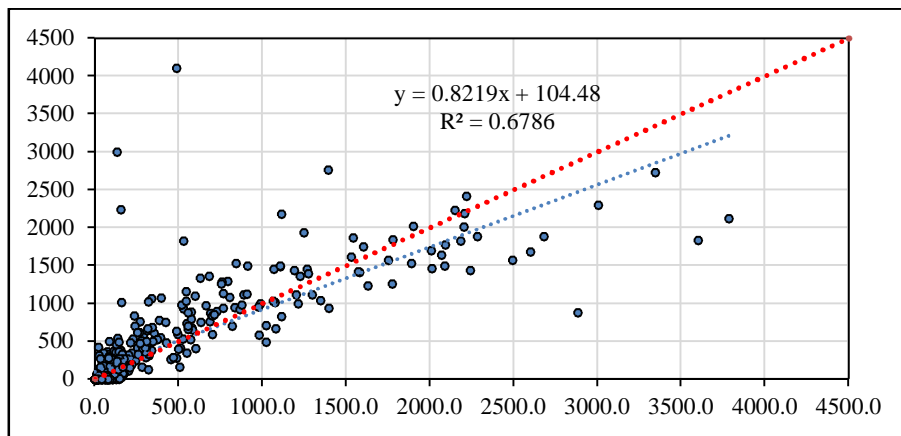
Fig. 5.7 Scatter plot showing pre-calibrated observed and simulated discharge
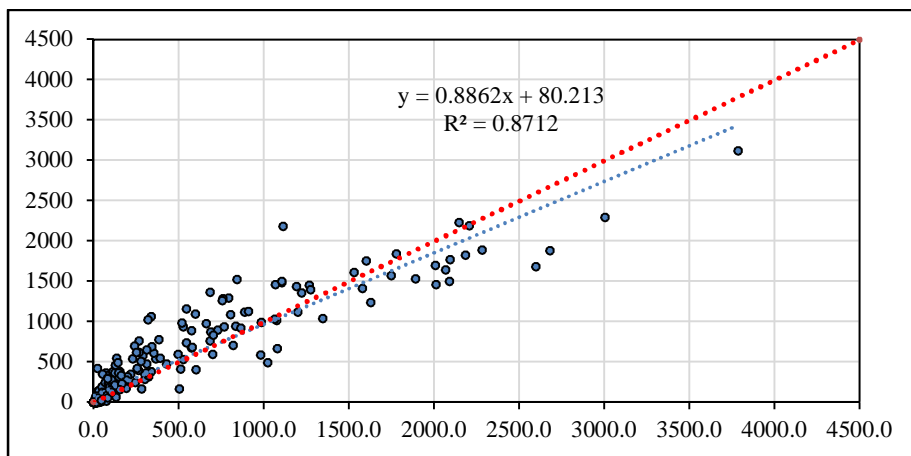
Fig. 5.8 Scatter plot showing calibrated observed and simulated discharge of the Tel basin

Further, the model efficiency was examined during the calibration period. Various measures of performance as mentioned earlier are calculated and reported in Table 5.5.

Table 5.5: Results of statistical analysis and model performance before and after calibration during 1972-1998

Parameters	Discharge during calibration Period (1972-1998)		
	Observed	Pre-calibrated	Calibrated
Mean	305.97	347	310.15
Standard Deviation	116.02	122.58	119.15
Maximum	3783.8	2299	3125
Coefficient of determination	-	0.67 (Good)	0.87 (Very Good)
Nash-Sutcliffe efficiency	-	0.37 (Unsatisfactory)	0.75 (Very Good)

It is evident from Table 5.5 that though the coefficient of determination (R^2) during the calibration period without any revision of the parameters is very good (0.87), but the other performance measure such as Nash-Sutcliffe efficiency (NSE) is highly unsatisfactory. Overall, it may be concluded that the monthly predictions are generally satisfactory during the simulation period, except for the few months with extreme storm and hydrologic conditions. However, one can improve the efficiency provided the ground data is available which can be incorporated in the model for its improved efficiency.

The parameters of the model are tested by running the model during the validation period of (1999-2012). It was observed that during the validation period also, the discharge values are little over-estimated throughout the time steps as shown in Fig. 5.9.
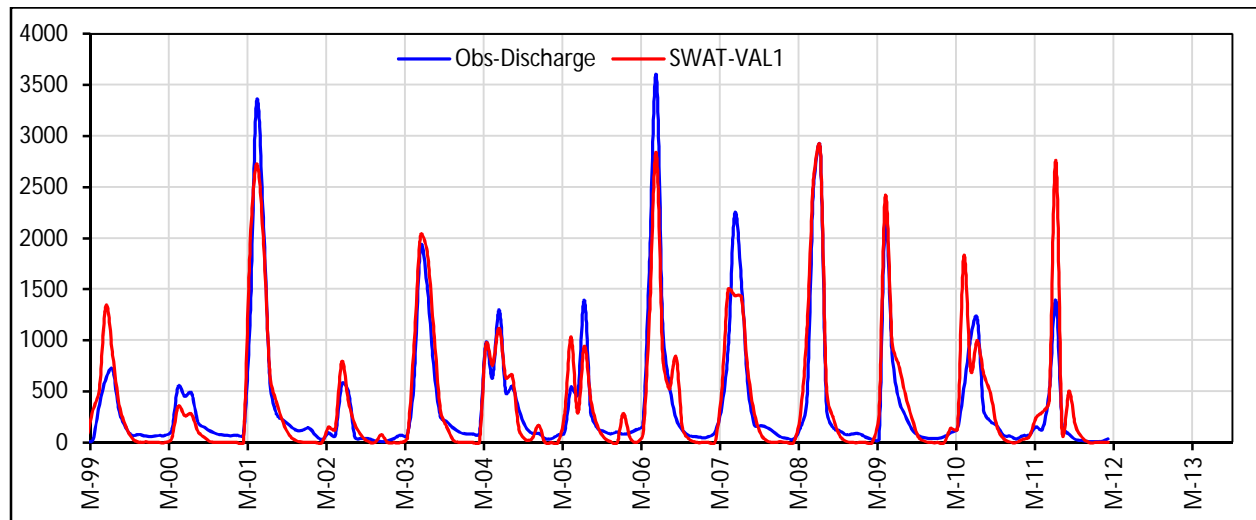
Fig. 5.9 Validated observed and simulated discharge of the Tel basin

The water balance components of the SWAT model is presented in Fig.5.10 for the Tel basin. The dependable annual flow for the basin at different dependability has been given in Table 5.6. Fig. 5.10 presents the flow duration curve for the basin.
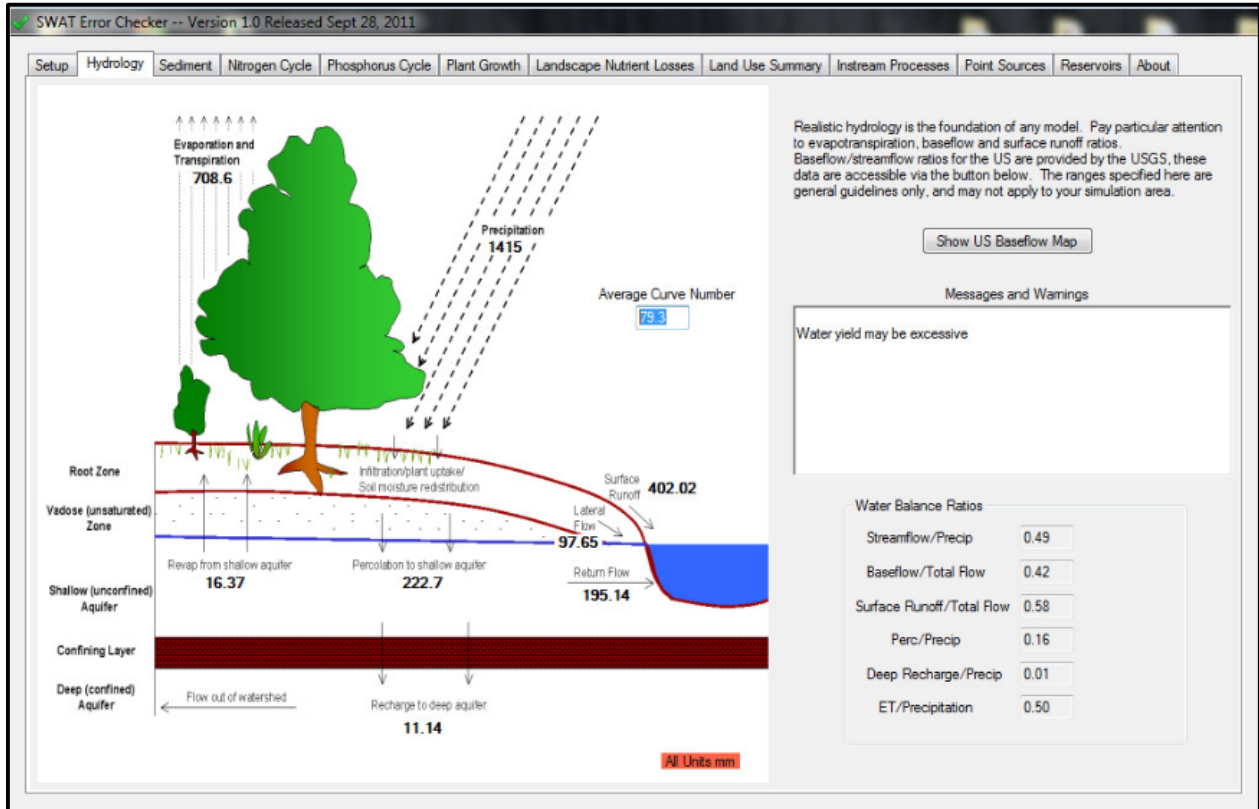
Fig. 5.10 Different water balance components based on SWAT model

Table 5.6: Annual dependable flows for the Tel basin

Year	Dependability	Annual Flow (MCM)
1991	50%	9977.07
2001	75%	6409.285
2007	90%	3777.33
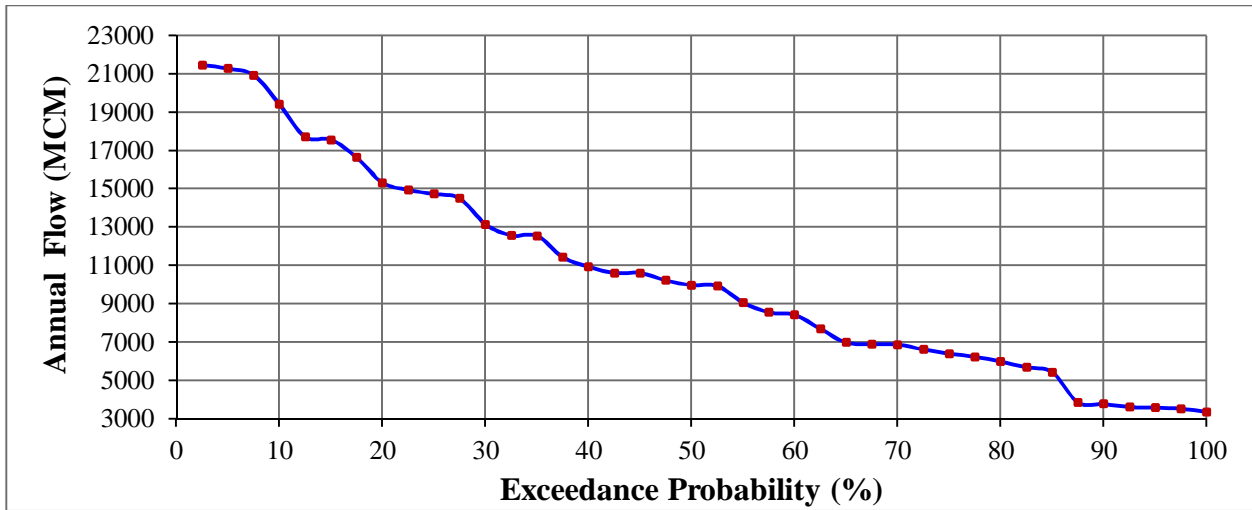
Fig. 5.11 Exceedance probability of annual flows of Tel basin

6

CONCLUSIONS

The KBK (Kalahandi-Koraput-Bolangir) region situated in the Southern-Western part of Odisha is prone to drought and poverty in spite of good rainfall and lot of agriculture activities. This can be attributed to several reasons including physiography, climate, soil, landuse-landcover, poor land and water management, human interventions, etc. To investigate the effect of climate change in the region, the study was conceptualized with three major objectives: (i) To analyze long-term historical climatic data to determine trend; (ii) To analyze the future climate in the region based on downscaled GCM data; and (iii) To assess the current potential and utilization gap of water resources in the region to develop management plan.

In this study, Mann-Kendall test and Sen's slope estimator test are utilized to investigate the trend for rainfall (110 years), temperature (102 years), and potential evapotranspiration (102 years). The year having considerable shift in rainfall and temperature pattern in the region has been detected using Pettitt's test and Standard Normal Homogeneity Test (SNHT). The results indicate significant decreasing annual rainfall trend at 5% significant level in the district of Nuapada and increasing trend in Malkangiri district. The southern districts with dominant forest coverage viz. Koraput and Rayagada are showing increasing rainfall trend though non-significant, whereas Bolangir, Kalahandi, Nabarangpur and Sonepur districts are showing decreasing trend. Monsoon rainfall shows decreasing trend in the districts of Nuapada, Kalahandi, Sonepur, Bolangir and Rayagada. The entire region is witnessing decrease in winter rainfall which plays a significant role for the rabi crops.

The future rainfall and temperature was downscaled for the region using HadCM3 Global Climate Model (GCM) for A2 and B2 scenarios. The KBK region is falling mainly in two sub-basins viz. Tel and Sabari sub-basins. Indravati project, Patora dam are few projects meeting the irrigation and drinking water demand in the region. Apart from this, few multipurpose projects (major and minor) are in pipe-line in the KBK region such as Ong irrigation project, Lower Suktel project, Tel project, etc. The water availability and utilization for Tel basin (sub-basin to Mahanadi basin) has been investigated. Daily discharge data for the Tel River for the duration

1972-2012 has been analyzed to compute annual dependable flow. The average annual yield for the basin is found to be about 9934 Mm^3 at 75% dependability. SWAT model has been applied to validate the results for the Kantamal G&D site. There are no major irrigation projects in the Tel basin at present. However, the combined annual utilization for drinking water, irrigation, and industry is about 4210 Mm^3.

The distinct climate variability of the Northern-Southern parts can be attributed to the distinct physiography of the region with a clear ridge line dividing the Northern and Southern districts. Northern districts are 'land-locked' with less coastal influence (about 300-350 km away) in comparison to South parts (100-150 km from the sea). Also the northern region is exposed to intense irrigated agriculture due to Hirakud reservoir and presence of lot of industries since 2003-04, whereas the southern districts viz. Malkangiri and Koraput have dense forest coverage influencing the climate in the region. Soils in district of Nuapada and Kalahandi are mostly 'Black Cotton' with high clay content resulting in poor retention of rainfall.

The important findings from the study are:

   i. Northern KBK region is getting drier (decreasing rainfall trend) whereas Southern KBK region is getting wetter.

  ii. Entire KBK region is 'warming', the Northern part is showing increasing rate of trend in last one decade, whereas Southern KBK region is showing a nearly constant rate of change in the temperature.

 iii. An increasing trend in the potential ET in the entire KBK region was noticed.

  iv. Precipitation and temperature (max) will likely to increase in future in the region as per HadCM3 A2 and B2 scenarios.

   v. The average annual water availability at 75% dependability in the Tel basin is about 10,000 Mm^3 sufficient to meet the water demand in the region with proper storage and water management practices.

  vi. The daily flow for the last 10 years (2003-04 to 2012-13) has been analyzed for the G&D site at Kantamal. The observations are:

   ✓ Average annual runoff has been found as 371 cumec.

- ✓ Average monsoon (Jul-Oct) and non-monsoon (Nov-May) flow is 832 cumec and 85.63 cumec respectively.
- ✓ Average annual yield for the basin is 9934 Mm^3 at 50% dependability.

REFERENCES

1. A.N. Pettitt, "A non-parametric approach to the change-point detection", *Appl. Statist.*, 28(2), pp 126-135, 1979.
2. A.N. Pettitt, "A non-parametric approach to the change-point detection", *Appl. Statist.*, 28(2), pp 126-135, 1979.
3. Alexandersson, H., Moberg, A., 1997. Homogenization of Swedish temperature data. Part I: A homogeneity test for linear trends. Int. J. Climatol. 17, 25–34.
4. Arora M, Goel NK, Singh P. 2005. Evaluation of temperature trends over India. *Hydrological Sciences Journal* 50(1): 81–93.
5. Asokan, S. M. and Dutta, D (2008) Analysis of water resources in the Mahanadi River Basin, India under projected climate conditions, Hydrological Processes, 22 (18), pp 3589-3603.
6. Basistha A., Aryan D. S. and Goel N. K., (2008). "Spatial pattern of trends in Indian sub-divisional rainfall", *Int. J. Climatol.* , DOI: 10.1002/joc.1706.
7. Basistha, D.S. Aryan and N.K. Goel, "Analysis of historical changes in rainfall in the Indian Himalayas", Int J Climatol, 29, pp 555–572, 2009.
8. Chow, V.T., Maidment D.R. and Mays, L.W. (1988) Applied Hydrology. McGraw-Hill International Editions, Civil Engineering Seires, pp 403-405.
9. Cohn, T.A. and Lins, H.F (2005) Nature's style: Naturally trendy. Geophysical Res. Letters, 32, L23402, doi:10.1029/2005GL024476.
10. De, U.S. & Prakash Rao, G.S. (2004) Urban climate trends-Indian scenario, J. of Ind. Geophys. Union, 8 (3), 199-203.
11. Ghosh S., Luniya V. and Gupta A., (2009). "Trend analysis of Indian summer monsoon rainfall at different spatial scales", *Atmospheric Science Letters*, DOI:10.1002/asl.235.
12. H. Alexandersson, "A homogeneity test applied to precipitation data", *J. Climatol*, 6, pp 661-675, 1986.
13. H. Alexandersson and A. Moberg, "Homogenization of Swedish temperature data. Part I: A homogeneity test for linear trends", *Int. J. Climatol*, 17, pp 25–34, 1997.
14. H.B. Mann, "Nonparametric tests against trend", *Econometrica*, 13, pp 245–259, 1945.
15. H. Theil, "A rank invariant method of linear and polynomial regression analysis", Part 3, Netherlands Akademie van Wettenschappen, Proceedings 53, pp 1397–1412, 1950.
16. Http://en.wikipedia.org/wiki/Moving_average.
17. Hundecha Y, Bardossy A (2005) Trends in daily precipitation and temperature extremes across western Germany in the second half of the 20th century. Int J Climatol 25:1189–1202.
18. H.V. Storch, "Misuses of statistical analysis in climate research. Analysis of climate variability: applications of statistical techniques, 2nd ed.", *Proceedings of an Autumn School organized by the Commission of the European Community on Elba from October 30 to November 6, 1993*", Springer, Berlin, 11–26, 1993.
19. IPCC (Intergovernmental Panel for Climate Change): 2001, Climate Change 2001 – the Scientific Basis, Contribution of Working Group I to the Third Assessment Report of the Intergovernmental Panel for Climate Change.

20. IPCC (Intergovernmental Panel for Climate Change): 2007, Climate Change 2007 – the Scientific Basis, Contribution of Working Group I to the Fourth Assessment Report of the Intergovernmental Panel for Climate Change.

21. Pal, and A.Al-Tabbaa, "Long-term changes and variability of monthly extreme temperatures in India", *Theor Appl Climatol*, 100, pp 45–56, 2010, DOI 10.1007/s00704-009-0167-0.

22. Jhajharia, D and Singh, V.P. 2011. Trends in temperature, diurnal temperature range and sunshine duration in Northeast India. *Int. J. Climatol.* 31: 1353–1367.

23. J.M.A. Duncan, J. Dash and P.M. Atkinson, "Analysing temporal trends in the Indian Summer Monsoon and its variability at a fine spatial resolution", *Climatic Change*, 2012, DOI 10.1007/s10584-012-0537-y.

24. J. Kyselý, "Trends in heavy precipitation in the Czech Republic over 1961–2005", *Int J Climatol*, 29, pp 1745–1758, 2008.

25. J.M. Cunderlik and D.H. Burn, Local and regional trends in monthly maximum flows in Southern British Columbia, *Canadian Water Resources Journal*, 27(2), pp 191-212, 2002.

26. J.M. Cunderlik and D.H. Burn, "Linkages between regional trends in monthly maximum flows and selected climatic variables", *ASCEJournal of Hydrologic Engineering,* 9(4), pp 246–256, 2004.

27. J.P. Patra, A. Mishra, R. Singh and N.S. Raghuwanshi, "Detecting rainfall trends in twentieth century (1871-2006) over Orissa State, India", *Climatic changes*, 111, pp 801-817, 2012.

28. Kothawale DR, Rupa Kumar K (2005) One the recent changes in surface temperature trends over India. Geophys Res Lett 32: L18714. doi:10.101029/2005GL023528.

29. Kundzewicz, Z. W., Robson, A.J (2004) Change detection in hydrological records-a review of the methodology. Hydrological Sciences Journal, 49(1), pp 7-19.

30. M. Bayazit, and B. Onoz, "To prewhiten or not to prewhiten in trend analysis?", *Hydrological Sciences Journal,* 52 (4), pp 611–624, 2007.

31. M. G. Kendall, "Rank correlation methods", London: Charles Griffin, 1975.

32. M.M.Q. Mirza, "Climate change and extreme weather events: can developing countries adapt?" *Climate Policy,* 3, pp 233–248, 2003.

33. M.N. Khaliq and T.B.M.J. Ouarda, "Short Communication on the critical values of the standard normal homogeneity test (SNHT)", *Int. J. Climatol*, 27, pp 681-687, 2007.

34. Modarres, R., da Silva, R.V.P. (2007) Rainfall trends in arid and semi-arid regions of Iran. Journal of Arid Environment 70, 344–355.

35. P.K. Sen, "Estimates of the regression coefficient based on Kendall's tau", *J Am Stat Assoc.*, 63(324), pp 1379–1389, 1968.

36. Rai R. K., Upadhyay A. and Ojha C. S. P. (2010) Temporal Variability of Climatic Parameters of Yamuna River Basin: Spatial Analysis of Persistence, Trend and Periodicity, *The Open Hydrology Journal,* 4, 184-210.

37. S.K. Jain and V. Kumar, "Trend analysis of rainfall and temperature data for India", *Current Science, 102*(1), pp 37–49, 2012.

38. S. Yue and M. Hashino, "Long term trends of annual and monthly precipitation in Japan", *J. Am. Water Resour. Assoc.*, 39(3), pp 587-596, 2003.

39. S. Yue, P. Pilon, R. Phinney and G. Cavadias, "The influence of autocorrelation on the ability to detect trend in hydrological series", *Hydrol Process*, 16, pp 1807–1829, 2002.

40. S. Yue, P. Pilon and R. Phinney, "Canadian streamflow trend detection: impact of serial and cross-correlation" *Hydrol Sci J*., 48(1), pp 51–63, 2003.

41. V. Kumar and S.K. Jain, "Trends in seasonal and annual rainfall and rainy days in Kashmir Valley in the last century", *Quaternary International*, 212, pp 64–69, 2010.

42. V. Kumar, S.K. Jain and Y. Singh, "Analysis of long-term rainfall trends in India", *Hydrological Sciences Journal,* 55(4), pp 484–496, 2010.

43. Yevjevich V. (1971) Stochastic Processes in Hydrology. Water Resources Publications, Fort Collins: CO.

44. Yue S and Pilon P. (2004) A comparison of the power of the t test, Mann-Kendall and bootstrap tests for trend detection. *Hydrological Sciences Journal* 49(1): 21–37.

45. Z.W. Kundzewicz, U. Ulbrich, T. Brucher, D. Graczyk, A. Kruger, G.C. Leckebusch, L. ,Menzel, I. Pinskwar, M. Radziejewski and M. Szwed, "Summer floods in central Europe—climate change track?", *Nat Hazards*, 36, pp 165–189, 2005.

46. Z.X. Xu, K. Takeuchi and H. Ishidaira, "Monotonic trend and step changes in Japanese precipitation", *J Hydrol*, 279, pp 144–150, 2003.

47. Aksornsingchai P, Srinilta C. 2011. Statistical downscaling for rainfall and temperature prediction in Thailand. Proceedings of the International MultiConference of Engineers and Computer Scientists, Vol. I, March 16-18, Hong Kong.

48. Bardossy A. 1997. Downscaling from GCM to local climate through stochastic linkages. J. Environ. Manage. 49:7-17.

49. Brekke, L.D., Kiang, J.E., Olsen, J.R., Pulwarty, R.S., Raff, D.A., Turnipseed, D.P., Webb,

R.S., and White, K.D., 2009, Climate change and water resources management—A federal perspective: U.S. Geological Survey Circular 1331, 65 p.

50. Chaturvedi R., Joshi J., Jayaraman M., Bala G. and Ravindranath N. (2012), Multi-model climate change projections for India under representative concentration pathways, Curr. Sci., 103(7), 1–12.

51. Fowler, H. J., and Wilby, R. L. (2007). Beyond the downscaling comparison study. International Journal of Climatology, 27: 1543–1545 (2007).

52. Fowler, H.J., Blenkinsop, S., and Tebaldi, C., 2007, Review: Linking climate change modeling to impacts studies—Recent advances in downscaling techniques for hydrological modelling: International Journal of Climatology, v. 27, p. 1547–1578.

53. Ghosh S, Mujumdar PP. 2006. Future rainfall scenario over Orissa with GCM projections by statistical downscaling. Current Science 90(3):396-404.

54. Hassan Z, Harun S. 2012. Application of statistical downscaling model for long lead rainfall prediction in Kurau river catchment of Malaysia. Malaysian J. of Civil Engineering 24(1):1-12.

55. Hewitson BC, Crane RG. 1996. Climate downscaling: techniques and application. Climatic Research 7:85-95.

56. Jones, R.G., Noguer, M., Hassell, D.C., Hudson, D., Wilson, S.S., Jenkins, G.J. and Mitchell, J.F.B. 2004. Generating high resolution climate change scenarios using PRECIS, Met Office Hadley Centre, Exeter, UK, 40pp.

57. MOEF (2010). Climate change and India: A "4X4" assessment. Ministry of Environment & Forests, New Delhi.

58. Ojha CSP, Goyal MK, Adeloye AJ. 2010. Downscaling of precipitation for lake catchment in arid region in India using multiple linear regression and neural networks. The Open Hydrology J. 4:122-136.

59. Pechlivanidis, I.G., Olsson, J., Sharma, D., Bosshard, T. and Sharma, K.C. (2015). Assessment of the climate change impacts on the water resources of the Luni region, India. GlobalNEST Jr., 17(1), 29-40.

60. Prudhomme C, Jakob D, Svensson C. 2003. Uncertainty and climate change impact on the flood regime of small UK catchments. J. of Hydrology 277:1-23.

61. Raje D, Mujumdar PP. 2009. A conditional random field-based downscaling method for assessment of climate change impact on multisite daily precipitation in the Mahanadi basin. Water Resources Research 45:1-20.

62. Robock A, Turco RP, Harwell MA, Ackerman TP, Andressen R, Chang HS, Sivakumar M VK. 1993. Use of general circulation model output in the creation of climate change scenarios for impact analysis. Climatic Change 23:293-335.

63. Wilby RL, Dawson CW. 2007. User manual on SDSM 4.2-a decision support tool for the assessment of regional climate change impacts, 1-94.

64. Wilby RL, Wigley TML. 1997. Downscaling general circulation model output: a review of methods and limitations. Progress in Physical Geography 21:530:548.

65. Wilby, R.L., T.M.L. Wigley, D. Conway, P.D. Jones, B.C. Hewitson, J. Main and D.S. Wilks. 1998. Statistical downscaling of general circulation model output: A comparison of methods, Water Resources Research, 34: 2995-3008.

66. Wilby, R.L., Charlas, S., Mearns, L.O., Whetton, P., Zorito, E. and Timbal, B. 2004. Guidelines for Use of Climate Scenarios Developed from Statistical Downscaling Methods. IPCC Task Group on Scenarios for Climate Impact Assessment (TGCIA).